January 2012

Evaluation Of Thermophysical Properties, Friction Factor And Heat Transfer Of Alumina Nanofluid Flow In Tubes

Sanjib Tiwari

EVALUATION OF THERMOPHYSICAL PROPERTIES, FRICTION FACTOR, AND HEAT TRANSFER OF ALUMINA NANOFLUID FLOW IN TUBES

by

Sanjib Tiwari
Bachelor of Engineering, Tribhuvan University, 2009

A Thesis

Submitted to the Graduate Faculty

of the

University of North Dakota

In partial fulfillment of the requirements

for the degree of

Master of Science

Grand Forks, North Dakota
December
2012

The Thesis, submitted by Sanjib Tiwari in partial fulfillment of the requirements of the Degree of Masters of Science from the University of North Dakota, has been read by the faculty advisory committee under whom the work has been done and is hereby approved.

_____

Dr. Clement Tang, Chairperson

_____

Dr. Forrest Ames

_____

Dr. Nanak Grewal

This, thesis meets the standard for appearance, conforms the style and format requirements of the graduate school of the University of North Dakota and is hereby approved.

_____

Dr. Wayne Swisher

Dean of Graduate School

_____

Date

PERMISSION

Title	Evaluation of Thermophysical Properties, Friction Factor and Heat Transfer of Alumina Nanofluid Flow in Tubes
Department	Mechanical Engineering
Degree	Masters of Science

In presenting this thesis in partial fulfillment of the requirements for a graduate degree from the University of North Dakota, I agree that the library of this University shall make it freely available for inspection. I further agree that permission for extensive copying for scholarly purposes may be granted by the professor who supervised my thesis work or, in his absence, by the chairperson of the department or the dean of the Graduate School. It is understood that any copying or publication or other use of this thesis or part thereof for financial gain shall not be allowed without my written permission. It is also understood that due recognition shall be given to me and to the University of North Dakota in any scholarly use which may be made of any material in my thesis.

Signature

12/05/2012

Date

TABLE OF CONTENTS

LIST OF FIGURES

LIST OF TABLES

ACKNOWLEDGEMENTS

I would first like to thank the University of North Dakota for providing me with an excellent opportunity to pursue my Master's program. I would like to thank my advisor Dr. Clement Tang for his continual support as well as his guidance in the contents of the research which led to the timely completion of my thesis. Dr. Tang has given me vast amount of ideas to conduct research efficiently for which I will be highly indebted to him throughout my life. I am very much indebted to the Professor Forrest Ames and Professor Nanak Grewal their continual guidance and encouragement for the time during my master's program.

I also would like to acknowledge Matthew Cox for his continual efforts and help during the research. I would like to thank John Roche of Emerson Rosemount for donating three pressure transducers which were critical for the outcome of this research.

I would also like to thank my family members, my mother Shanta Tiwari, my sister Samriddi Tiwari and my brother in law Sushil Joshi whose continual emotional support has helped me to stay focused and organized. I am very much grateful to my friend Samira Kharel for her continuous encouragement and help. Finally I would like to thank Gary Dubuque, Jay Evenstad and Teri Berg, staff of the Department of Mechanical Engineering, University of North Dakota for their continuous help.

In Loving Memory of my father, Dr. Dirgha Nidhi Tiwari

ABSTRACT

Various thermophysical properties, fluid flow parameter and heat transfer characteristics were measured for nanofluid with 6% volume concentration of solid Al_2O_3 nanoparticles in water. Thermal conductivity measurements showed that there is a definite enhancement in thermal conductivity of the nanofluid compared to that of water. At 7°C, the enhancement was 16% which decreased to 6.96% at 50°C.

The viscosity measurements of the 6% volume concentration Al_2O_3/water nanofluid showed that its viscosity is higher by a factor of 1.25 to 10.24 than the viscosity of water. Also the measurements of the viscosity of different volume concentration of Al_2O_3/water nanofluid showed that, the viscosity decreases as the volume concentration decreases. The plot between the shear stress and strain rate for the 6% volume concentration Al_2O_3/water nanofluid showed that it is a Newtonian fluid for the range of strain rate between 6–122 s^{-1}. Several readings of viscosity were taken by subjecting the nanofluid to heating and cooling cycle. It was found that above 62.65°C, the 6% volume concentration Al_2O_3/water nanofluid experiences an irrecoverable increase in viscosity and when cooled from beyond this temperature, a hysteresis effect on the viscosity is seen.

The friction factor results for laminar flow for the 6% volume concentration Al_2O_3/water nanofluid showed that it matches the value given by the Hagen-Poiseulle equation

($f = 64/Re$). The transition from laminar flow to turbulent was found to occur at a Reynolds number of approximately 1500.

The convective heat transfer results were in agreement with that proposed by the Lienhard correlation (Lienhard and Lienhard, 2008). For fully developed laminar flow, the Nusselt number under constant heat flux condition was found to be within ±7% of 4.36. In the laminar flow regime, the Nusselt numbers for thermally developing flow were within ±10% of the value calculated from the Lienhard correlation.

NOMENCLATURE

A	Particle radius [m]
B	Ratio of nanolayer thickness to particle radius
D_o	Outside diameter[m]
D_{in}	Inside diameter [m]
d	diameter of particle[m]
du/dy	Velocity gradient, shear rate [s^{-1}]
d_{BF}	Base fluid molecular diameter [nm]
d_p	Diameter of nanoparticles [nm]
d_N	Diameter of the nanoparticle [nm]
f	Friction Factor
h	Convective heat transfer coefficient[$W/m^2.K$]
h_x	Convective heat transfer coefficient at distance x [$W/m^2.K$]
I	Current supplied [Amp]

k	Thermal conductivity [$Wm^{-1}K^{-1}$]
k_l	Thermal conductivity of base liquid[$Wm^{-1}K^{-1}$]
k_{BF}	Base fluid thermal conductivity [$Wm^{-1}K^{-1}$]
k_b	Boltzmann constant (= 1.3807×10^{-23} J/K)
k_{eff}	Nanofluid effective thermal conductivity [$Wm^{-1}K^{-1}$]
k_f	Thermal conductivity of the base fluid [$Wm^{-1}K^{-1}$]
k_m	Effective thermal conductivity of the fluid caused by convection
k_O	Thermal conductivity of base fluid [$Wm^{-1}K^{-1}$]
k_{low}	Lower limit of thermal conductivity [$Wm^{-1}K^{-1}$]
k_p	Thermal conductivity of the particles [$Wm^{-1}K^{-1}$]
k_i	Thermal conductivity of the interfacial shell [$Wm^{-1}K^{-1}$]
L	Length of the test section [m]
l_{BF}	Mean free path for water (= 0.17 nm)
M	Dynamic viscosity [Nsm^{-2}]
$\dot{m}$	Mass flow rate [kg/s]
n	Empirical shape factor (= $3/\Psi$)

Nu	Nusselt number
Pr	Prandtl number
Q	Heat/power supplied [W]
q	Heat flux [W/m^2]
R	Thickness of capping layer (= 1 nm)
R_b	Interfacial resistance [Km^2W^{-1}]
Re	Reynolds number
T	Temperature [°C]
t	Interfacial shell thickness [nm]
T_c	Half of the base fluid boiling temperature [°C]
T_b	Bulk fluid temperature [°C]
$T_{b,out}$	Outlet fluid bulk temperature [°C]
$T_{b,in}$	Inlet fluid bulk temperature [°C]
T_o	Reference temperature [°C]
ΔT	Temperature difference [°C]
V	Voltage supplied [Volts]

V_{Br}	Brownian velocity of the nanoparticles [m/s]
ΔV	Voltage drop [Volts]
x	Axial distance [m]
x^+	Dimensionless distance
x_{et}	Thermal entry length [m]
y	Distance from the surface [m]

Greek Symbols

α	Parameter defined by Eq. 2.18
$\partial T/\partial y$	Temperature gradient [K/m]
η_{nf}	Viscosity of nanofluid [Pa.s]
η_{bf}	Viscosity of base fluid [Pa.s]
μ	Dynamic Viscosity [Pa.s, cP]
v	Kinematic viscosity of liquid [m^2/s]
μ_{bf}	Viscosity of base fluid [Pa.s]
μ_{nf}	Viscosity of nanofluid [Pa.s]

μ_r	Relative viscosity
Φ	Particle volume fraction
Ψ	Sphericity
ρ	Density [kg/m^3]
ρ_N	Density of the nanoparticle [kg/m^3]
τ	Shear stress [N/m^2]
ξ	Thermal conductivity enhancement

Abbreviations

NF	6% volume fraction Al_2O_3(47 nm)/water nanofluid

CHAPTER I

INTRODUCTION

Modern researchers are in search for a suitable means of efficient heat dissipation for increased range of temperature operation, compact design, cost reduction etc. The conventional cooling fluids such as water and air are proving inadequate to achieve the required trend of current needs. Many studies have suggested the use of two phase fluids consisting of suspension of micro/millimeter sized particles in base fluids such as water or oil due to the higher thermal conductivities of the suspended solids (Eastman et al., 1996, Beck et al., 2006, Minsta et al., 2007). Although such two phase fluids show improvement in the heat transfer characteristics, they inherit problems such as clogging, sedimentation and abrasive action of the particles. These problems are much more amplified when using these fluids in micro/mini channels.

It was not until the mid-1990's when advancement in manufacturing technology led to a development in nanoparticles, a new class and size of material whose size range is around 1-100 nm. A nanometer is equivalent to one billionth of a meter (see Figure 1.1). These nanoparticles show promising new applications in the field of heat transfer and flow due to their size which permits them to stay as a stable suspension indefinitely in liquid base fluid. Also, nanoparticles have much more surface area per unit volume when compared

with millimeter/micrometer sized particles which can be beneficial for heat transfer. Nanofluid is essentially a two phase solid suspended in liquid mixture in which the solid particles size ranges in nanometers. Typical solid particles can be metals such as aluminum, copper, nickel, etc. or oxides of such metals. The liquid or the base fluid can be water or other organic compounds such as ethylene glycol, oils etc. Nanofluids are believed to have better heat transfer capabilities while eliminating problems such as sedimentation, corrosion and clogging.

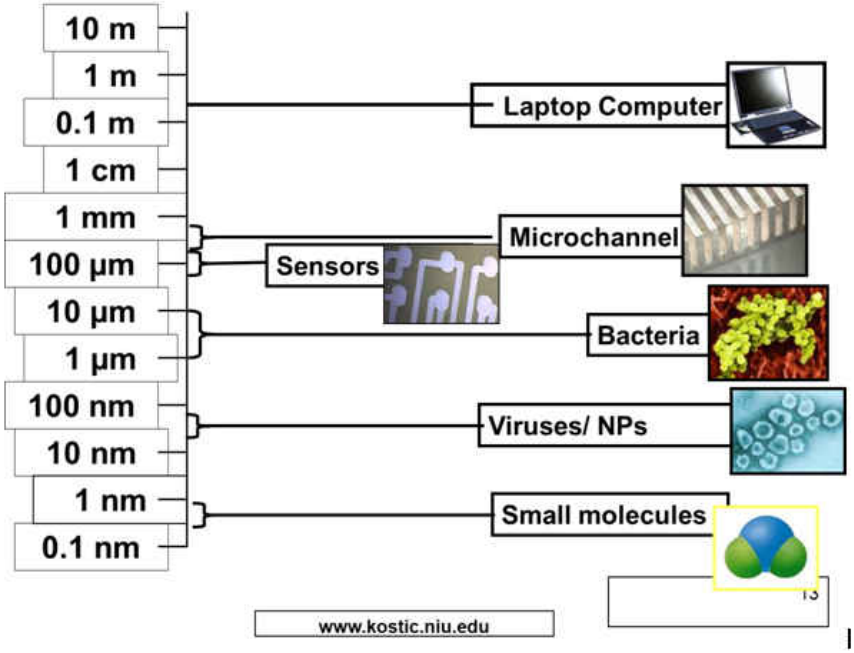

Figure 1.1 Comparison of size of nanoparticles with other substances (nanoparticles are indicated as NPs), Choi et al. (2004).

Although Nanofluids are still mainly in the research phase, applications of Nanofluids have been found in variety of operations, such as cooling applications in industry,

cooling of desktop CPUs, automotive coolants etc. It has also been suggested to be used as cooling fluids in nuclear reactors, which is an ongoing research project conducted at MIT (Wong et al., 2010). Wong et al. (2010) reported that nanofluids have been used as coolant in radiators of trucks, which has led to a more compact design and hence reduction in drag.

For nanofluid to be used as a cooling fluid in variety of operations, proper characterization of various parameters such as viscosity, pressure drop, mass flow rate, heat transfer coefficient and concentration of nanoparticles must be done. These properties are very important in designing the cooling flow system. There have been numerous studies on these parameters. However, studies on heat transfer and other parameters are done separately and there is a need to study all these parameters together to have a better understanding on the influence of each parameter on the other.

There are many properties to be considered for a fluid to be considered in heat transfer and flow applications. Some of the properties are discussed below

Viscosity

Viscosity is an important factor when considering flow applications because it affects the pumping power requirement and the workability of the fluid. Viscosity is the measure of internal friction of the fluid. This friction is created when layers of fluid slide past each other. When the layers of fluid slide past each other, shearing occurs between the layers of fluid. There is always a force required to cause this shearing, greater the force greater will be the shearing.

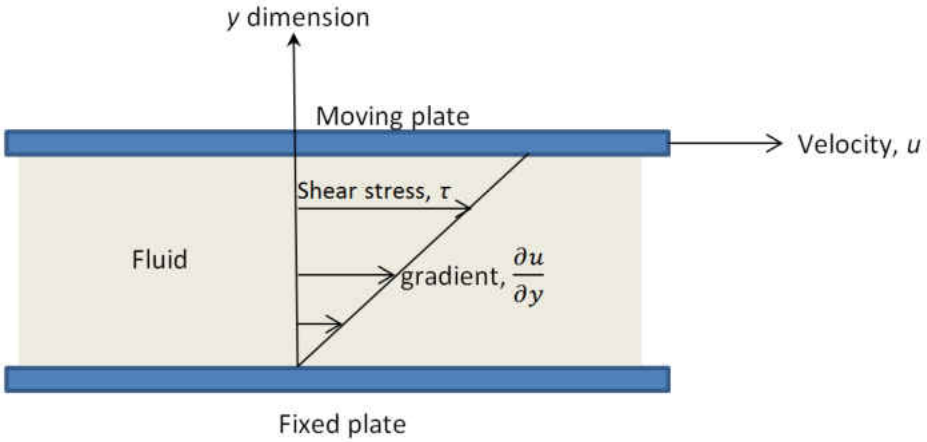

Figure 1.2 velocity gradient formed between two parallel plates.

If we consider two parallel plates (see Figure 1.2) separated by a distance y between which fluids are enclosed, and apply a force (F) in one of the plate that causes it to move, there will exist a velocity gradient (du/dy) in the fluid. In this case the applied force will be proportional to the velocity gradient and the area. Mathematically, it can be expressed as

$$F = \mu A \frac{du}{dy} \tag{1.1}$$

where μ is a is called the absolute viscosity or dynamic viscosity.

The term du/dy measures the speed at which different layers of fluid move with respect to each other and is termed the strain rate. The term F/A gives the force per unit area and is a measure of the unit force required to produce the shearing of the liquid and is termed as the shear stress. The shear stress is denoted as τ.

There are different types of material which show different types of behavior based on their viscosity. They are categorized as

I. Newtonian Fluid: A Newtonian fluid is such fluid whose value of viscosity does not change when the strain rate is varied at a given temperature. Some of the examples of Newtonian fluid are water and air.

II. Non-Newtonian fluid: A non-Newtonian fluid is which whose value of viscosity varies as the strain rate is varied at a given temperature. This means that when the strain rate is varied, the shear stress does not change in the same proportion at a given temperature. There are different types of non-Newtonian fluids depending upon whether their viscosities increases or decreases as the strain rates are increased. If the fluid displays a decreasing viscosity while the strain rate is increasing, it is termed as pseudoplastic and the fluid is said to undergo a shear-thinning behavior. If the fluid displays an increasing viscosity while the strain rate is increasing, it is termed as dilatant and the fluid is said to undergo a shear-thickening behavior.

III. Some fluids undergo a change in viscosity over time under constant shear rate. If the viscosity decreases under constant shear rate over time, it is said to exhibit a thixotropic behavior and if the viscosity increases, a rheopectic behavior.

There are other factors upon which the viscosity is dependent. For fluids, viscosity is a strong function of temperature. For fluids containing many constituents, it depends upon the concentration of the constituents and their properties.

Thermal Conductivity

The thermal conductivity is the measure of heat (Q) flow per unit area (A) in the direction of the temperature gradient (dT/dy).

$$\frac{Q}{A} = k\frac{dT}{dy} \tag{1.2}$$

The Newton's law of cooling is given as

$$\frac{Q}{A} = h(T_s - T_\infty) \tag{1.3}$$

when combing the Fourier's law (Eq. 1.2) and the Newton's law of cooling (Eq. 1.3), we get

$$h = -k\frac{\partial T \;\; \partial y \;\Big|_{y=0}}{T_s - T_\infty} \tag{1.4}$$

Equations 1.2–1.4 show that estimating and knowing the behavior of thermal conductivity is crucial in heat transfer. The values of thermal conductivity can significantly affect the heat transfer. Due to this higher thermal conductivity materials are mostly used in heating or cooling application while lower thermal conductivity materials are used for insulation purposes. Thermal conductivity is affected by factors such as temperature, phase change of materials, constituents of the material and also the material structure.

Mass Flow Rate

The mass flow rate ($\dot{m}$) is an important factor while determining the heat transfer rate. Mass flow rate is related to the heat transfer by

$$Q = mc_p\Delta T \tag{1.5}$$

where c_p is the specific heat capacity of the substance in [J/kg.K].

Pressure Drop

The pressure drop is quantified in terms of friction factor and is an important factor when considering flow applications. A high friction factor (f) or pressure drop would indicate a high power requirement. The pressure drop (Δp) can be expressed from the Darcy-Weisbach equation given by

$$\Delta p = f\frac{L}{D_i}\rho\frac{V^2}{2g} \tag{1.6}$$

where L is the length of the channel in [m], D_i is its inside diameter in [m], ρ is the fluid density in [kg/m^3], V is the average velocity in [m/s], and g the acceleration due to gravity in [m/s^2].

Convective Heat Transfer

The convective heat transfer is quantified in terms of a dimensionless number called the Nusselt number. The Nusselt number is the ratio of the convective heat transfer to the conductive heat transfer. A high Nusselt number indicates active convection and a low

Nusselt number refers to a laminar or slug flow and less active convection. Mathematically, it is given as

$$Nu_L = hL/k \tag{1.7}$$

The Nusselt number is highly dependent upon the Reynolds number and the Prandtl number of the fluid and also depends upon the type of flow (laminar or turbulent) and whether the flow is fully developed or not. A turbulent flow is characterized by a high Nusselt number. For a developing laminar flow, the Nusselt number slowly decreases from a higher value and approaches to a constant value of 4.36 under fully developed conditiosn for constant heat flux and a value of 3.66 under a fully developed isothermal condition. The curve of Nusselt number versus the developing distance for laminar flow for high Prandtl number fluids decreases sharply and takes a relatively long distance for the thermal profile to develop fully while for a low Prandtl number is flat and the thermal profile quickly develops. It is therefore very important to know whether the flow is fully developed or not. This distance is termed as the thermal entry length and is given by Lienhard and Lienhard (2008) as

$$\frac{x_{et}}{D} \cong 0.034 Re_D Pr \tag{1.8}$$

where x_{et} is the thermal entry length in [m], D is the diameter in [m], Re_D is the Reynolds number based on diameter, and Pr is the Prandtl number.

1.1 Research Objectives

The main objective of this research is to devise an accurate experimental setup and methodology for the measurement of various thermophysical properties, pressure drop and heat transfer for nanofluid. This experimental setup will be used get a throughout understanding of the nanofluid in terms of its thermophysical properties, pressure drop and heat transfer. The thermophysical properties such as thermal conductivity and viscosity have important effects on the flow and heat transfer characteristics. Understanding and accurately quantifying these terms are critical in understanding the flow and heat transfer characteristics of nanofluids. The data collected from this research provide an absolute value of nanofluid properties; however comparison of the results should be made with a standard fluid preferably water in order to know where the nanofluid lies in terms of their properties and characteristics. Before conducting the research, one should try to answer the following question

1. Does the experimental setup and procedure work well for a standard fluid? Do the results compare well to the well-established correlations?
2. Is there an enhancement in the thermal conductivity of nanofluid when compared to water? If yes, what does the enhancement at different temperature look like? What is the trend of this enhancement? Does the thermal conductivity of nanofluid compare well to established correlations.
3. Is the viscosity of the nanofluid too high causing flow problems? What is it viscosity compared to water? Is the viscosity a strong function of temperature?

What does the temperature-viscosity profile look like? Is the nanofluid Newtonian, Non-Newtonian or does its viscosity changes over time?

4. Does the friction factor compare well to that of water? Will we have more head loss pumping the nanofluid through the loop?
5. Does the nanofluid show an abnormal enhancement in the heat transfer characteristics or will it compare to that of water? Can the heat transfer be quantified by a well-established correlation for a single phase?

To answer these questions following tasks were employed

1. A literature review was performed to determine the results regarding the thermal conductivity, viscosity, friction factor, heat transfer and experimental procedure.
2. A lab setup for measuring the thermophysical properties, flow and heat characteristics of fluid.
3. The experimental facility and procedure was validated using a standard fluid
4. The comparison of experimental results for standard fluid, water with the nanofluid.
5. The assessment of correlations available in the literature for single phase in predicting the behavior of nanofluid.
6. The collection and comparison of findings from the research in literature on related properties of nanofluids.

1.2 Outline of the Study

The subjects in this manuscript provide an insight about the experimental setup for measuring the thermophysical properties, fluid flow and heat transfer characteristics as well as the analysis of all these properties and parameters of nanofluids. Chapter II includes the review of literature from various sources regarding the thermal conductivity, viscosity, friction factor and convective heat transfer phenomena of a nanofluid. Chapter IV discusses the experimental setup, instrument calibration and the uncertainty associated with the measurements. Chapter V presents the results of the study, validates the experimental procedure and compares the results with established correlations. Chapter VI derives the conclusions from the results and gives recommendations to further improve the research.

CHAPTER II

LITERATURE REVIEW

2.1 Thermal Conductivity of Nanofluids

One of the early studies in the thermal conductivity enhancement was done by Eastman et al. (1996). The thermal conductivity was measured using the hot wire transient method. They found out that the thermal conductivity increases linearly with increasing nanoparticle volume fraction. They achieved a significant increase in thermal conductivity by 60% compared to the base fluid (water) for 5% volume fraction of CuO. Less increment in thermal conductivity for Al_2O_3/H_2O nanofluid is reported. They even suggested that larger increase in thermal conductivity can be obtained if metals are used instead of metallic oxides due to the larger values of thermal conductivity for metals.

Sridhara and Satapathy (2011) reviewed different papers related to Al_2O_3 based nanofluids. They report a maximum increment in thermal conductivity by 32% for 4% vol. fraction for water based Al_2O_3 nanofluids. In the case of ethylene glycol based nanofluid an enhancement of 30% for the same volume concentration is reported. There is not a clear correlation between the effects of particle size on the thermal conductivity of nanofluids. They report the least enhancement in thermal conductivity for water based

nanofluids compared to other non-water based nanofluids for same volume concentration. They suggest that there is a noticeable enhancement in thermal conductivity with increment in temperature.

There is no definite correlation that serves to give an estimation of thermal conductivity of nanofluids. However, Murugesan and Sivan (2010) developed correlation for the lower and upper limits of thermal conductivity of nanofluids. The lower limit is based on Maxwell

model. They reduced the Maxwell equation in terms of volume concentration and is given as

$$k_{low} = \frac{k_{eff}}{k_1} = 1 + 3\Phi \tag{2.1}$$

where k_{low} is the lower limit of thermal conductivity in [$Wm^{-1}K^{-1}$], k_{eff} is the effective thermal conductivity in [$Wm^{-1}K^{-1}$], k_1 is the thermal conductivity of base liquid in [$Wm^{-1}K^{-1}$], and Φ is the volume fraction of nanoparticles.

The upper limit for thermal conductivity is based on particle shape, nanolayer thickness in the particle fluid interface and Brownian motion. This is given as

$$k_{upp} = \frac{k_{eff}}{k_1} = \frac{k_p + \ n-1\ k_1 + (n-1)\ 1+\beta\ ^3\Phi(k_p - k_1)}{k_p + \ n-1\ k_1 - (1+\beta)^3\Phi(k_p - k_1)} + C\frac{\Phi(T - T_o)}{\mu a^4 k_1} \tag{2.2}$$

where k_p is the thermal conductivity of the particle in [$Wm^{-1}K^{-1}$], $n = 3/\Psi$ is an empirical shape factor that is the function of sphericity (Ψ), β is the ratio of nanolayer thickness to particle radius, μ is the dynamic viscosity in [Nsm^{-2}], a is the particle radius in [m], T is

temperature in [K], T_o is the reference temperature at 273 K, and the constant $C = 7 \times 10^{-36}$.

To validate their correlation, they performed experiments with different nanofluids with different particle sizes (13−38.4 nm), different volume fraction (0−5%) and with different temperature (21−51°C). Majority of their data is within the upper and lower limit. They even observed the drift of data from lower to upper limit as the temperature is increased.

Beck et al. (2010) measured the thermal conductivity of alumina nanoparticles with an average diameter of 12 nm dispersed in water, ethylene glycol, and ethylene glycol + water mixtures. They used the transient wire method to measure the thermal conductivity at temperature between 296 and 410 K. They found out that the thermal conductivity vs temperature pattern of the alumina nanofluid with water as base fluid follows the trend as that of water with a maximum value of thermal conductivity near 400 K (see Figure 2.1). They found a similar pattern with ethylene glycol and 50% (w/w) water + ethylene glycol base nanofluids concluding that the temperature dependence of the effective thermal conductivity of nanofluid is mainly due to the base fluid.

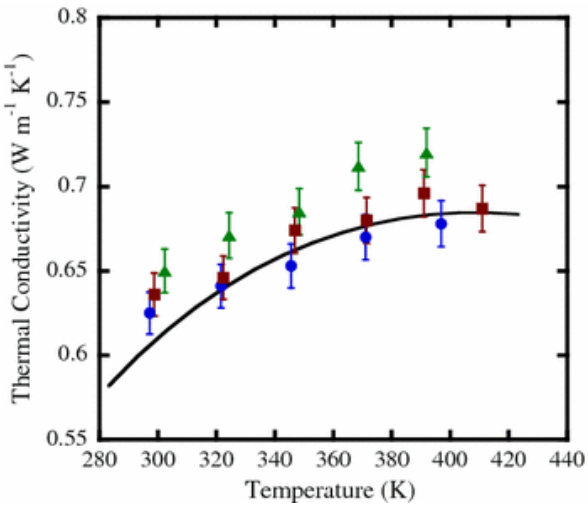

Figure 2.1. Thermal conductivity of water and alumina nanofluids with water as the base fluid [*d* = 12 nm at Φ = 1% (filled circle), Φ = 3% (filled square), Φ = 4% (filled triangle)]. The smooth curve shows the thermal conductivity of water. This shows that the curve trend of nanofluid is same that of the base fluid (water), Beck et al. (2006).

Chon et al. (2005) developed a correlation for the thermal conductivity of Al_2O_3 nanofluids as a function of the nanoparticle size and temperature. For developing the correlation they choose three Al_2O_3-water nanofluid samples containing 11 nm, 47 nm and 150 nm sized Al_2O_3 nanoparticles. They placed their apparatus inside a thermal bath to provide the temperature range of 21 to 71°C with ±0.01°C accuracy at each temperature. They used the transient hot wire method to measure the thermal conductivity of the nanofluid with an uncertainty of 3.90%. They present their correlation to be a strong function of the Brownian velocity which increases with increasing temperature and decreases with increasing nanoparticle size. Their correlation is based on the Buckingham-Pi theorem with a linear regression for the experimental results given as

$$\frac{k_{eff}}{k_{BF}} = 1 + 64.7\Phi^{0.7460} \left(\frac{d_{BF}}{d_p}\right)^{0.3690} \left(\frac{k_p}{k_{BF}}\right)^{0.7476} Pr^{0.9955} Re^{1.2321} \quad (2.3)$$

where d_{BF} is the base fluid molecular diameter, d_p is the diameter of nanoparticles, k_{eff} is the nanofluid effective thermal conductivity, k_{BF} is the base fluid thermal conductivity, k_p is the thermal conductivity of the particles, and Φ is the volume fraction of nanoparticles. The Prandtl number is given as

$$Pr = \frac{\mu}{\rho_{BF}\alpha} \quad (2.4)$$

where μ is the base fluid viscosity given as

$$\mu = A10^{B/(T-C)} \quad (2.5)$$

where, A, B and C are constants given as 2.414×10^{-5}, 247.8 and 140, respectively, for water.

The Reynolds number is given as

$$Re = \frac{\rho_{BF}\, V_{Br}\, d_p}{\mu} = \frac{\rho_{BF}\, k_b\, T}{3\,\pi\,\mu^2\, l_{BF}} \quad (2.6)$$

where l_{BF} = 0.17 nm is the mean free path for water, k_b = 1.3807×10^{-23} J/K is the Boltzmann constant, V_{Br} is the Brownian velocity of the nanoparticles based on the Einstein diffusion theory given by

$$V_{Br} = \frac{k_b T}{3\,\pi\mu\, d_p l_{BF}} \quad (2.7)$$

Minsta et al. (2007b) measured the thermal conductivities of nanofluid containing 29 nm CuO nanoparticles and 36 nm and 47 nm Al_2O_3 nanoparticles. They used the KD2 Pro thermal property analyzer from Decagon to measure the thermal conductivity. Nanofluid was placed in an insulated heated enclosure. They used a stirrer placed 15 mm from the thermal probe to ensure a better temperature profile of the nanofluid. They found that the effective thermal conductivity of nanofluids increases with temperature. From 20°C to 40°C they found an increase in thermal conductivity by approximately 16% for each type of nanofluid. They found out almost a linear relationship between the nanoparticle volume fraction and the measured thermal conductivity. The data for thermal conductivity with mixing induced by the stirrer was found to be higher than without mixing. This observation was attributed to the fact that less sedimentation occurs while using a stirrer. However, thermal conductivity measurements using a transient hot wire method is very much susceptible to free convection caused by disturbances.

Yoo et al. (2007) measured the thermal conductivity of different nanofluids. They used a two-step procedure to prepare TiO_2, Al_2O_3, Fe and WO_3 nanofluids with particle diameter of 25 nm, 48 nm, 10 nm and 38 nm, respectively. Deionized water was used as the base fluid. Transient hot wire method was used to measure the thermal conductivity. For 1% volume fraction of nanoparticles, Al_2O_3 based nanofluid shows 4% enhancement in thermal conductivity while TiO_2 based nanofluid shows an enhancement of 14.4%. Even though the thermal conductivity of Al_2O_3 is more than that of TiO_2, TiO_2 based nanofluid exhibit a higher thermal conductivity. For 0.3% vol. fraction of nanoparticles Fe based nanofluid shows 16.5% enhancement in thermal conductivity, whereas WO_3 based nanofluid shows an enhancement of 13.8%. This suggests that thermal conductivity of

nanofluid is not a strong function of particle thermal conductivity rather it is strongly dependent on the particle size. However there are different research and studies that indicate that the nanofluid thermal conductivity is a function of particle thermal conductivity.

Beck et al. (2009) measured the thermal conductivity of seven nanofluids containing alumina nanoparticles with diameters of 8–282 nm to determine the effect of particle size on the thermal conductivity of nanofluids. They utilized the transient hot wire method to measure the thermal conductivity. They also present a correlation for the thermal conductivity enhancement which is expressed as

$$\xi = \frac{k-k_1}{k_1} = \xi_{max}(1 - e^{-0.025d}) \tag{2.8}$$

with the limiting value given by,

$$\xi_{max} = 4.4134\Phi \tag{2.9}$$

For polydispersed nanoparticles,

$$\xi_{max} = 5.527\phi \tag{2.10}$$

where ξ is the thermal conductivity enhancement, k is the thermal conductivity of nanofluid in [$Wm^{-1}K^{-1}$], d is the diameter of particle in [m], Φ is the volume fraction of nanoparticles, and k_1 is the thermal conductivity of base fluid in [$Wm^{-1}K^{-1}$].

With the experimental findings, Beck et al. (2009) presents the fact that there is a limiting factor for thermal conductivity of nanofluids in terms of particle size. They report a maximum thermal conductivity enhancement for particle size of 50 nm. As the particle

size decreases, the thermal conductivity enhancement also decreases. This result however contradicts to the fact that the thermal enhancement of nanofluid is caused by increase in the surface to volume ratio of nanofluid.

For measuring the thermal conductivity Lee et al. (2008) used the transient hot wire method. They measured the thermal conductivity of Al_2O_3-water nanofluid for a concentration range of 0.01 to 0.3% vol. They found out that the thermal conductivity of Al_2O_3-water nanofluid increases almost linearly with volume concentration of nanoparticles with maximum enhancement of 1.44% at 0.3% vol. concentration compared to that of the base fluid (see Figure 2.2).

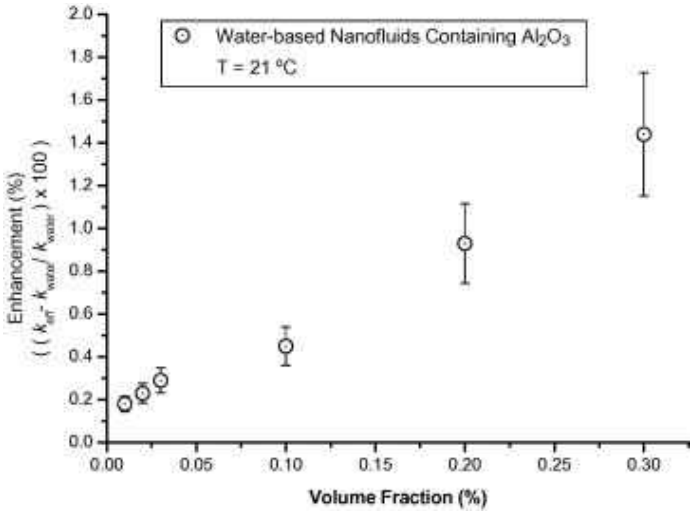

Figure 2.2. Linear increment in nanofluid thermal conductivity with particle volume fraction, Lee et al. (2008).

Sobhan and Thomas (2011) reviewed the different techniques used for thermal conductivity measurement of nanofluid. They described the transient and steady state

methods for measuring the thermal conductivity of fluids. They present a comparison between the different experimental techniques and conclude that the transient hot wire method to be the most accurate and reliable means of measurement of thermal conductivity of nanofluids.

Dey and Kole (2010) used alumina nanoparticles (<50nm diameter) with car engine coolant as the base fluid to prepare nanofluids with volume fraction of nanoparticles ranging from 0.001 to 0.035. In order to stabilize the suspension they used oleic acid as surfactant along with ultrasonication for 3 hours. They then homogenized the suspension for 1 hour by magnetic force agitation. The stability was then tested for 80 days without any trace of sedimentation.

They used the transient hot wire method to determine the thermal conductivity of the nanofluid with an uncertainty ±0.5%. They observed that the thermal conductivity increases almost linearly with nanoparticles volume fraction. Also the temperature dependence of nanofluid is presented to follow the trend of base fluid. They also present the fact that thermal conductivity enhancement of the nanofluid relative to the base fluid is independent of temperature. For 0.035 volume fraction of alumina, they observed an enhancement in thermal conductivity of 10.41% and 11.25% at 30°C and 8°C, respectively.

Abbaspoursani et al. (2011) presented a model for predicting the effective thermal conductivity of nanofluids based on dimensionless groups. They assume that the effective thermal conductivity of nanofluids (k_{eff}) is a function of the thermal conductivity of the base fluid (k_f), the solid particle (k_p), the interfacial shell (k_i), the particle diameter (d_p),

the volume fraction of the particle (Φ), the interfacial shell thickness (*t*), the temperature of nanofluid (*T*), and the half of the base fluid boiling temperature (T_c). They present their equation as

$$\frac{k_{eff}}{k_f} = 1 + m\frac{\Phi^{\alpha}}{{d_p}^{\beta}}T^{\delta} + n\Phi \quad 1 - \frac{d_c}{d_p} \quad T \quad \text{for} \quad d_p \geq d_c \tag{2.11}$$

where, *m, α, β, n,* d_c and δ are the model parameters given in Table 2.1. The accuracy of this model was tested by experimental data. This model shows a good agreement with the experimental findings.

Table 2.1. Model parameters for Al2O3-water nanofluids, Abbaspoursani et al. (2011).

Parameter	Value for Al_2O_3-water system
m	10
A	0.350
B	2.6
n	0.0121
d_c	21
δ	1

Hamilton and Crosser (1962) developed an elaborate model for measuring the effective thermal conductivity of two component fluid mixture. The effective thermal conductivity is given as a function of the thermal conductivity of the pure material, the shape of the particles and the properties of the component mixture and is given as

$$k = k_o \frac{k + (n-1)K_o - (n-1)\Phi(k_o - k_p)}{k_p + (n-1)k_o + \Phi(k_o - k_p)} \tag{2.12}$$

where k is the thermal conductivity of nanofluid, k_o is the thermal conductivity of base fluid, k_p is the thermal conductivity of nanoparticle, Φ is the volume fraction, $n = 3/\Psi$ is the empirical shape factor as a function of the sphericity (Ψ) of the nanoparticle and is taken as 1 for alumina nanoparticle.

Jang and Choi (2004) gave a correlation for the effective thermal conductivity of nanofluid based on the Brownian motion of the nanoparticles, concentration of the nanoparticles, size of nanoparticles and the temperature of the nanofluid. They developed their theoretical model based on kinetics, Kapitza resistance and convection involving four modes of energy transport in nanofluids presented schematically in Figure 2.3.

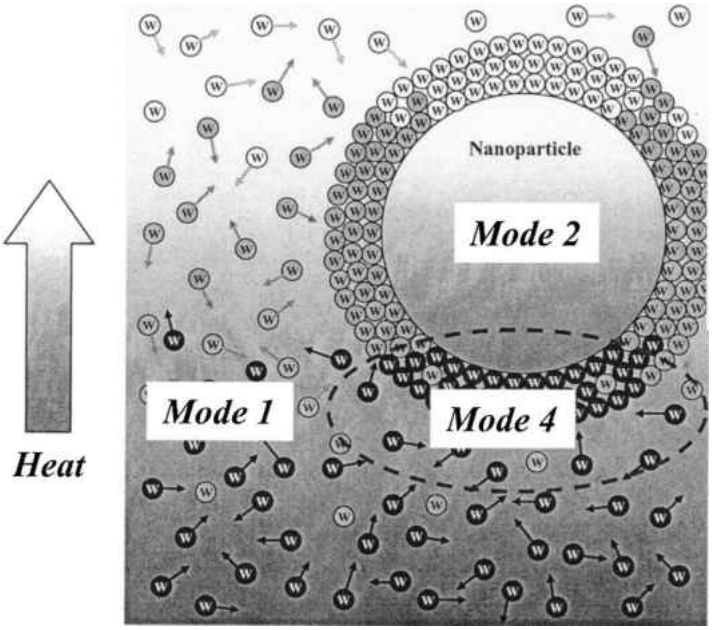

Figure 2.3. Modes of energy transport in nanofluids. The first mode is collision between base fluid molecules; the second mode is the thermal diffusion in nanoparticles suspended in fluids; the third one is collision between nanoparticles (not shown); and the fourth mode is the thermal interactions of dynamic or dancing nanoparticles with base fluid molecules, Jang and Choi (2004).

They present their equation as

$$k_{eff} = k_{BF}\ 1-\Phi\ + k_{nano}\Phi + 3C_1\frac{d_{BF}}{d_{nano}}K_{BF}Re_{d_{nano}}^2 Pr\Phi \tag{2.13}$$

where k_{eff} is the effective thermal conductivity, d_{nano} is the diameter of the nanoparticle, k_{nano} is the thermal conductivity of the particle, k_{bf} is the thermal conductivity of the base fluid, Φ is the volume fraction of nanoparticles, Pr is the Prandtl number, d_{BF} is the diameter of base fluid molecule, C_1 is a proportional constant, and Re_{dnano} is the Reynolds number defined by

$$Re_{d_{nano}} = \frac{C_{RM}d_{nano}}{\nu} \tag{2.14}$$

where C_{RM} and v are the random motion velocity of nanoparticles and kinematic viscosity of the base fluid. The random motion velocity (C_{RM}) is defined as

$$C_{RM} = \frac{D_o}{l_{BF}} \tag{2.15}$$

where l_{BF} = 0.17 nm is the mean free path for water, and the nanoparticle diffusion coefficient (D_o) is given by

$$D_o = \frac{k_b T}{3\pi\mu d_{nano}} \tag{2.16}$$

where $k_b = 1.3807 \times 10^{-23}$ J/K is the Boltzmann constant.

To validate their correlation, they compared their correlation with experimental data. Excellent agreement between model predictions and experimental results are shown.

Prasher et al. (2005) developed a correlation for estimating the thermal conductivity of nanofluids. They show that the increase in the thermal conductivity is primarily caused by convection due to the Brownian movement of the nanoparticle, translation Brownian motion and the existence of interparticle potential. They present their model as

$$\frac{k}{k_f} = \left(1 + ARe^m Pr^{0.003} \Phi\right)\left(\frac{1 + 2\alpha + 2\Phi(1-\alpha)}{1 + 2\alpha - \Phi(1-\alpha)}\right) \tag{2.17}$$

where k is the enhancement in thermal conductivity, k_f is the thermal conductivity of the base fluid, Φ is the particle volume fraction, Pr is the Prandtl number, A and m are constants and have the values of 40000 and 2.75, respectively, for alumina nanofluids, and α is given as

$$\alpha = \frac{2R_b k_m}{d} \tag{2.18}$$

where $R_b = 0.77 \times 10^{-8}$ $\mathrm{Km^2W^{-1}}$ is the interfacial resistance for water, d is the particle diameter, k_m is the effective thermal conductivity of the fluid caused by convection and is given as

$$k_m = k_f \left(1 + \frac{1}{4} RePr\right) \tag{2.19}$$

The Reynolds number (Re) is given as

$$Re = \frac{1}{\nu} \sqrt{\frac{18k_b T}{\pi \rho_N d_N}} \tag{2.20}$$

where ν is the kinematic viscosity of the liquid, ρ_N is the density of the particle, d_N is the diameter of the particle, T is the temperature, and $k_b = 1.3807 \times 10^{-23}$J/K is the Boltzmann constant.

2.2 Viscosity of Nanofluids

Hosseini et al. (2010) developed a model based on dimensionless group to describe the viscosity of nanofluids. Their model includes the effect of the viscosity of base fluid, particle volume fraction, particle size, temperature and thickness of the capping layer on nanoparticle. They present their model as

$$\frac{\eta_{nf}}{\eta_{bf}} = \exp\left(m + \alpha \frac{T}{T_o} + \beta \phi_h + \gamma \frac{d}{1+r}\right) \tag{2.21}$$

where η_{nf} is the viscosity of nanofluid, η_{bf} is the viscosity of base fluid, m is the shape factor that depends on the properties of the solid nanoparticles, the base fluid and their interactions, d is the diameter of nanoparticle, T_o is the reference temperature at 20°C, r = 1 nm is the thickness of capping layer, and α, β and γ are empirical constants calculated from a set of experimental data for alumina-water nanofluids using least square regression, their values are given in the Table 2.2.

Table 2.2 Empirical constants for Al2O3-water, Hosseini et al. (2010).

m	α	β	γ
0.72	−0.485	14.94	0.0105

Mintsa et al. (2007a) measured viscosity of Al2O3-water (particle diameter of 36 nm and 47 nm) and CuO-water (particle diameter of 29 nm) nanofluids using a piston type calibrated viscometer with a heating jacket. The measurement is based on the Couette flow inside a cylindrical measurement chamber. The piston is submerged in the sample and time for the piston to complete a cycle under an alternating magnetic force is calibrated in terms of fluid viscosity with an accuracy of ±1% for the range of 0–20 cP. They observed that the viscosity increases with increasing particle concentration. For 47 nm alumina-water nanofluid, the relative viscosity increased from 1.12 to 1.6 to 3.0, and then to approximately 5.3 for particle concentration increasing from 1% to 4% to 9%, and finally to 12%. For 36 nm alumina-nanofluid similar tendency was observed. They also found out that for relatively same concentration of nanoparticles, the viscosity of

nanofluid with 36 nm particle size are lower than for nanofluid with 47 nm particle size. This difference was found to me more prominent for volume fraction higher than 5%. With temperature they observed that the gradient of viscosity vs. temperature is maximum around 22 to 40°C. They also found out that the gradient is much steeper for higher particle fraction. They also developed a correlation for the viscosity of nanofluid for 4% particle concentration as a function of the viscosity of base fluid and temperature and is give n as

$$\mu_{nf} = \mu_{bf}\ 2.1275 - 0.0215T + 0.0002T^2 \tag{2.22}$$

where μ_{nf} is the viscosity of nanofluid, μ_{bf} is the viscosity of base fluid, and T is the temperature in °C.

They also observed that after certain temperature, the viscosity curve is almost flat with an increase in temperature. They also mentioned a critical temperature above which if a nanofluid is cooled, a hysteresis effect on viscosity is observed (see Figure 2.4).

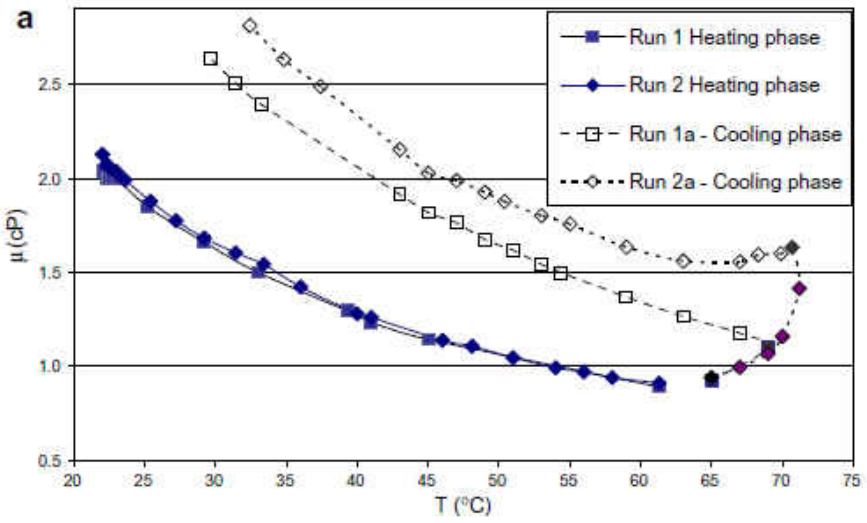

Figure 2.4. Hysteresis observed on viscosity for alumina (47 nm, 7%)- water nanofluid, Mintsa et al. (2007).

Lee et al. (2008) measured the effective viscosities and thermal conductivity of Al_2O_3-water nanofluid for low volume concentration of nanoparticles ranging from 0.01% to 0.3%. They used ultrasonic vibration for 5 hours to finely disperse the particle into the solution. They used the oscillation type viscometer to measure the viscosity of nanofluid for a temperature range of 21 to 39°C. They tested their experimental setup with DI water with a measurement uncertainty of ±1.8%. A maximum increment in viscosity by 2.9% at concentration of 0.3% compared to the base fluid is reported. They found a nonlinear relationship between the viscosity and temperature (see Figure 2.5) even at low volume concentration (0.01%−0.3%). This was found to contradict the Einstein model that serves to be valid for particle concentration less than 2 % vol. which predicts a linear relationship between the viscosity and temperature.

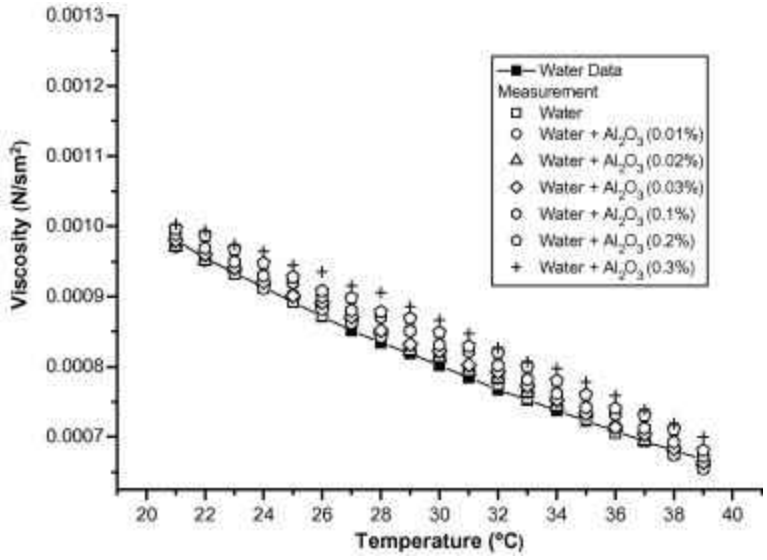

Figure 2.5. Nanofluid Viscosity vs. Temperature for low volume fraction of nanoparticles, Lee et al. (2008).

Dey and Kole (2010) measured the viscosity of Al_2O_3 nanofluid based on car engine coolant. They measured the viscosity by a Brookfield programmable viscometer connected to a temperature bath to vary the fluid temperature between 10 and 80°C. They found out that addition of small quantities of Al_2O_3 particles does not change the Newtonian behavior of the base fluid (engine oil).The curve between the viscosity and shear rate are all horizontal straight lines. However, for a volume fraction greater than 0.004, the shear stress varies non-linearly with the shear strain rate indicating a non-Newtonian shear thinning behavior. With increasing temperature they found out that the viscosity of the nanofluid decreases exponentially. Also, the viscosity of the nanofluid is found to be increasing with increasing nanoparticle concentration.

Zhou et al. (2010) experimentally investigated the viscosity of alumina nanofluids. The nanofluids they used are suspension of alumina nanospheres or nanorods in PAO

lubricant mixed with certain surfactant. The nanospheres they used had a nominal diameter of 10 nm and that of the nanorod is 800 nm. They prepared four samples of nanofluid containing 1% alumina nanospheres, 3% alumina nanospheres, 1% alumina nanorods and 3% alumina nanorods. They used a stress-controlled rheometer in a cone plate configuration to measure the rheological behavior of the base fluid and the nanofluid. Their operating temperature was set at 25°C and the shear rate varied between 500 to 0.01 s^{-1}. They used an Ubbelohde capillary viscometer to measure the viscosity at different temperatures by placing the viscometer in a temperature controlled bath.

They found out that for the same volume fraction, the viscosity of nanofluids containing nanorods is higher than that of nanofluid containing nanospheres due to the higher aspect ratio of rods than that of spheres. For 3% volume fraction nanorods nanofluid, they found out that it showed a non-Newtonian behavior for shear rate higher than 1 s^{-1} and shows a shear-thinning behavior. The base fluid showed a perfect Newtonian behavior in the shear rate range under test. For the nanospheres nanofluid with 1% vol. concentration, showed a Newtonian behavior for shear rates between 0.1 s^{-1} and 20 s^{-1}. For higher shear rate a small shear thinning behavior is noticed. For the nanospheres nanofluid with 3% volume concentration, a shear thinning trend was seen for shear rates above 20 s^{-1}.

Zhou et al. (2010) has emphasized mainly on the relative viscosity dependence upon temperature. Relative viscosity is the ratio of viscosity of a solution to the viscosity of a solvent. They found out that the relative viscosity is independent of temperature for relatively low volume concentration of nanoparticles except for the nanofluid with3% alumina nanorods (see Figure 2.6). This trend was even investigated on water based

titanium dioxide and water based copper oxide nanofluids. For low volume fraction, the relative viscosity was found independent to temperature. They reported this trend by the fact that the rheological behavior of nanofluids is mainly dominated by base fluid.

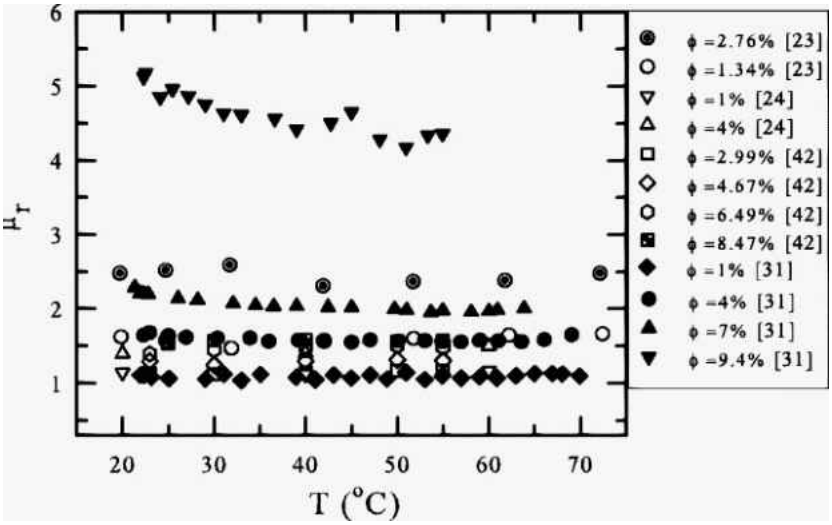

Figure 2.6. The relative viscosity (μ_r) as a function of temperature in water based alumina nanofluids. The relative viscosity curve stays flat with temperature except for higher concentration of 9.4%, Zhou et al. (2010).

2.3 Heat Transfer and Pressure Drop of Nanofluids

Wongwises and Duangthongsuk (2009) measured the heat transfer and pressure drop characteristics of 0.2 % by volume of TiO_2/water nanofluid. The TiO_2 nanoparticles had a mean diameter of 21 nm. They used surface activators and ultrasonication to achieve better suspension characteristics of the nanofluids. The experimental setup (see Figure 2.7) they used consist of a test section, two receiver tanks, a magnetic gear pump, a hot water pump, a cooler tank, a hot water tank and a collection tank. Their test section was a

1.5 m long counter flow horizontal double-tube heat exchanger with nanofluid flowing inside the inner tube with inner diameter of 8.13 mm and outer diameter of diameter 9.53 mm. Hot water flowed through the annular PVC tube with inside diameter of 27.8 mm and outside diameter of 33.9 mm. Differential pressure transmitter and T-type thermocouples were mounted at both ends of the test section to measure the pressure drop and bulk temperatures. Thermocouples were mounted at different locations along the test section on the inner tube surface for measuring the heat transfer.

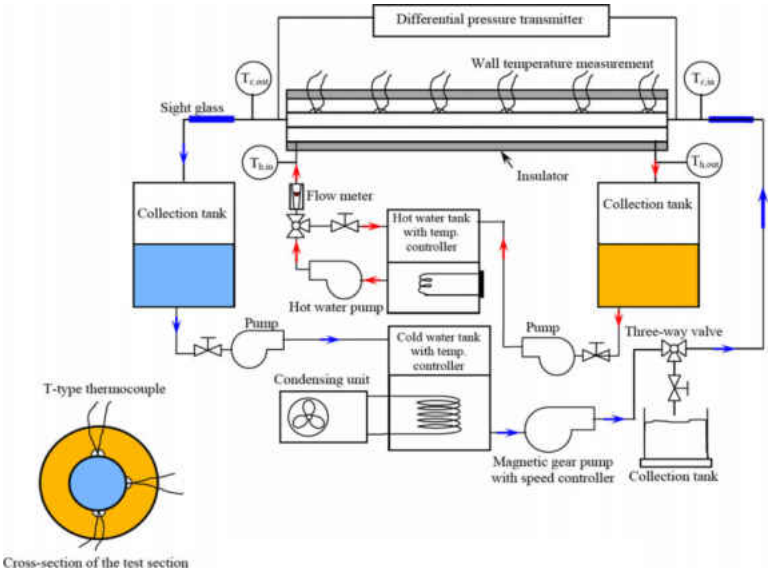

Figure 2.7. Schematic of Experimental Setup to measure heat transfer and pressure drop of nanofluid, Wongwises et al. (2009).

Wongwises et al. (2009) found that the heat transfer coefficient of nanofluid increases with an increasing Reynolds number. They show that the 0.2% vol. TiO_2/water nanofluid has a higher heat transfer coefficient than that of water by around approximately 6–11%.

For 0.2% vol. TiO_2/water nanofluid, they found out that the friction factor does not change compared to that of water. This is attributed to the fact that the small addition of nanoparticles in the liquid does not change the flow behavior in the fluid and can be treated as a single phase flow.

Chandrasekar et al. (2010) investigated the friction factor and heat transfer of Al_2O_3/water nanofluid flowing through a uniformly heated horizontal tube. The 43 nm Al_2O_3 nanoparticles were prepared from an aqueous solution of aluminum chloride by microwave assisted chemical precipitation method. Nanofluid with specified volume concentration was prepared by ultra-sonication of the solution to get a stable Al_2O_3/water nanofluid.

For the heat transfer measurement, Chandrasekar et al. (2010) built a test loop consisting of a reservoir, a peristaltic pump, cooling section, test section and a collecting station. A straight copper tube of 1200 mm in length and 4.85 mm in diameter was used as the test section. RTDs are placed along the test section for heat transfer measurements. Pressure ports are connected at the inlet and outlet to the test section to measure the pressure drop.

For 0.1% volume fraction, they found out that the Nusselt number increased by 12.24% at Re = 2275 compared to distilled water. This increase in Nusselt number is attributed to mixing effects near the wall, Brownian motion of the particles, increased thermal conductivity, particle migration and rearrangement, reduction in boundary layer thickness and delay in boundary layer development. For 0.1% volume concentration, for laminar flow they found no significant increase in the friction factor compared to distilled water.

The reason for this may be attributed to the fact that the nanofluid has a low volume concentration (around 0.1%) of nanoparticles.

Hu et al. (2009) measured the convective heat transfer and pressure drop for alumina water and zirconia-water nanofluid in a vertical heated tube. Their experimental setup consisted of a flow loop made up of stainless steel tubing. The loop consisted of a gear pump to pump the fluid, a turbine meter for volumetric flow measurement; control valve, pressure transducer, and a heat exchanger to cool the fluid coming out from the test section (see Figure 2.8). The test section was kept vertical made up of stainless tube with an inner diameter of 4.5 mm and outer diameter of 6.4 mm and a length of 1.01 m. T-type thermocouples were cemented along the length of the test section and two T-type thermocouples were inserted into the flow channel before and after the test section for bulk fluid temperature measurement. The test section was heated with a DC power supply.

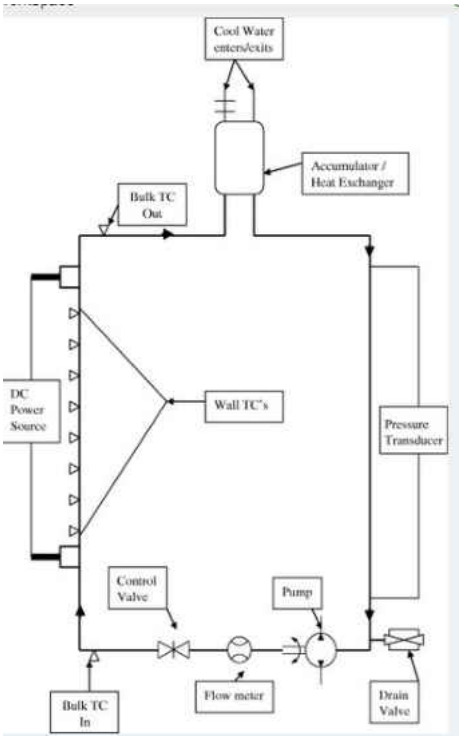

Figure 2.8. Schematic of Experimental Setup for Convective Heat Transfer and Viscous Pressure Drop Measurement, Hu et al. (2006).

They used alumina/water and zirconia/water nanofluids with 6% and 3% volume concentration of nanoparticles with particle size of 50 nm. They measured the thermal conductivity of these nanofluids with transient hot wire method with measurement accuracy of ±2%. The viscosity of the nanofluid was measured with a capillary viscometer submerged in a temperature controlled bath with measurement accuracy of 0.5%. They found out that the thermal conductivity dependence on temperature of the nanofluid is same that of the base fluid or water. They also proposed correlations for thermal conductivity and viscosity for alumina-water nanofluids and are given as

$$k\ \Phi, T\ = k_f\ T\ (1 + 4.5503\Phi) \tag{2.23}$$

$$\mu\ \Phi,T\ = \mu_f\ T\ \exp\ \frac{4.91\Phi}{0.2092-\Phi} \tag{2.24}$$

For heat transfer, Hu et al. (2006) used the following relation for their Nusselt number for laminar range

$$Nu = 1.302\ \ \frac{x^+}{2}\ ^{\frac{1}{3}} - 0.5,\ \ x^+ \leq 0.003 \tag{2.25}$$

$$Nu = 4.364 + 0.263\ \ \frac{x^+}{2}\ ^{-0.506}\ e^{-41\ \frac{x^+}{2}}\ ,\ \ x^+ > 0.003 \tag{2.26}$$

where

$$x^+ = \frac{2\ x\ \ D}{RePr} \tag{2.27}$$

For fully developed laminar flow, Hu et al. (2006) found that the heat transfer enhancement for 6% vol. fraction alumina nanofluid and 1.32% vol. fraction zirconia nanofluids are 27% and 3% respectively. For 6% volume fraction of alumina nanofluids, they found out that the viscosity is around 7.2 times higher than that of water, resulting similar increase in pressure loss.

Selvakumar et al. (2012) carried out experiments on the convective heat transfer and frictional factor characteristics of CuO/water nanofluid under laminar flow and constant heat flux. The CuO particles were prepared by sol-gel method with average particle size of 15.7 nm. The sol-gel method involves a reaction of copper chloride and sodium hydroxide. The particles formed from the reaction is filtered, washed, dried, scraped off and then ground to obtain the nanoparticles. They prepared nanofluid with concentration

of 0.1%, 0.2% and 0.3% by dispersing required amount of nanoparticles in water by using ultrasonic agitation.

The thermal conductivity of the CuO/water nanofluid is measured with a KD2 thermal property analyzer from Decagon Devices. The thermal conductivities of 0.1%, 0.2% and 0.3% volume concentrations of CuO/water nanofluids was reported to be 0.671, 0.682 and 0.727 W/m.K, respectively. The viscosity was measured with a Brookfield DV-I+Pro viscometer. The viscosities of 0.1%, 0.2%, and 0.3% volume concentrations of CuO/water nanofluids were reported to be 0.83, 0.86, and 0.88 cP, respectively, at 27°C.

Their experimental loop setup consists of a test section pipe of 4.85 mm in diameter and 800 mm in length, heat exchanger, flow measurement device and a reservoir. Pressure transducer ports are connected to the inlet and outlet of the test section and thermocouples are attached at different locations along the test section for measuring the friction factor and heat transfer. For a Reynolds number of 2200, the experimental Nusselt for 0.1, 0.2 and 0.3% volume concentrations of CuO nanoparticles were reported to be 6, 9.9 and 12.6 %, respectively, higher than that obtained with distilled water. The friction factor for for 0.1, 0.2 and 0.3% volume concentrations of CuO nanoparticles were reported to be 8, 13 and 20.7 %, respectively, higher compared to that of distilled water.

Yu et al. (2012) investigated the thermophysical properties and convective heat transfer phenomenon of Al_2O_3-polyalphaolefin (PAO) nanofluids containing both spherical (NF1) and rod (NF2) like particles. The nanofluids were prepared by dispersing alumina nanoparticles in PAO under ultrasonication. Special dispersants were added to the PAO to lessen the aggregation of the nanoparticles and stabilize the nanofluid. The diameter of

the spherical nanoparticles was found to be 60 nm with the aid of a dynamic light scattering (DLS) instrument. The diameter and length of the rod like nanoparticles was found to be 7 nm and 85 nm, respectively.

The viscosity was measured with a capillary viscometer under static condition at a temperature of 25°C for particle volume fractions of 0.33, 0.49, 0.65 and 1.3% volume. It was seen that the viscosity of the nanofluid clearly increases with the nanoparticle loading. For the nanofluids containing rod like particles, the viscosity was found to be higher than that of nanofluids containing spherical nanoparticles for the same volume concentration of nanoparticles. Yu et al. (2012) also gave a correlation for estimating the relative viscosity of nanofluids containing spherical nanoparticles which is valid for volume concentration less than 1.3%.

$$\mu_r = 1 + 13.67\Phi + 185.42\Phi^2 \tag{2.28}$$

The thermal conductivity is measured by a thermal property analyzer (KD2 Pro from Decagon Devices) with an uncertainty of 5%. For spherical nanoparticles, they developed a correlation using the least squares method and it is given as a function of the volume concentration of nanoparticles.

$$\frac{k}{k_f} = 1 + 7.6661\Phi \tag{2.29}$$

The experimental setup of convective heat transfer and pressure drop measurements established by Yu et al. (2012) consists of a gear pump, turbine flow meter, heat exchanger, pressure transducer and thermocouples (see Figure 2.9). All the data were collected by a data acquisition unit. The test section is a circular tube made up of stainless

steel with 1.09 mm inner diameter, 0.25 mm wall thickness and 306 mm length. The test section was heated using a DC power supply. Pressure transducers and thermocouples were placed in the inlet and outlet of the test section for measuring the pressure drop and bulk fluid inlet and outlet temperature. Thermocouples were also placed along the test section for measuring the heat transfer. The experimental setup is shown schematically below

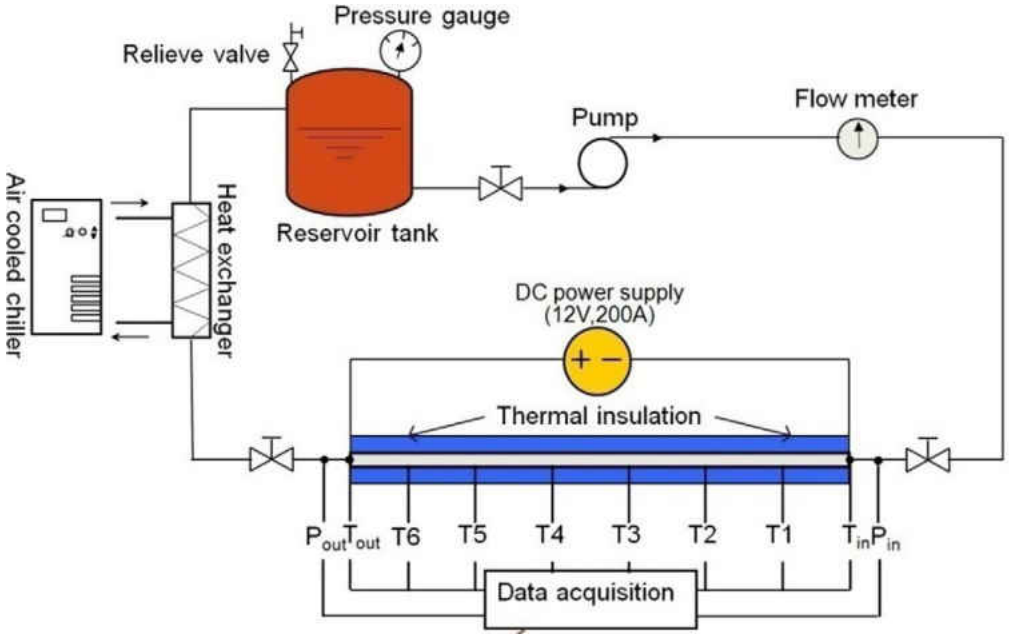

Figure 2.9. Schematic of experimental setup for measuring pressure drop and heat transfer, Yu et al. (2012).

The pressure drop experiment was conducted for a maximum Reynolds number of 460 which was limited due to the high viscosity of PAO as well as the nanofluid. They conducted the experiment for 0.65% vol. and 1.3% vol. of spherical and rod shaped

particles, respectively. They found out that the nanofluids incur higher pressure drop than the base fluid and the difference get higher with increasing volume concentration of nanoparticles. Also the pressure drop of the nanofluid containing non-spherical nanoparticles was found to be always greater than the spherical particles for the same volume fraction. For medium to high Reynolds number (200−400), the friction factor for the nanofluids containing non spherical particles was seen to drop below than that given by Hagen-Poiseuille equation ($fRe = 64$). This is attributed to the strong alignment of the nanorods under the shear stress causing the effective viscosity of nanofluids to decrease in a manner similar to shear thinning.

The convective heat transfer experiments were conducted for 0.65% vol. and 1.3% vol. of spherical and non-spherical nanoparticles, respectively. The local heat transfer coefficients were measured at 5 axial locations for Reynolds numbers of 350 and 490. They found out that the heat transfer of nanofluids is enhanced than that of the base fluid and the increment increases proportionally to Reynolds number and the loading of nanoparticles. The local Nusselt number are plotted against a dimensionless parameter given by

$$x^* = \frac{x}{D.Re.Pr} \tag{2.30}$$

They found out that for spherical nanoparticles, the prediction for the local Nusselt number given by Shah-London equation closely matched their experimental data. The Shah-London equation (Shah et al., 1978) is given as

$$Nu_x = \begin{cases} 1.302/(x\hat{}*)\hat{}(1/3) - 1 & for\ x\hat{}* \leq 0.00005 \\ 1.302/\ x^{*\ \frac{1}{3}} - 0.5 & for\ 0.0005 \leq x^* \leq 0.0015 \\ 4.364 + 8.68\ 1000x^{*\ -0.506} e^{-41x^*} & for\ x^* \geq 0.0015 \end{cases} \quad (2.31)$$

However, for non-spherical particles, the local Nusselt number vs. the dimensionless parameter initially follows the Shah-London equation and then drops rapidly with a slope much steeper than the theoretical curve.

CHAPTER III

EXPERIMENTAL SETUP AND METHODOLOGY

A proper and sound experimental setup is necessary to minimize the measurement uncertainties and accurately obtain the data. There has been different speculation by different authors regarding the thermophysical, fluid flow and heat transfer parameters of nanofluids. These differences may be caused by the method of measuring and obtaining the data. Therefore a sound technique of measuring different parameters of the fluid is critical. This chapter discusses on the detailed experimental setup of obtaining the thermal conductivity, viscosity, pressure drop, and heat transfer measurements. The experimental setup is divided into 1) temperature control system, 2) viscosity measurements, 3) thermal conductivity measurement, 4) experimental loop, 5) instrument calibration, 6) experimental procedure and 7) experimental uncertainties. The experimental setup is fairly simple to operate and can be used to measure different types of fluids other than nanofluids.

3.1 Temperature Control System

To measure the physical and thermal properties of fluid at various operating temperatures, a proper system to maintain a specified temperature is required. This is achieved through a constant temperature bath form Brookfield Engineering (model TC-550MX), see Figure 3.1. This temperature bath can be operated within the range of −20°C to 135°C with a temperature stability of 0.07°C. The temperature bath has a reservoir that can hold 7.0 liters of fluid. An opening at the top allows measurement of different properties by submerging the sample into the bath or the fluid can be circulated through a tube to other instruments requiring a temperature controlled environment through constant speed pump.

Figure 3.1. TC 550MX constant temperature bath.

3.2 Viscosity Measurement

The viscosity is measured with a Brookfield viscometer (model DV II+Pro Extra) with an accuracy of ±0.1% of the full scale reading. It measures the viscosity and shear stress of the fluid sample at a given shear rate. The shear rate can be varied by varying the rotational speed of the spindle from 0.01 to 200 RPM, with 0.01 RPM increments from 0.01 to 0.99 RPM, and 0.1 RPM increments from 1 to 200 RPM. The spindle is immersed in the sample fluid and rotated at a specified rotational speed. The viscous drag force against the spindle is measured by a spring deflection. The spring deflection is measured in terms of torque by a rotary transducer. While taking measurements, the measured torque should be in between 10–90% of the full scale torque of the calibrated spring to obtain a good reading. The percentage of the torque will be displayed in the screen. For the DV II+Pro Extra model, the full scale torque is 0.0673 milliN.m. The measurement range of the instrument is determined by the rotational speed, size and shape of the spindle (various spindle come along for measuring various viscosity), and the container in which the spindle is rotating. The operating temperature is obtained with the help of a temperature bath. A 600 ml beaker filled with the sample can be placed into the reservoir of the water bath where the spindle can be immersed and readings can be taken. With the help of an Enhanced UL adapter with EZ-lock spindle coupling system, the fluid in the temperature bath can be circulated through a water jacketing system built around the sample chamber to take readings at a specified temperature (see Figure 3.2).

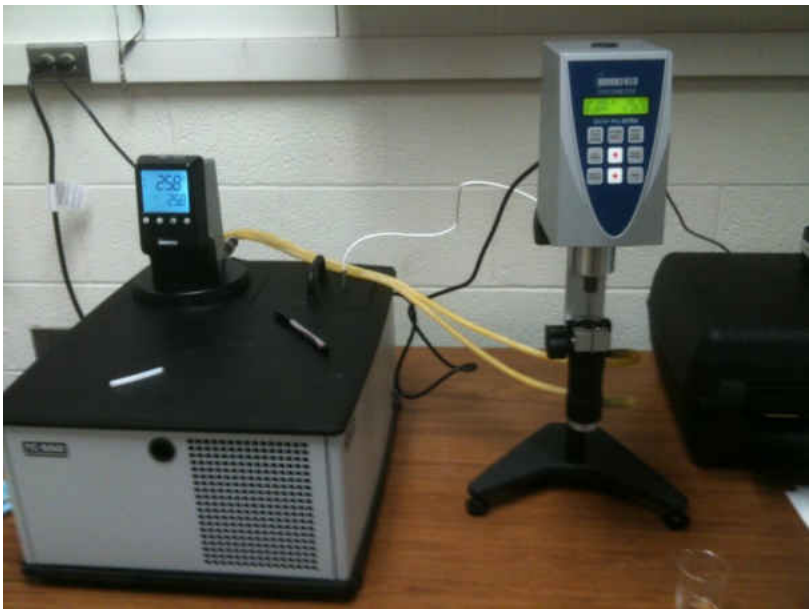

Figure 3.2. DV II+Pro Extra Brookfield viscometer connected to the TC-550MX temperature bath.

The viscometer is attached to a PC with a serial USB cable and all the readings are taken via Rheocalc V3.3 Build 49-1 software. All the communication with the viscometer is done via this software. This software is capable of programming the viscometer to operate it at different shear rate. All the readings from this software can be exported to MS Excel where further analysis of the data can be done.

Before taking any measurements, the use of the viscometer has to be validated for its accuracy. This is done with the help of a calibration fluid which comes along with the viscometer. The calibration fluid has a viscosity of 493 cP at 25°C. Readings are taken at this temperature at different rotational speed. The values are then placed into a standard template which determines whether the viscometer has passed the calibration test or not. For other samples, the following are the procedures that must be taken for accurate readings:

1. Ensure that the viscometer is level. This can be done by a leveling meter at the top of the viscometer and leveling screw at the bottom.
2. Turn on the viscometer and select external mode or standalone mode. The external mode allows the viscometer to be controlled with the help of the Rheocalc software, whereas in the standalone mode, the viscometer must be controlled with the touch dials located in the viscometer itself.
3. Ensure that the spindle is not attached to the viscometer. Then auto zero the torque in the spring. Make sure that at the end of the auto zeroing process, the percentage torque reads 0% or ±0.1 to ±0.2%.
4. Attach the desired spindle depending upon the readings to be taken. If using a beaker in the temperature bath, make sure that the volume of sample taken can fully immerse the spindle. If using the Enhanced UL adapter, 20 ml of the sample will be enough.
5. Set the temperature bath to the desired temperature with the RTD probe inserted into the reservoir. When the temperature bath reaches the specified temperature, wait 3 min before taking any readings. This ensures the sample temperature is in equilibrium with the bath temperature.
6. After taking the reading, increase the temperature of the bath by 5°C and follow the same procedure for taking the readings till the maximum desired temperature is reached.
7. Follow the same procedure by decreasing the bath temperature for the highest to the lowest.

3.3 Thermal Conductivity Measurements

The thermal conductivity is measured with the help of a thermal roperties analyzer from Decagon Devices (model KD2 Pro) with a measurement accuracy of ±5% over the range of 0.2 to 2 W/(m.K). It is also capable of measuring thermal resistivity, volumetric specific heat capacity and thermal diffusivity. All the data recorded by the instrument can be extracted to a PC with the help of a serial cable and the KD2 Pro utility software. The data can be exported to MS Excel where it can be analyzed.

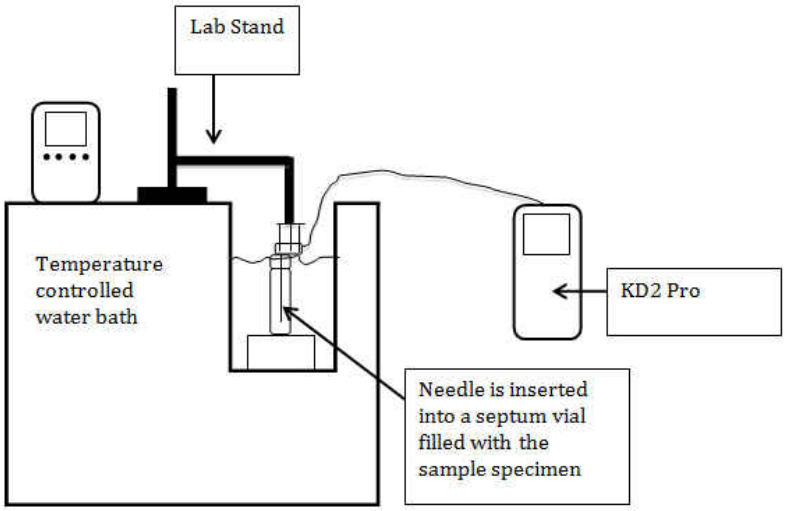

Figure 3.3. Schematic of thermal conductivity measurement using the KD2 Pro thermal property analyzer.

It has three sensors which is to be selected depending upon the type of sample (liquid or solid). This instrument operates on the principle of transient heat conduction. A small

amount of current is passed through the sensor needle immersed in the sample and the temperature of the sensor needle is monitored over time to get the thermal conductivity. Mathematically, this process of obtaining the thermal conductivity reading can be described by the following equation

$$k = \frac{q}{4\pi}\frac{d\ln\ t}{dT} \tag{3.1}$$

where k is the thermal conductivity in [$Wm^{-1}K^{-1}$], q is the applied heat per unit length in [W/m], t is the heating time in [s], and dT is the rise in temperature over the heating time in [K].

The amount of current input kept minimal so that the heat input is small which minimizes the sample movement from the sensor and free convection. The KD2 Pro is capable of resolving 0.001°C temperature so the small amount of heat added does not significantly affect the result.

The KD2 pro is well capable of measuring the thermal properties of liquids. However, extra care should be taken to minimize errors. Error may result from convection or bulk movement of the measuring samples. The sample should be in thermal equilibrium so that no thermal gradient exists in the sample to minimize free convection. To minimize error from forced convection, the sensor and the sample must be absolutely still. Readings must be done during the night time or the weekends so that we do not encounter any vibration from the HVAC. It is also a good practice to shut down other equipment in the lab before taking the thermal conductivity reading as they can be a source of vibration

which can induce forced convection. The sensor needle should be placed into the sample in a vertical position to get accurate readings.

Before taking any readings, the KD2 Pro and the experimental method should be checked for its accuracy. This can be done with the help of a provided thermal conductivity standard liquid whose thermal conductivity is 0.285 W/(m.K) at 20°C.

The following is a procedure which is followed to take a thermal conductivity reading:

1. Take 40 ml of the liquid sample in a septum vial. Ensure that it is completely filled. Insert the sensor needle into the vial. It must be noted that the sensor needle is not touching the walls of the vial and it almost lines up with the axis of the vial.
2. Place the vial along with the needle into the temperature bath
3. To have the sensor needle in a perfect vertical position, attach it to a lab stand.
4. Set the temperature bath at a specified temperature at which the reading is to be taken. Once the bath temperature indicator indicates that it has reached the specified temperature, keep running the bath at that temperature for 15 minutes to ensure no thermal gradients in the sample.
5. After that, turn off the temperature bath. Allow 1 min for everything to come to a still before taking a reading so that no vibration exists.
6. Take a reading; while taking the reading it should be noted that there are no disturbances or vibrations around.

3.4 Experimental Loop

This is a closed loop system consisting of 1) reservoir, 2) gear pump, 3) mass flow meter, 4) pressure transducers, 5) data acquisition, 6) thermocouples, 7) DC power supply unit and 8) heat exchangers which are all connected by a pipe network (see Figure 3.4). The piping network consists of a ¼ inch stainless steel tubing and flexible PVC tubing. The flexible tubing is incorporated in this experimental loop to accommodate different lengths of the test section. This flow loop can facilitate experiments for fluids flowing through tubes ranging from 6 mm to 500 μm I.D.

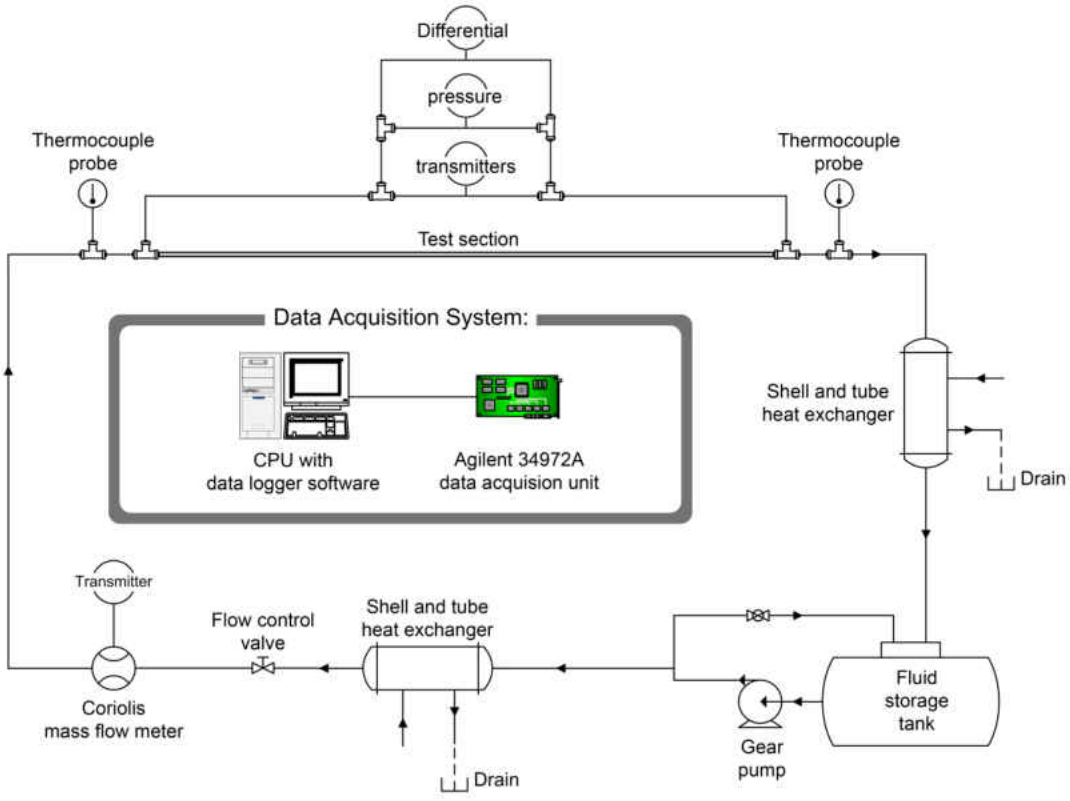

Figure 3.4. Schematic of experimental loop for conducting pressure drop and heat transfer measurements.

The working fluid is contained in a reservoir which is then pumped to the flow loop by a gear pump. A counter flow heat exchanger just after the gear pump removes the heat added by the pump on the fluid. A metering valve allows adjusting the mass flow rate in the loop. A Coriolis mass flow meter measures the mass flow rate. Pressure transducers are connected at the inlet and the outlet of the test section to measure the pressure drop. A DC power supply heats up the test section. Thermocouples are cemented along the test section for heat transfer analysis. A second heat exchanger right after the test section removes any heat gained by the fluid when passing through the heated test section. All the pressure transducer, DC power supply and the mass flow meter are connected to the data acquisition system which is used to gather and analyze data. The fluid after passing through the test section goes back to the reservoir.

3.4.1 Reservoir

Figure 3.5 shows the reservoir, which is a PVC made and in cylindrical shape with diameter of 0.25 m, length 0.3048 m and a capacity of 15 liters. The reservoir is kept 1 m above the gear pump so that the gear pump will have adequate pressure avoiding it to run dry. At the bottom of the reservoir a piping connects to the gear pump while at the top a bypass line and the line from the loop are connected.

Figure 3.5. Flow loop reservoir.

3.4.2 Gear Pump

The gear pump used for the experiment is a Liquiflow sealed gear pump (model 35 F), see Figure 3.6. It is rated for a maximum flow of 12.8 LPM and maximum ΔP of 6.9 bar. This pump is capable of operating at variable speed with maximum rated speed as 1750 RPM. The suction side of the pump is connected to the reservoir whereas the discharge side is connected to a T-connector which divides the flow through the closed loop and a bypass.

Figure 3.6. Liquiflow sealed gear pump.

3.4.3 Mass Flow Meter

The mass flow meter is a Micro Motion mass flow sensor (model CMFS010M) connected to a 1700R model transmitter (see Figure 3.7). It has an accuracy of ±0.05% of the flow rate. The maximum flow rate it can measure is 108 kg/hr. The mass flow meter operates on the principle of the Coriolis effect. The fluid is passed through a U-shaped tube in the mass flow sensor which is initially vibrating at a given frequency. When the fluid flows through the U- shaped tube due to its angular velocity and inertia causes the tube to twist. The twisting of the two legs of the U-shaped tube is sensed by an electromagnetic sensor in terms of a phase change. This phase change is measured in terms of mass flow.

Figure 3. 7 Micro Motion mass flow sensor connected to a 1700R transmitter.

The flow going through the mass flow meter is controlled by a metering or needle valve. The transmitter gives a DC current signal which is calibrated linearly in terms of flow rate. The transmitter also allows for the adjusting of the flow range through the display and switches located in the transmitter itself.

3.4.4 Pressure Transducers

There are three Rosemount pressure transmitters (model 3051) with accuracy of +0.65% of span connected to the inlet and outlet of the test section (see Figure 3.8). The three pressure transducers correspond to different pressure ranges. The lowest one can measure a pressure drop from 0 to 9 psi, the intermediate one can measure pressure drop from 0 to 36 psi and the largest one can measure pressure drop from 0 to 300 psi. All of them are connected in parallel so that each of them reads the same pressure drop for a given flow

rate. The main purpose of having the three pressure transmitter connected in parallel is that for a given pressure drop more accurate reading can be obtained. The pressure transmitter outputs DC current which is calibrated linearly in terms of pressure drop. If a pressure drop reading is above the maximum for a given transducer, the data acquisition unit is programmed to produce an alarm after which a valve on the pressure transmitter itself allows for the isolation of the particular transmitter.

Figure 3.8. Three Rosemount pressure transmitters (model 3051) connected in parallel.

3.4.5 Data Acquisition Unit

The data acquisition instrument used for the experiment is an Agilent data acquisition unit (model 34972A) with a 20 channel multiplexer (see Figure 3.9). All the thermocouples, mass flow meter, pressure transducer are attached to the channels of multiplexer. The data acquisition unit can sense the temperature based on the type of thermocouple. All the outputs of the pressure transducers and the mass flow meter are in

DC current which can be sensed and programmed linearly to give the output readings in psi and gm/sec, respectively.

The data acquisition unit is connected to the PC via a USB cable. Agilent Benchlink Data Logger 3 is used to program the channels, set the reading time and capture data. A read time of 0.1sec is used for all the experiments conducted.

Figure 3.9. Agilent data acquisition unit (model 34972A).

3.4.6 Thermocouples

There are two different thermocouples used for the experiment. The thermocouples used for the bulk fluid inlet and outlet temperatures in respect to the test section are thermocouples from Omega (model no. TMQSS-020U-6). It is a T-type thermocouple with 0.020 inches sheath diameter and 6 inches length. The tip of the thermocouple is inserted into the middle of the flow path of the fluid with the help of a Tee and a reducing compression fitting from Omega (part no. SSLK-116-18, 1/16*1/8). The thermocouple is

then attached to the data acquisition unit where the bulk temperature are recorded and analyzed.

Another type of thermocouples is made up from a 36 AWG thermocouple wire from Omega (model TT-T-36-SLE-1000). The two tips of the thermocouples were welded to form a thermocouple tip with the help of a thermocouple welder. Special care is taken so that the tip is small as possible. The tips are then cemented along the test section (see Figure 3.10) with the help of a high temperature and thermally conductive epoxy from Omega (part no. 08-101-16). This epoxy is highly thermally conductive but acts as an insulator for DC current. This protects the thermocouple and enables accurate temperature readings.

Figure 3.10. Thermocouple wire tip cemented to the test section outer wall with the help of Omega bond cement.

3.4.7 DC Power Supply

The DC power supply used in the experiment is the N5761A DC power supply from Agilent Technologies (see Figure 3.11). It has a rated output of 6 V / 180 A, 1080W. It has a measurement accuracy of ±300mA for current and ±6mV for voltage. The output from the DC power supply is connected to the test section through a copper strip soldered to the test section. The DC power supply has a remote load sense circuit which is connected to the same copper strips so that the DC power supply can compensate for the voltage drop in the wires between the test section and the DC power supply itself.

Figure 3.11. N5761A Agilent DC power supply unit.

3.4.7 Test Section

Three stainless steel 304 tubing from Small Parts are used for the experiment. The first one is a stainless steel 304 hypodermic tubing of 6 gauge, 0.203 inches in OD, 0.175 inches in ID and 36 inches in length. The second one is a stainless steel 304 hypodermic tubing of 10 gauge, 0.134 inches in OD, 0.118 inches in ID and 36 inches in length. The third tubing is the same as the second one except its length is 22 inches. They are connected to the test loop with the help of polyimides ferrules made up of graphite which are supplied by Small Parts. The polyimide ferrules acts as a reducing fitting and acts as a sealing between the experimental loop and the test section. The thermocouple wires are connected to the test sections (see Figures 3.12−3.14) by the procedure explained in section 3.4.6. Also the DC power supply is connected to the test section with the help of copper strips.

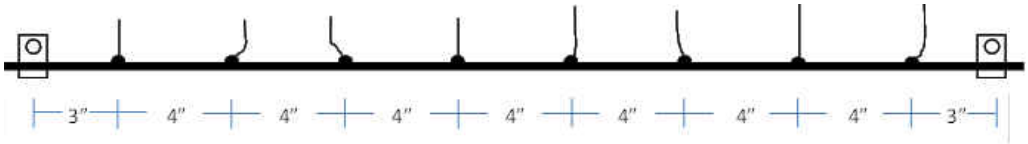

Figure 3.12.Stainless steel 304 hypodermic tubing of 6 Gauge, 0.203 inches OD, 0.175 inches ID and 36 inches length. Thermocouples tip are cemented along the test section with two copper strips at the end for supplying DC power.

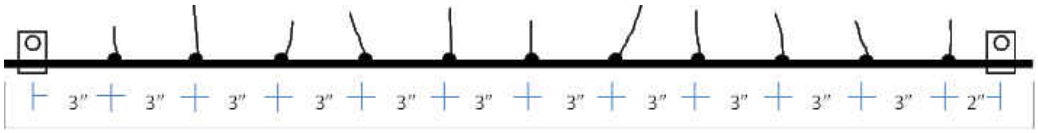

Figure 3.13. Stainless steel 304 hypodermic tubing of 10 Gauge, 0.134 inches OD, 0.118 inches ID and 36 inches length. Thermocouples tip are cemented along the test section with two copper strips at the end for supplying DC power.

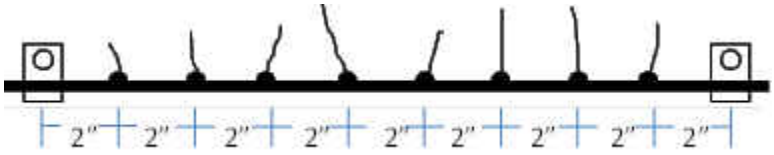

Figure 3.14. Stainless steel 304 hypodermic tubing of 10 Gauge, 0.134 inches OD, 0.118 inches ID and 18 inches length. Thermocouples tip are cemented along the test section with two copper strips at the end for supplying DC power.

3.4.8 Heat Exchangers

Two counter flow heat exchangers are fitted coaxially to the ¼ inch tubing in the experimental loop. One heat exchanger is placed just after the gear pump to eliminate the heat added from the pump and maintain a steady inlet temperature to the test section. Another heat exchanger is fitted just after the test section to remove the heat added during heating of the test section for heat transfer experiments.

The heat exchangers are ½ inch diameter stainless steel tubing with length of 38 inches. Each of the heat exchangers is fitted in the test loop with the help of a ½ inch Tee connection and a bore through fitting from Swagelok on each end. The bore through fitting has a ½ inch thread at one end and a ¼ inch compression fitting in the other end. The threaded end is connected to the Tee while the compression fitting maintains a seal

in between the ½ inch tubing and the ¼ inch tubing. The other free end of the tube is connected to a cold water supply by a ½ inch PVC tubing.

3.5 Instrument Calibration

3.5.1 KD2 Pro Thermal Property Analyzer Calibration

Before taking any thermal conductivity measurement, the KD2 Pro was calibrated with the help of a standard calibration fluid from the manufacturer to test the accuracy of the experimental setup and procedure. By following the same procedure as described in section 3.3, the measured values are compared with the standard value of the calibration fluid (see Figure 3.15).

The calibration fluid was specified with a value of thermal conductivity of 0.285 W/m.K ±5% at 20°C. The measurements were performed by keeping the bath temperature at 20°C. It can be seen that the measurement process gives repeatable values with a standard deviation of 0.0005 W/m.K for the thermal conductivity. The average of these values deviated from the standard value by −1.05% which is well within the uncertainty limit of the given thermal conductivity value of the standard calibration fluid. This can conclude that our experimental procedure for thermal conductivity measurement gives accurate results.

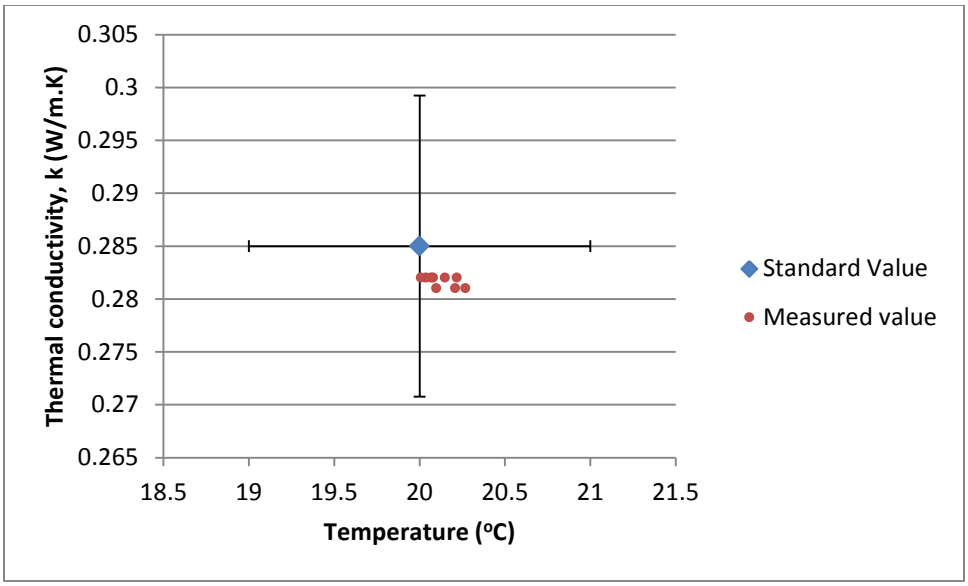

Figure 3.15. Thermal conductivity measurement for a standard calibration fluid at a temperature of 20°C. The error bar represents ±5%.

3.5.2 Pressure Transmitters Calibration

The three pressure transducers are calibrated using a pneumatic hand pump from Ametek (model T-970, range 0 to 580 psi), see Figure 3.16, and a digital electronic gage from Dwyer (model DPG-107, range 0–300 psi) and model DPG-104, range 0–50 psi).The calibration was performed by recording the output voltage from the transducers when certain amount of pressure is applied by the hand pump. The following is the procedure followed for calibration of the pressure transducers:

1. Connect the digital pressure gauge to the hand pump. Then connect the hand pump to the high pressure side of the pressure transmitter.
2. Apply certain amount of pressure by pumping the hand pump. Leave the system for about 2 minutes. If the pressure has reduced, check the connections for leak using soap solution.

3. Apply certain amount of pressure and record the voltage corresponding to the pressure.
4. Increase the applied pressure by 5 psi and record the voltage. Repeat this step until the higher range of the pressure transmitter has been reached.
5. Repeat the same steps for other two pressure transmitters.

These steps were followed and Figures 3.17−3.19 show the calibration results for the three pressure transmitters. A linear trend line is also shown in each of the graphs along with respective R^2 value. This trend line is a curve fit for the linear relation between the applied pressure and output voltage. The linear equation is also shown in the graph. This equation is set as a gain ($Mx + B$) in the data acquisition unit to read the output directly in terms of pressure drop.

Figure 3.16Ameterk hand pump for calibration of the pressure transducers.

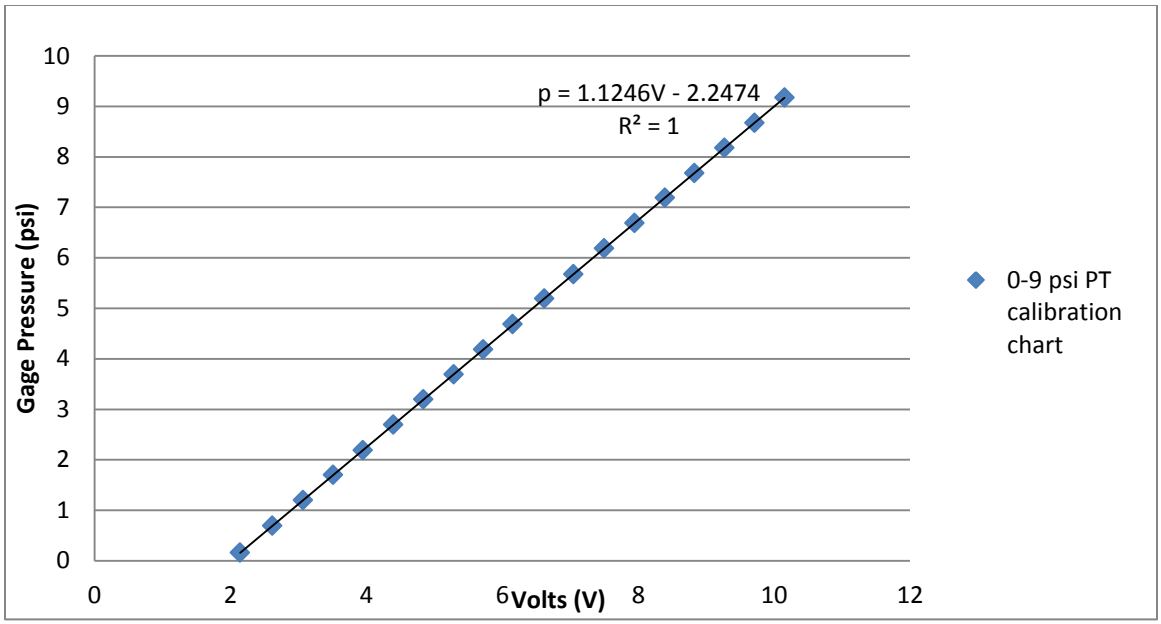

Figure 3.17. Calibration graph for 0–9 psi pressure transmitter.

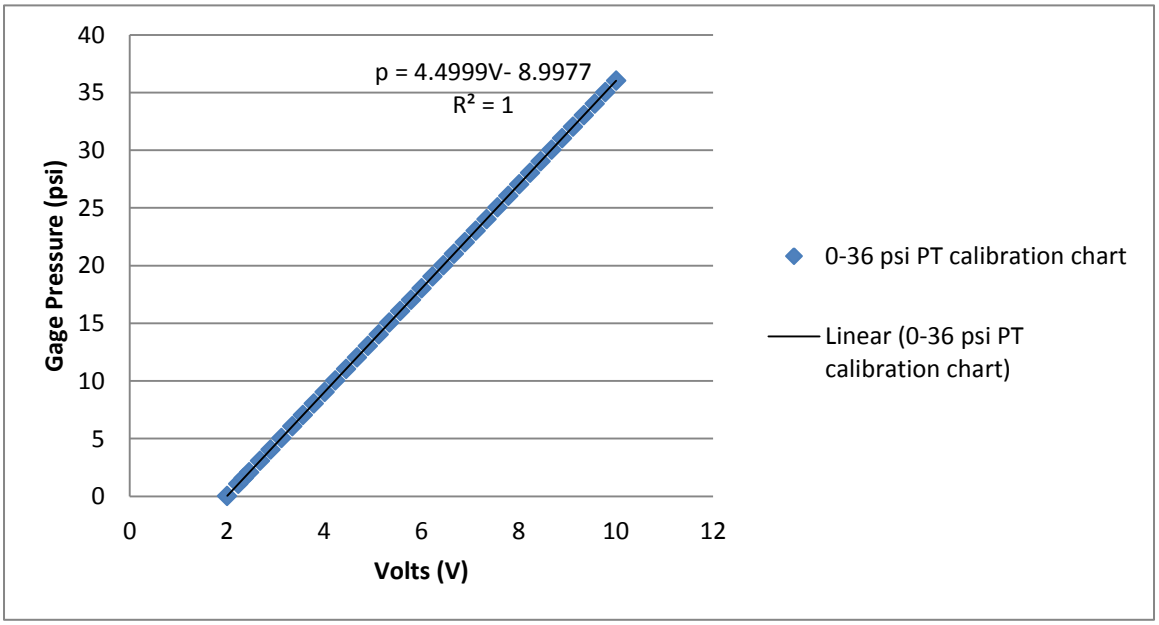

Figure 3.18. Calibration graph for 0–36 psi pressure transmitter.

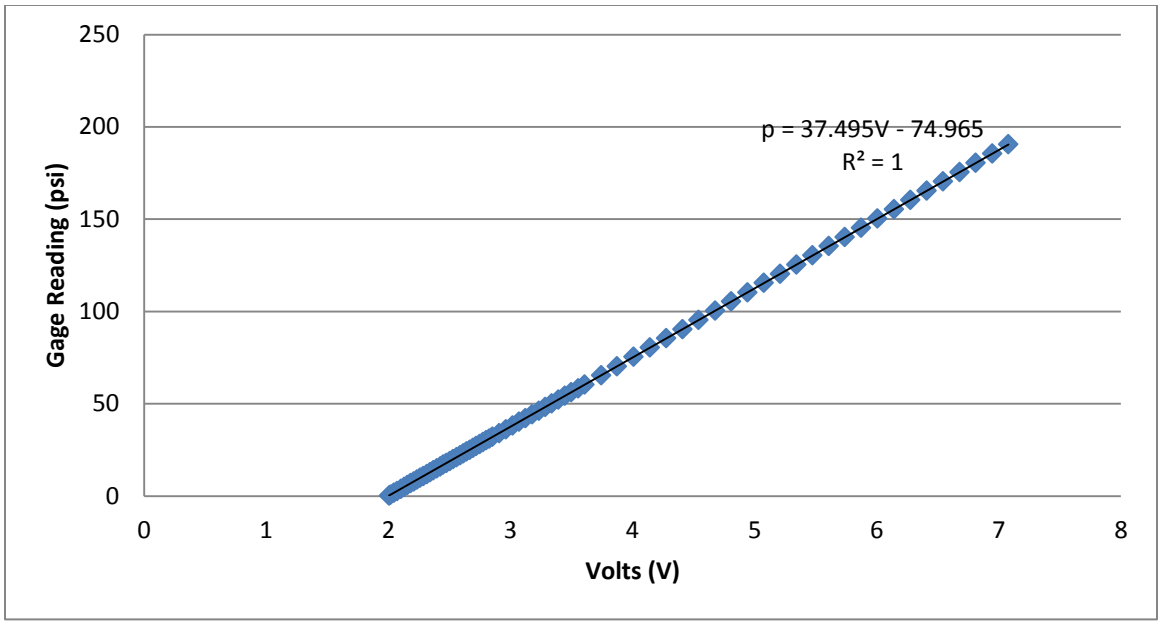

Figure 3.19. Calibration graph for 0–300 psi pressure transmitter.

3.5.3 Viscometer Calibration

The Brookfield viscometer is factory calibrated. Still our process needs to be checked for accuracy. This is done with the help of a standard calibration fluid. The calibration fluid has a viscosity of 493 cP at 25°C. The exact procedure outlined in Section 3.2 is followed by using the enhanced UL adapter. The results of the calibration for the standard viscosity fluid are shown in Figure 3.20.

It can be seen that the cooling curve follows the same path as the heating curve. While heating, the viscosity at 25°C is found to be 493.09 cP, while cooling, the viscosity at 25°C is found to be 494.39 cP. These values fall well within the uncertainty of the

instrument (±2 cP). Thus, it can be concluded that our procedure for taking the viscosity measurements is accurate.

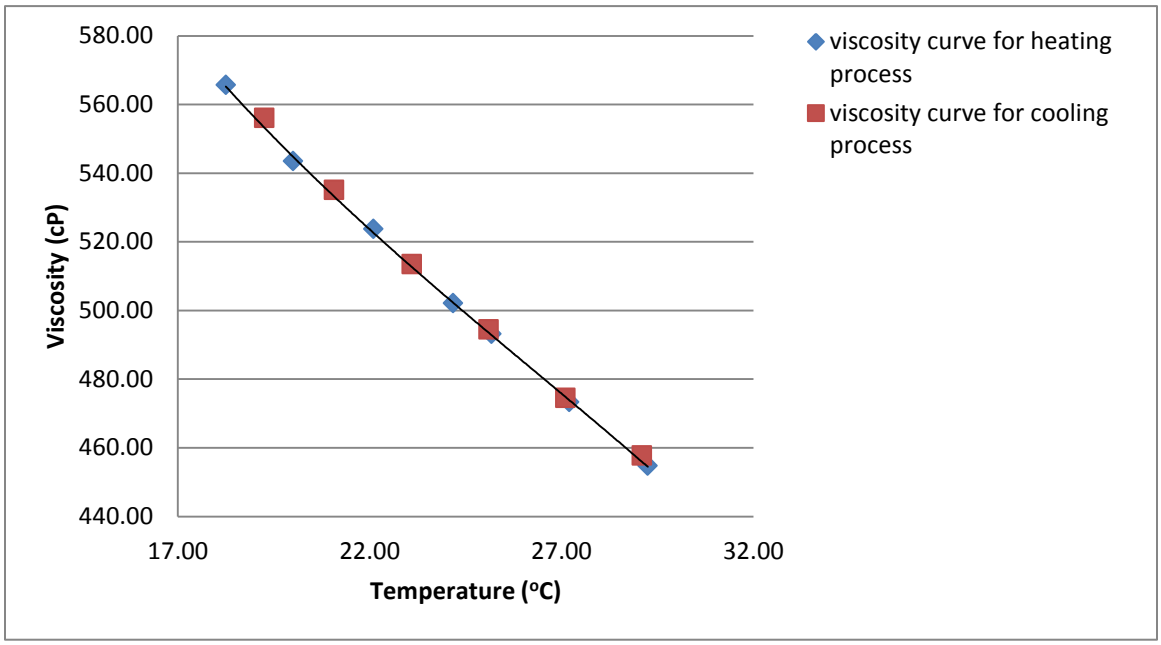

Figure 3.20. Viscosity vs. temperature curve for the given standard viscosity fluid. The fluid has a viscosity of 493 cP at 25°C.

3.5.4 Thermocouples Calibration

The heat transfer results are directly affected by the temperature measurements. Thus, all the thermocouples used in this experiment must be calibrated to determine their accuracy. Both types of thermocouples were calibrated using the temperature bath and an RTD. The temperature range for calibration was from around 7–70°C, which falls under the operating temperature range for this experiment. It can be seen from Figures 3.21 and

3.22 that the thermocouple readings are in close agreement with the RTD readings in the temperature range of 7–70°C. The maximum difference between the calibrated thermocouples and the RTD is 0.31°C.

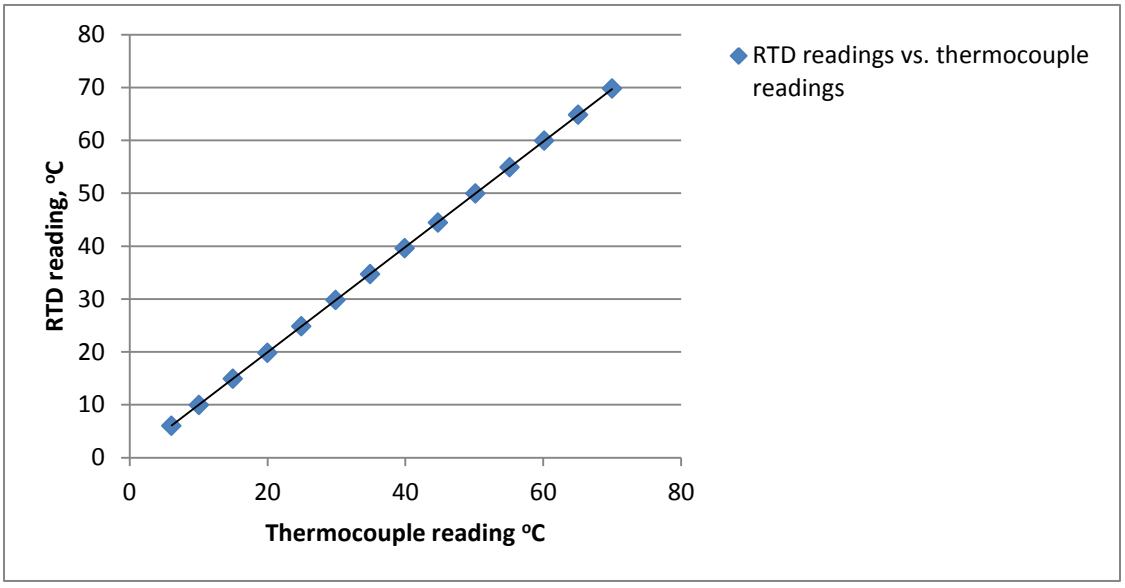

Figure 3.21. RTD readings vs. thermocouple readings for the TT-T-36-SLE-1000 thermocouple.

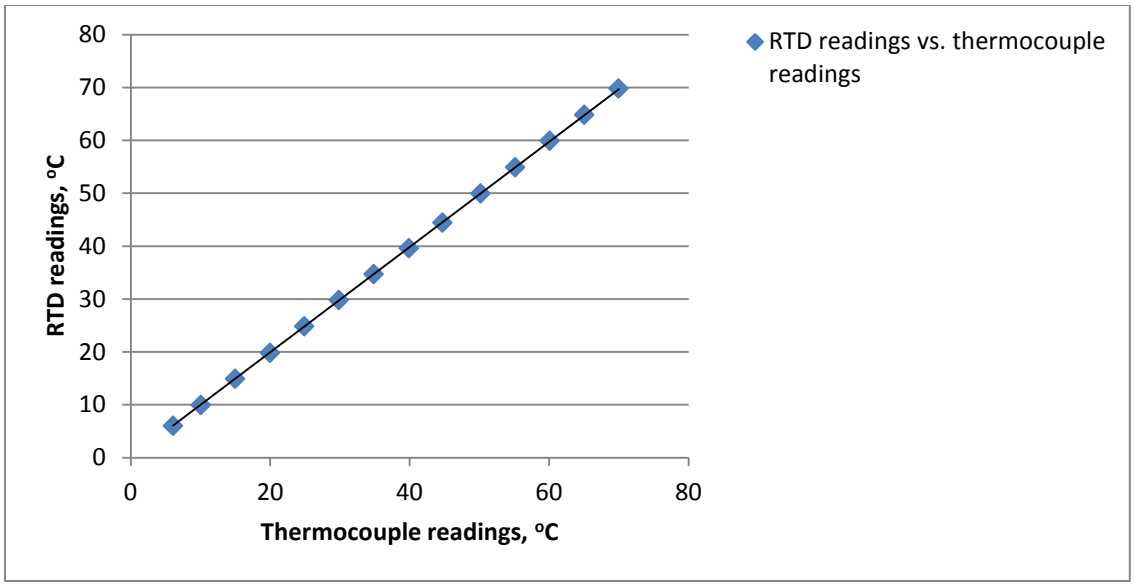

Figure 3.22. RTD readings vs. thermocouple readings for the TMQSS-0.0U-6 thermocouple.

3.6 Experimental Procedure

3.6.1 Pressure Drop Measurement

1. Start up the pump, mass flow meter, data acquisition unit and the pressure transducers.

2. Set the pump speed to match the desired flow rate and Reynolds number.

3. Make sure that the bypass valve is open to limit the strain in the pump.

3. Supply the heat exchangers with cold tap water.

4. Adjust the metering valve to fine tune the flow rate.

5. See if the all the pressure transducers are stable and reading the same value.

6. Wait 5 min to allow the system to be in steady state.

7. Start recording the outputs from the mass flow meter, pressure transducers and bulk temperature measuring thermocouples for 5 minutes.

8. See if all the recordings indicate a steady state process.

9. Increase the flow rate by 1 gm/s by fine tuning the metering valve or increasing the speed of the pump and repeat the process until the maximum Reynolds number or flow rate is reached.

3.6.2 Heat Transfer Measurements

1. Stick the thermocouples along the length of the test section with the help of Omega bond.

2. Use fiber glass insulation (R-25) to insulate the test section. Make sure that the test section is well insulated.

3. Turn on the pump, mass flow meter, pressure transducers and the data acquisition unit.

4. Make sure the bypass valve is open.

5. Supply the heat exchanger with cold tap water.

6. Fine tune the metering valve or increase the speed of the pump to maintain a desired flow rate.

7. Turn on the DC power supply.

8. Wait for 15 minutes for the system to be in a steady state.

9. Start recording the data for 6 minutes.

10. Verify the data recorded represents a steady state process.

11. Increase the flow rate by 1 gm/sec by fine tuning the metering valve or increasing the speed of the pump.

12. Repeat the process until maximum flow rate has been achieved. If the bulk fluid temperature difference between the inlet and the outlet becomes less than 2.5^{o}C, stop the process.

14. Make sure that the DC power supply is turned off first and then the pump. Turning the pump first might cause excessive temperature in the test section damaging the thermocouples and the test section. For nanofluid, excessive heat can cause dry out and clog up the test section.

3.7 Experimental Uncertainties

3.7.1 Friction Factor

The friction factor is given by the Darcy equation which is expressed mathematically as

$$f = \frac{2\Delta P D_i}{\rho L V^2} \tag{3.2}$$

The velocity term in this equation is computed as

$$V = \frac{m}{\rho A_i} \tag{3.3}$$

The flow area is given by

$$A = \frac{\pi D_i^2}{4} \tag{3.4}$$

Therefore, the velocity can be written as,

$$V = \frac{4m}{\rho \pi D_i^2} \tag{3.5}$$

Finally, the friction factor can be written as

$$f = \frac{\Delta P D_i^5 \rho \pi^2}{8 L m^2} \tag{3.6}$$

From Eq. 3.6, it can be seen that the friction factor depends upon 1) pressure drop, 2) inside diameter of the tube, 3) density of the fluid flowing through the tube, 4) length of the tube, and 5) mass flow rate of the fluid.

The uncertainty of measuring the pressure drop, mass flow rate and the length of the tube can be controlled depending upon the procedure of taking the data. However, uncertainty in the tube diameter depends upon the manufacturer's accuracy and methods.

The accuracy of the pressure transmitter is specified as +0.65% of span by the manufacturer. While taking readings, careful attention was given so that the process reached steady state and all of the three transducers were reading the same pressure drop. However, when taking readings with water at low Reynolds number and higher tube diameter, the uncertainty in the measurement of pressure drop seemed to be high which were indicated by slightly different reading of the three pressure transmitters. The

situation seemed better when using nanofluid as the working fluid. In this case the readings from the lower range pressure transmitter were used for data analysis.

The uncertainty in the inside diameter of the test section is a major factor that affects the measurement of friction factor. From equation 3.5 it is clear that the friction factor relates to the fifth power of the inside diameter. The tolerance provided by the manufacturer is ±0.002 inches.

The accuracy of the mass flow meter is specified as ±0.05% of the flow rate. Here also extra attention was given to capture a steady state process.

The uncertainty of the tube length is determined by the accuracy of the measurement scale used for measuring the tube. The least count of the measurement scale used is ± 0.25 inches. Repeated measurements were taken to avoid any error. The uncertainty for the length of the tube is given as ± 0.25 inches.

The nanofluid density is taken as 1.19 gm/cc. The operating range of the experiment was from 5°C till 70°C. It is assumed that the particle density stays constant over this range whereas the density of water may change slightly. The maximum uncertainty in density is calculated as 1.69%.

The uncertainties of the friction factor were estimated within ±5.65 to ±8.53%, as shown in Table 3.1.

Table 3.1. Uncertainty in friction factor.

Uncertainty in pressure drop	Uncertainty in inside diameter	Uncertainty in length	Uncertainty in mass flow rate	Uncertainty in density	Uncertainty in friction factor measurement
±40.43 Pa	1.69%	0.64%	0.05%	1.69%	5.65 to 8.53%

3.7.2 Heat Transfer

The heat transfer is quantified in terms of the Nusselt number. The Nusselt number is given as

$$Nu = \frac{hD_i}{k} \tag{3.7}$$

where Nu is the Nusselt number, h is the convective heat transfer coefficient in [W/m^2.K], D_i is the tube inside diameter in [m], and k is the thermal conductivity in [W/m.K].

The convective heat transfer coefficient is calculated from the following equation

$$h = \frac{q}{T_{wi} - T_b} \tag{3.8}$$

where q is the heat flux per unit area and is given as

$$q = \frac{dQ}{\pi D_i dx} \tag{3.9}$$

where Q is the total heat input to the test section and x is the axial distance along the heated section.

The inside wall temperature T_{wi} is calculated from the outer wall temperature T_{wo} by using the conduction equation given as

$$T_{wi} = T_{wo} - \frac{qD_i x}{2k_s L} \ln \frac{D_o}{D_i} \tag{3.10}$$

where L is the length, D_o is the outside diameter, D_i is the inside diameter of the test section, and k_s is the thermal conductivity of the wall. For stainless steel 304, the thermal conductivity values are given in tabular form by Ho et al. (1977). A temperature dependent equation for thermal conductivity of stainless steel 304 is obtained by curve fitting the data from Ho et al. (1977), and is given as

$$k_s = 0.0156T_{wo} + 14.53 \tag{3.11}$$

The bulk fluid temperature is assumed to vary linearly from the inlet of the test section to the outlet and for any axial distance along the test section, it is given as

$$T_{b,x} = T_{b,in} + \frac{x}{L}(T_{b,out} - T_{b,in}) \tag{3.12}$$

where $T_{b,in}$ is the inlet fluid bulk temperature in [°C] and $T_{b,out}$ is the outlet fluid bulk temperature in [°C].

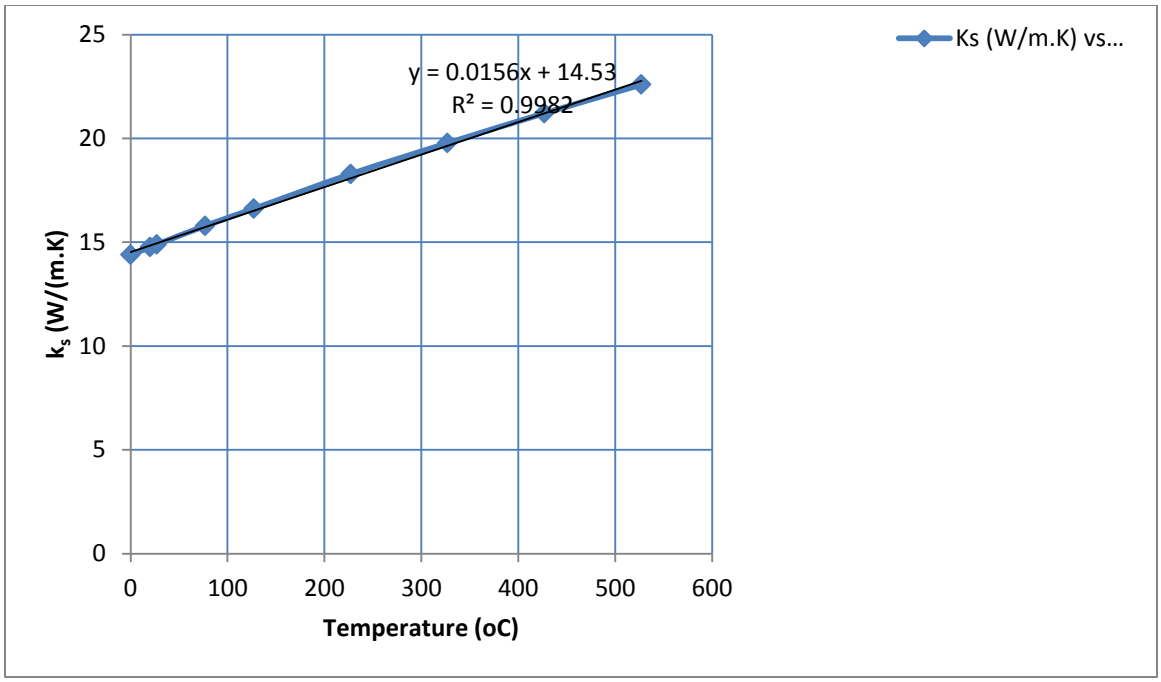

Figure 3.23. Stainless steel thermal conductivity vs. temperature, Ho et al. (1977).

Therefore in final form, the Nusselt number can be written as,

$$Nu = \frac{IV'}{\pi D_i x \left[T_{wo} - T_{bin} + \frac{x}{L} \left(T_{bout} - T_{bin} \right) - \frac{IV}{2\pi k_s L} \ln \frac{D_o}{D_i} \right]} \frac{D_i}{k} \tag{3.13}$$

It can be therefore said that the Nusselt number is a function of 1) thermal conductivity of the fluid, 2) bulk fluid inlet and outlet temperatures, 3) tube outer wall temperature, 4) length of the heated section, length of each axial locations, 5) thermal conductivity of the tube, 6) tube inside diameter, 7) tube outside diameter, 8) current supplied by the DC power supply, and 9) Voltage supplied by the DC power supply.

The uncertainty in measurement by the thermocouple is given as ±0.5°C by the manufacturer for T-type thermocouples. However, when we compared the thermocouples with a RTD, the maximum deviation found was ±0.31°C.

The thermal conductivity of the fluid is measured with the help of the KD2 pro whose accuracy is within ±5% for the range 0.2−2 W/m.K.

The thermal conductivity of the 304 stainless steel is obtained from an equation from a curve fitted value. Here the maximum uncertainty found is 0.617%.

Using these uncertainties, the uncertainty in the measurement of Nusselt number is 6.54% (see Table 3.2).

Table 3.2. Uncertainty in measurement of Nu_d.

Uncertainty in measurement of h	Uncertainty in measurement of q	Uncertainty in measurement of T_b	Uncertainty in measurement of T_{wi}	Uncertainty in measurement of Nu_d
4.72%	3.14%	1.96%	1.08%	6.91%

CHAPTER IV

RESULTS AND DISCUSSION

This chapter discusses on the experimental findings and the comparison of the results with results from different researchers. For most of the experiments, a validation of the experimental setup and procedure is checked by gathering the data with distilled water. All the experiments for nanofluid are conducted with 6.0% vol. fraction Al_2O_3/water nanofluid with average nanoparticle size of 47 nm. For the viscosity measurements different concentration of nanofluid were also considered and analyzed.

4.1 Results for Experimental Setup Validation Using Water

Before conducting experiments in the flow loop with nanofluid, it was necessary to conduct experiments with distilled water and see if the results matched with theory. This was also done to predict the accuracy of the flow loop and different instruments connected to it. With water, experiments were conducted with a Reynolds number above 2300. Laminar flow could not be achieved with water due to its low viscosity and the sensitivity/accuracy of the instruments.

4.1.1 Thermal Conductivity Measurements with Water

The thermal conductivity of water was first measured with the procedure outlined in Section 3.3. The plot between the thermal conductivity and temperature for water is shown in Figure 4.1. It can be seen that the measured value for thermal conductivity of water well represents the standard values available in textbooks, such as Holman (2010). The measured thermal conductivity of water tends to increase with temperature. The thermal conductivity of

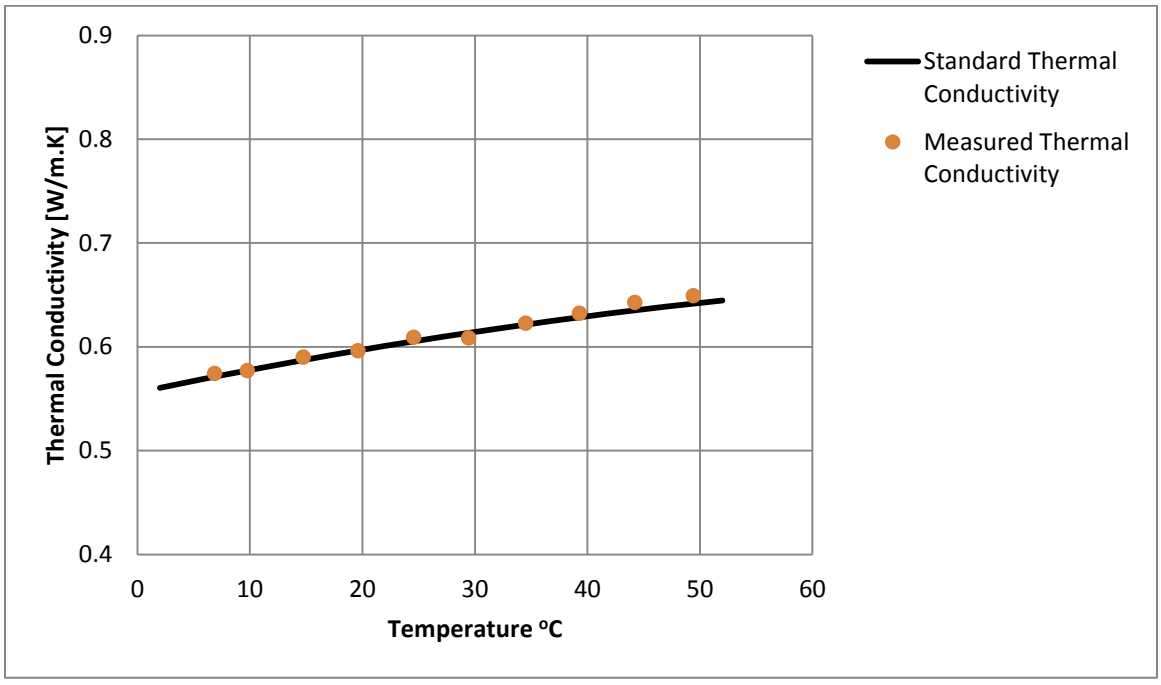

Figure 4.1. Comparison between measured value of thermal conductivity for distilled water at temperature range from 7°C to 50°C with the standard value.

water as measured at 7°C is 0.5742 W/m.K and at 50°C is 0.649 W/m.K. Above 50°C measurements were not taken as the accuracy of measuring thermal conductivity depends upon the viscosity of the liquid. A higher viscosity implies that it will dampen out the disturbances and the readings will be more accurate. Above 50°C due to the lower viscosity of water, readings were not stable and scattered and did not represent a true value for the thermal conductivity of water. Since the measured values of thermal conductivity for water is in close agreement with that of the standard value, the procedure of taking the thermal conductivity measurement is validated and further experiment were carried out with the NF using the same procedure.

4.1.2 Friction Factor Measurements with Water

The friction factor was calculated with the help of the Darcy-Weisbach equation given as

$$f = \frac{\Delta P D_i^5 \rho \pi^2}{8 L m^2} \tag{4.1}$$

From the equation, it is clear that the friction factor involves the measurement of the pressure drop and the mass flow rate. These values of friction factor were plotted against the Reynolds number. Two tubes of diameter 0.175 inch and 0.118 inch with the same length of 36 inches were taken as the test section. Most of the values of friction factor were measured at Reynolds number greater than 4000 for distilled water. The values measured was compared with different correlations available from the literature which are given below

Blasius (1913) for $4000 \leq Re \leq 10^5$,

$$f = 0.316Re^{-0.25} \tag{4.2}$$

Drew et al. (1932) for $4000 \leq Re \leq 5 \times 10^6$,

$$f = 0.0056 + 0.5Re^{-0.32} \tag{4.3}$$

Churchill (1977) for laminar to turbulent region,

$$f = 8 \left(\frac{8}{Re} \right)^{12} + \frac{1}{(A+B)^{1.5}}^{1/12} \tag{4.4}$$

where

$$A = 2.457 \ln \frac{1}{7 \left(Re^{0.9} + 0.27 \epsilon / D \right)}^{16} \tag{4.5}$$

$$B = \frac{37530}{Re}^{16} \tag{4.6}$$

Bhatti and Shah (1987) for $4000 \leq Re \leq 10^7$,

$$f = 0.00512 + 0.4572Re^{-0.311} \tag{4.7}$$

A plot between the measured values of friction factor vs. Reynolds number for water for both the tube diameter is shown in Figure 4.2. Comparison of the measured value with other correlation is also done in the same figure. It can be seen that the measured values are in agreement with that given by the correlation. Further the comparisons between the measured values of friction factor with those given by the correlations are shown in Figures 4.3−4.6. It can be seen that the measured values are within ±5% of those

predicted by the correlations. Thus, it can be concluded that the experimental procedure for measuring the friction factor is accurate and validated.

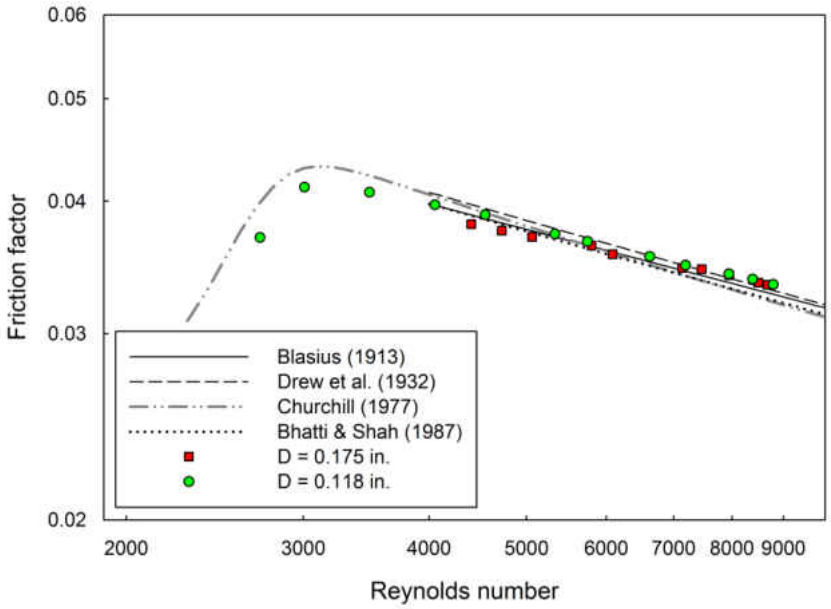

Figure 4.2 Plot between the measured friction factor of water in different tube diameter vs. the Reynolds number. Friction factor calculated from other correlation vs. Reynolds number are also shown.

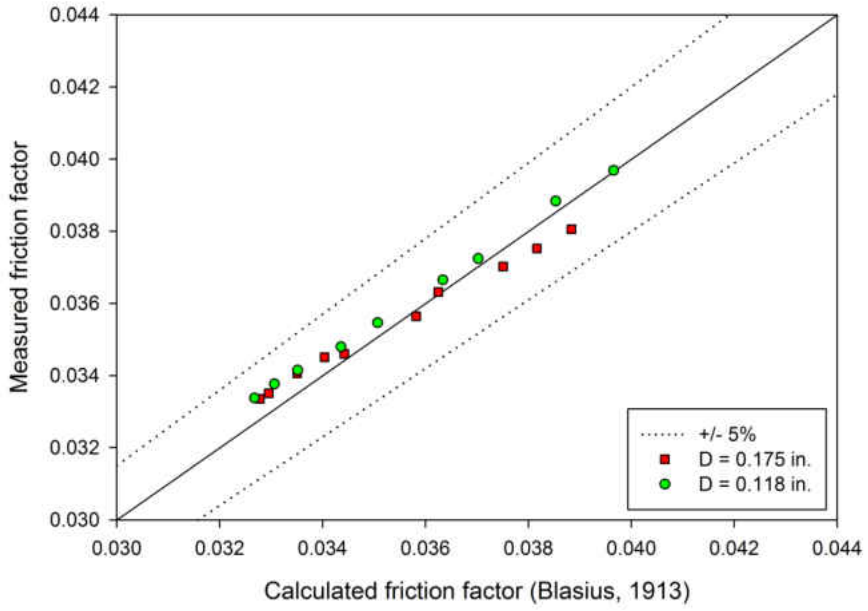

Figure 4.3 Comparison of the measured friction factor of water in different tube diameter with the value of friction factor calculated from the Blasius correlation. Dotted lines represent ± 5% error.

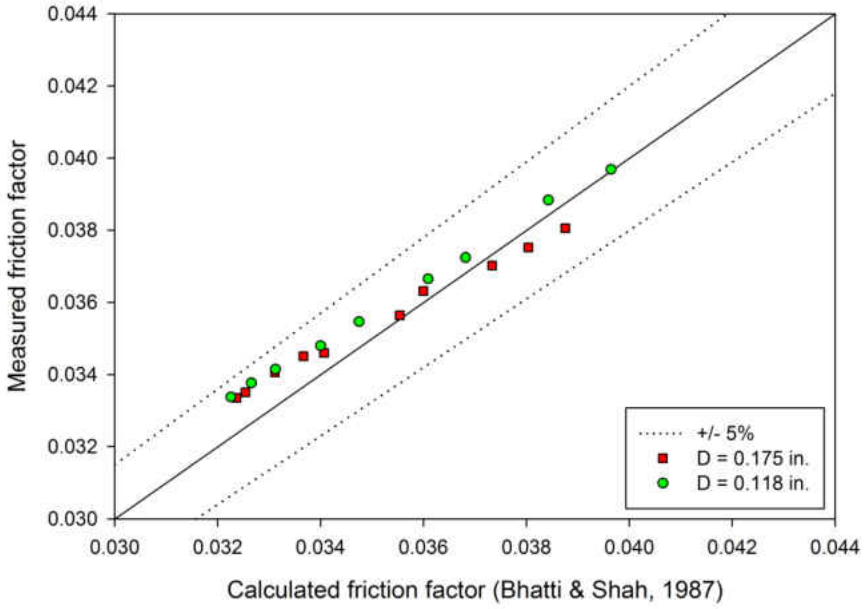

Figure 4.4. Comparison of the measured friction factor of water in different tube diameter with the value of friction factor calculated from the Bhatti and shah correlation. Dotted lines represent ± 5% error.

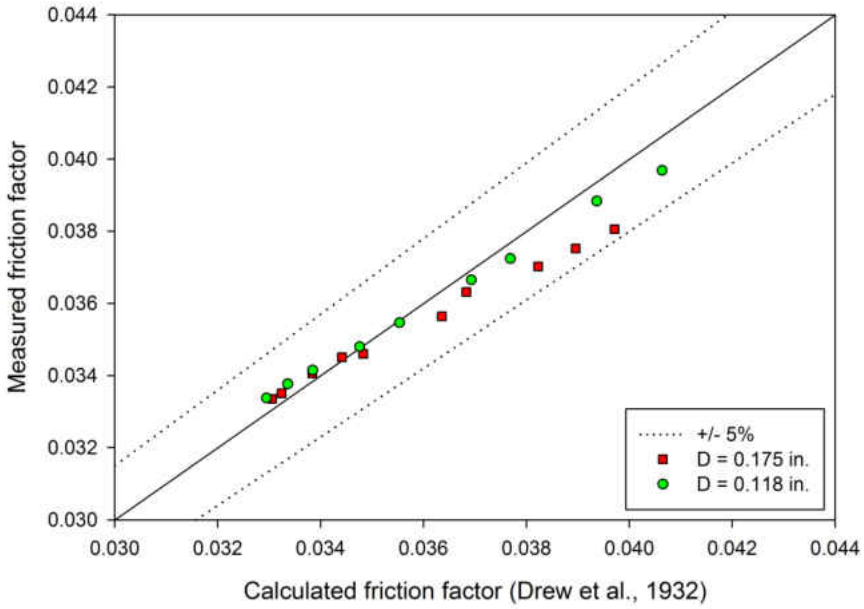

Figure 4.5. Comparison of the measured friction factor of water in different tube diameter with the value of friction factor calculated from the Drew et al. (1932) correlation. Dotted lines represent ± 5% error.

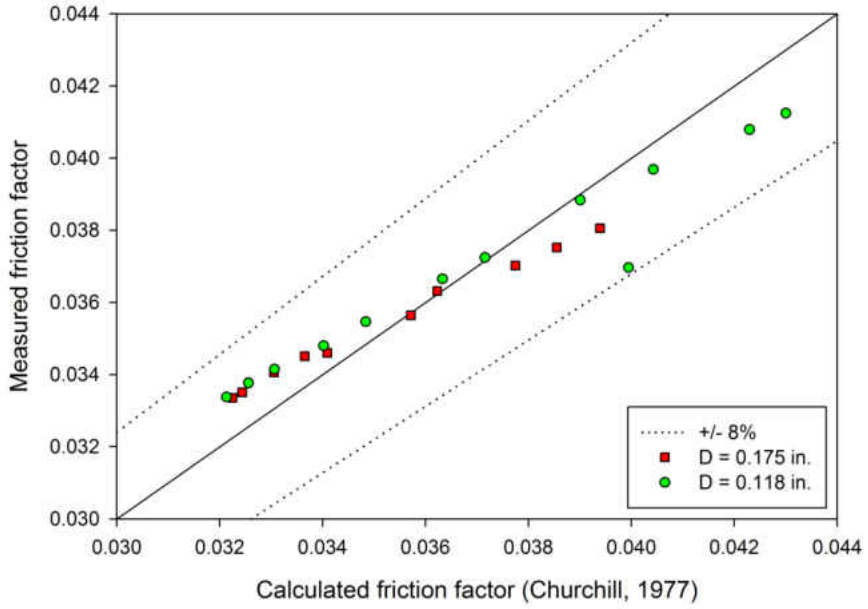

Figure 4.6. Comparison of the measured friction factor of water in different tube diameter with the value of friction factor calculated from the Churchill (1977) correlation. Dotted lines represent ± 5% error.

4.1.3 Heat Transfer Measurements with Water

The heat transfer is characterized in terms of Nusselt number which is expressed mathematically as

$$Nu = \frac{hD_i}{k} \tag{4.8}$$

where Nu is the Nusselt number, h is the convective heat transfer coefficient in [W/m^2.K], D_i is the tube inside diameter in [m], and k is the thermal conductivity in [W/m.K].

The convective heat transfer coefficient is calculated from the following equation

$$h = \frac{q}{T_{wi} - T_b} \tag{4.9}$$

where q is the heat flux per unit area and is given as

$$q = \frac{1}{\pi D_i}\frac{dQ}{dx} \tag{4.10}$$

where Q is the total electrical heat input to the test section, and x is the axial distance along the heated section.

The inside wall temperature (T_{wi}) is calculated from the outer wall temperature (T_{wo}) by using the conduction equation given as

$$T_{wi} = T_{wo} - \frac{qD_i x}{2k_s L} \ln \frac{D_o}{D_i} \tag{4.11}$$

where L is the length, D_o is the outside diameter, D_i is the inside diameter of the test section, and k_s is the thermal conductivity of the wall. For stainless steel 304, the thermal conductivity values are given by Ho et al. (1977). A temperature dependent equation for thermal conductivity of stainless steel 304 is obtained by curve fitting the data from Ho et al. (1977),

$$k_s = 0.0156T_{wo} + 14.53 \tag{4.12}$$

The bulk fluid temperature is assumed to vary linearly from the inlet of the test section to the outlet and for any axial distance along the test section, it is given as

$$T_{b,x} = T_{b,in} + \frac{x}{L}(T_{b,out} - T_{b,in}) \tag{4.13}$$

where $T_{b,in}$ is the inlet fluid bulk temperature in [°C] and $T_{b,out}$ is the outlet fluid bulk temperature in [°C].

Since the values of Reynolds number for the experiment were in the range $3000 \leq Re \leq 12000$, the results were compared with the correlations given by Dittus and Boelter (1930) and Gnielinski (1976). The Dittus and Boelter correlation is valid for fully turbulent flow and for Prandtl number ranging from 0.6 to 100 and is given as

$$Nu_d = 0.023\, Re_d^{0.8} Pr^{0.4} \tag{4.14}$$

The Gnielinski correlation is valid for $3000 < Re < 5 \times 10^6$ and for Prandtl number ranging from 0.5 to 2000, and is given as

$$Nu = \frac{f\ 8\ \ Re - 1000\ Pr}{1 + 12.7\ f\ 8\ ^{0.5}\ Pr^{2\ 3} - 1} \tag{4.15}$$

The plot between the measured Nusselt number and the Reynolds number (see Figure 4.7) shows that the Nusselt number increases with the Reynolds number. The plot for the Nusselt numbers for 0.175 inch ID tube shows that the measured Nusselt numbers are in agreement with that calculated by Dittus and Boelter (1930) and Gnielinski (1976) correlations. For both correlations, most of the value lies within ±15% that of the expected value (see Figures 4.8 and 4.9). For the 0.118 inch ID, 36 inch long tube, most of the value lies within ±15% when compared with the Dittus and Boelter correlation, and within ±10% when compared with the Gnielinski correlation (see Figures 4.10 and 4.11). For the 0.118 inch ID, 18 inch long tube most of the value lies within ±18% when compared with the Dittus and Boelter correlation and within ±5% when compared with the Gnielinski correlation (see Figures 4.12 and 4.13). This shows that the Gnilenski

correlation compares better with the measured data using water than the Dittus and Boelter correlation. The Gnielinski correlation is generally considered to be more accurate than the Dittus and Boelter correlation. Since the measured values of Nusselt number are in agreement with these correlations for different tubes, the experimental procedure is validated and experiments for heat transfer of nanofluid can be carried out.

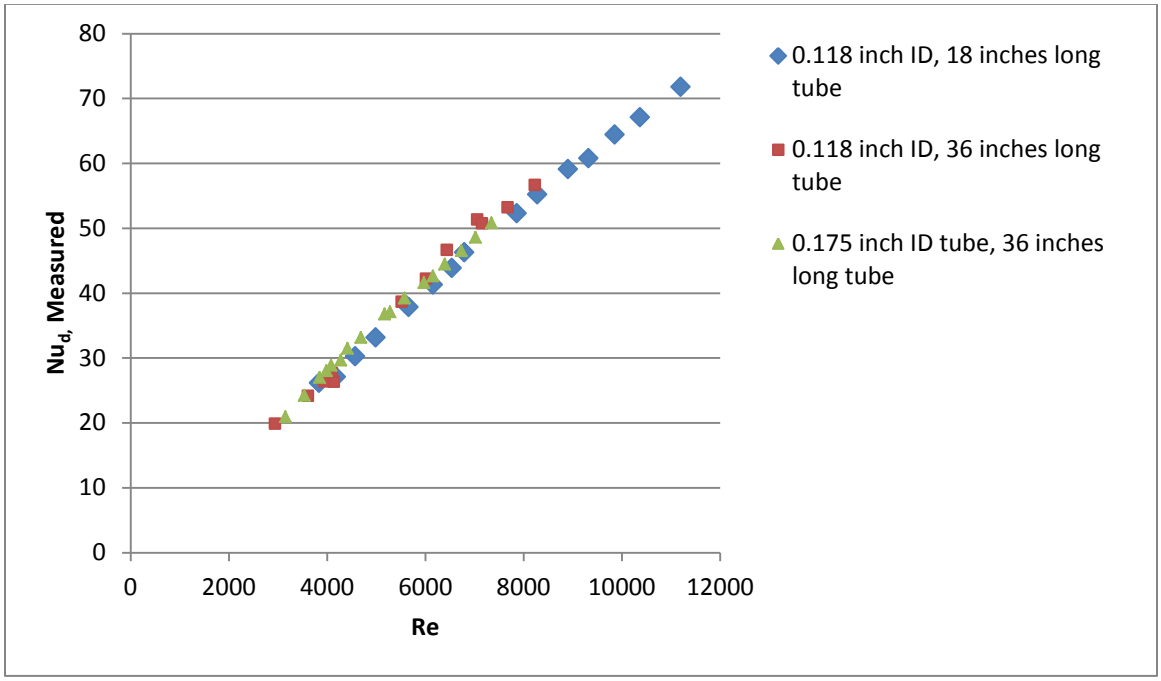

Figure 4.7. Measured Nusselt number vs. Reynolds number for water flowing in different tubes.

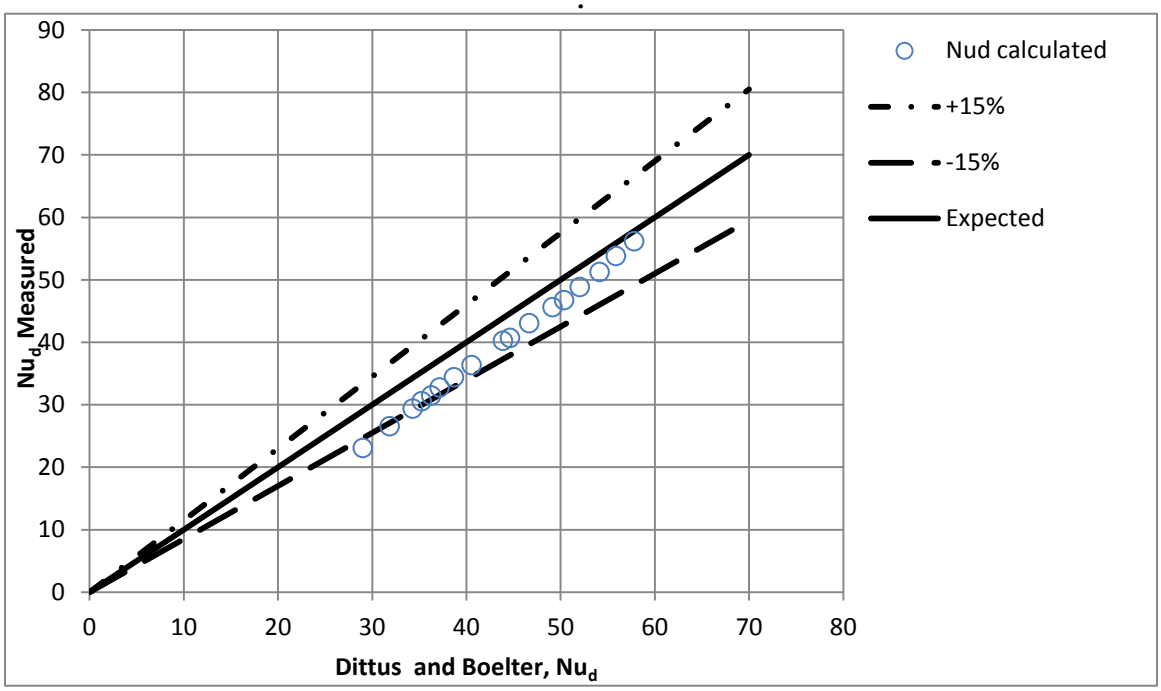

Figure 4.8. Plot showing comparison of the measured Nusselt number and the Nusselt number given by the Dittus and Boelter correlation for the 0.175 inch ID tube.

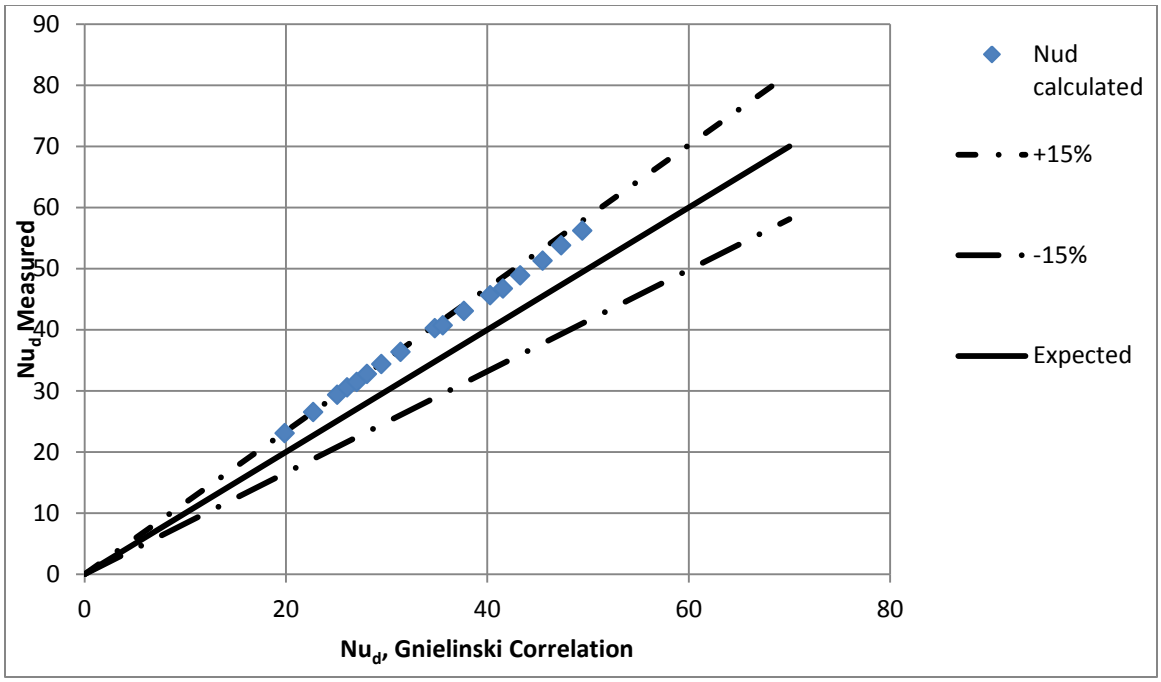

Figure 4.9. Plot showing comparison of the measured Nusselt number and the Nusselt number given by the Gnielinski correlation for the 0.175 inch ID tube.

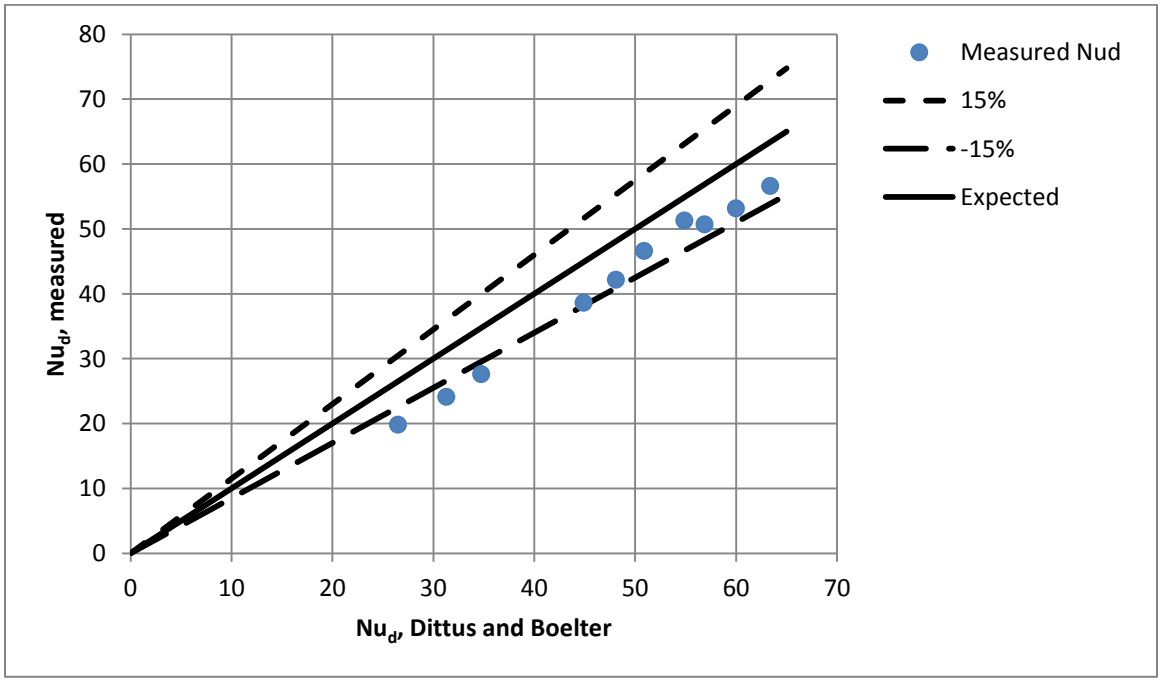

Figure 4.10. Plot showing comparison of the measured Nusselt number and the Nusselt number given by the Dittus and Boelter correlation for the 0.118 inch ID, 36 inch long tube.

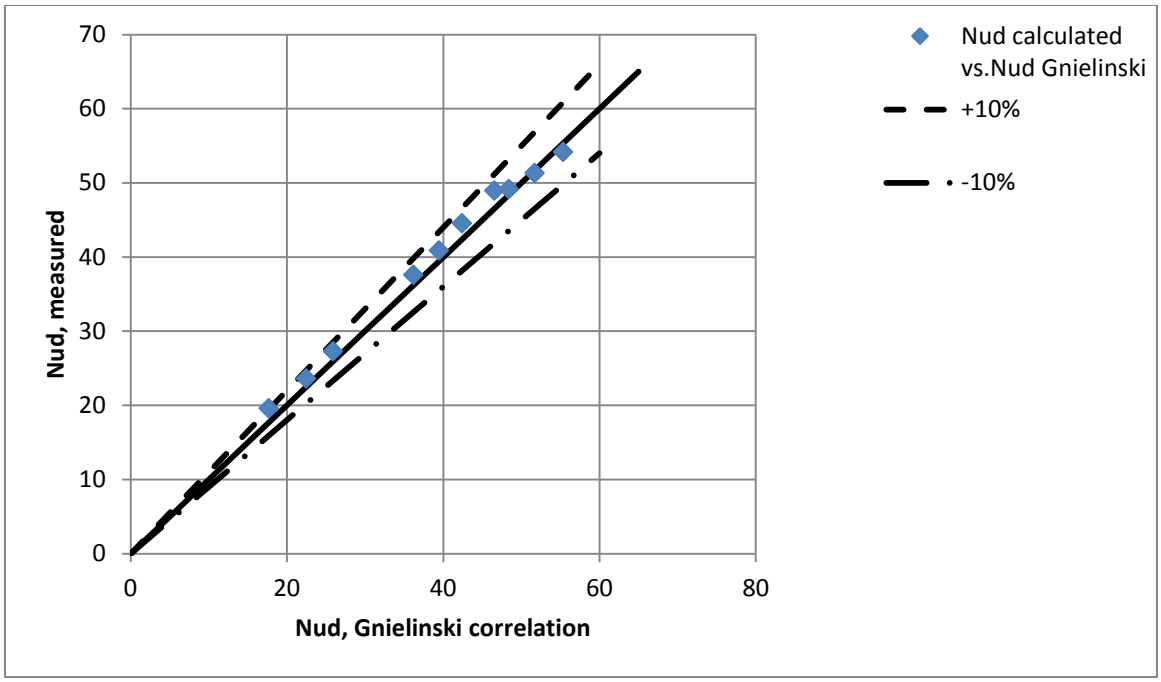

Figure 4.11. Plot showing comparison of the measured Nusselt number and the Nusselt number given by the Gnielinski correlation for the 0.118 inch ID, 36 inch long tube.

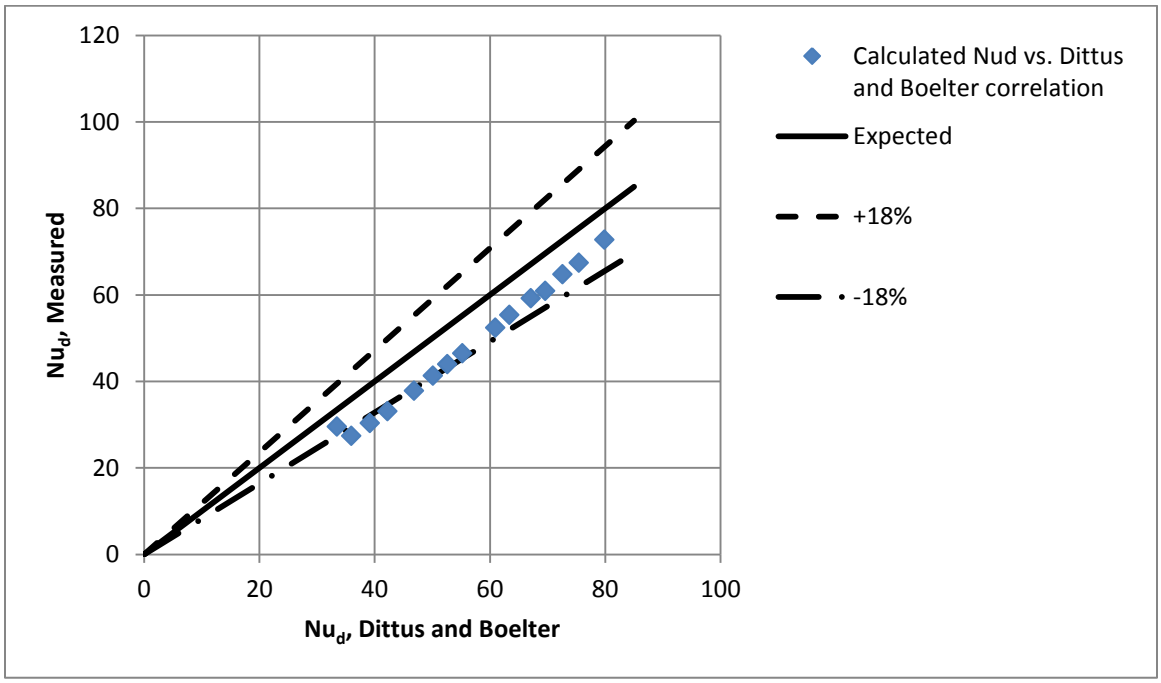

Figure 4.12. Plot showing comparison of the measured Nusselt number and the Nusselt number given by the Dittus and Boelter correlation for the 0.118 inch ID, 18 inch long tube.

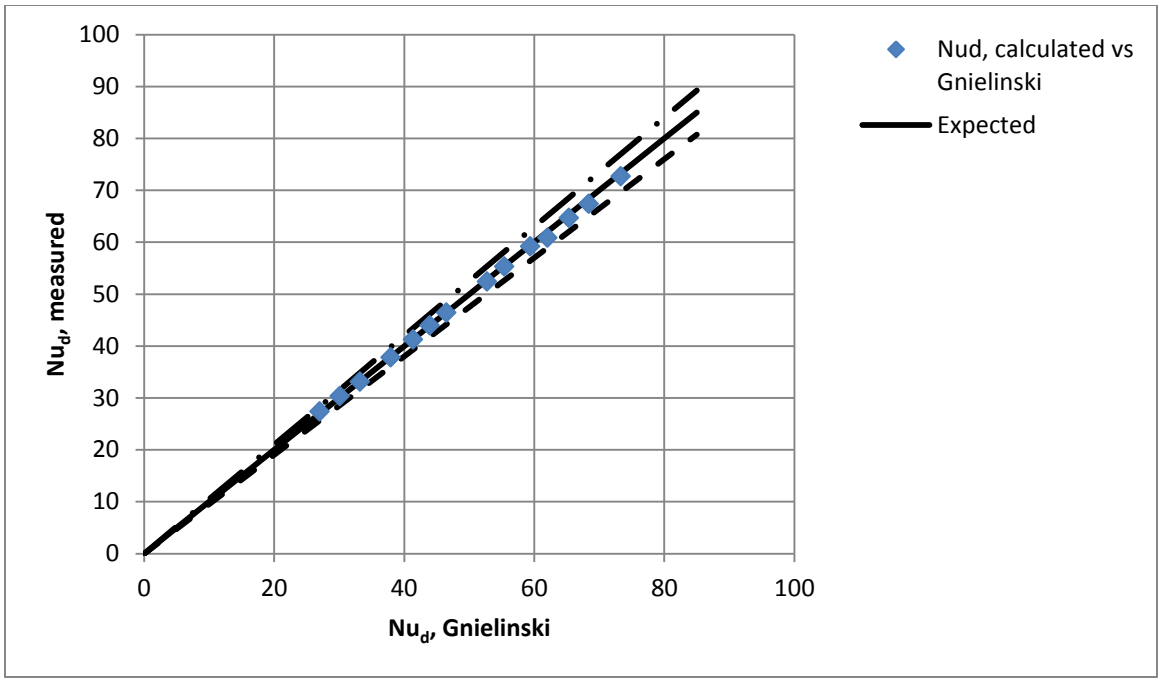

Figure 4.13. Plot showing comparison of the measured Nusselt number and the Nusselt number given by the Gnielinski correlation for the 0.118 inch ID, 18 inch long tube.

4.2. Thermal Conductivity Results of Nanofluid

The plot for the thermal conductivity measurement of NF vs. temperature is shown in Figure 4.14. It can be seen from the plot that from 7°C to 50°C the thermal conductivity of the NF does not increase that much as compared to water. For water the increase in thermal conductivity from 7°C to 50°C is 13%, whereas for NF it is 3.65%. The maximum enhancement in thermal conductivity of NF as compared to water is 16.6% at 7°C, which decreases with increasing temperature, and at 50°C the enhancement is 6.96%.

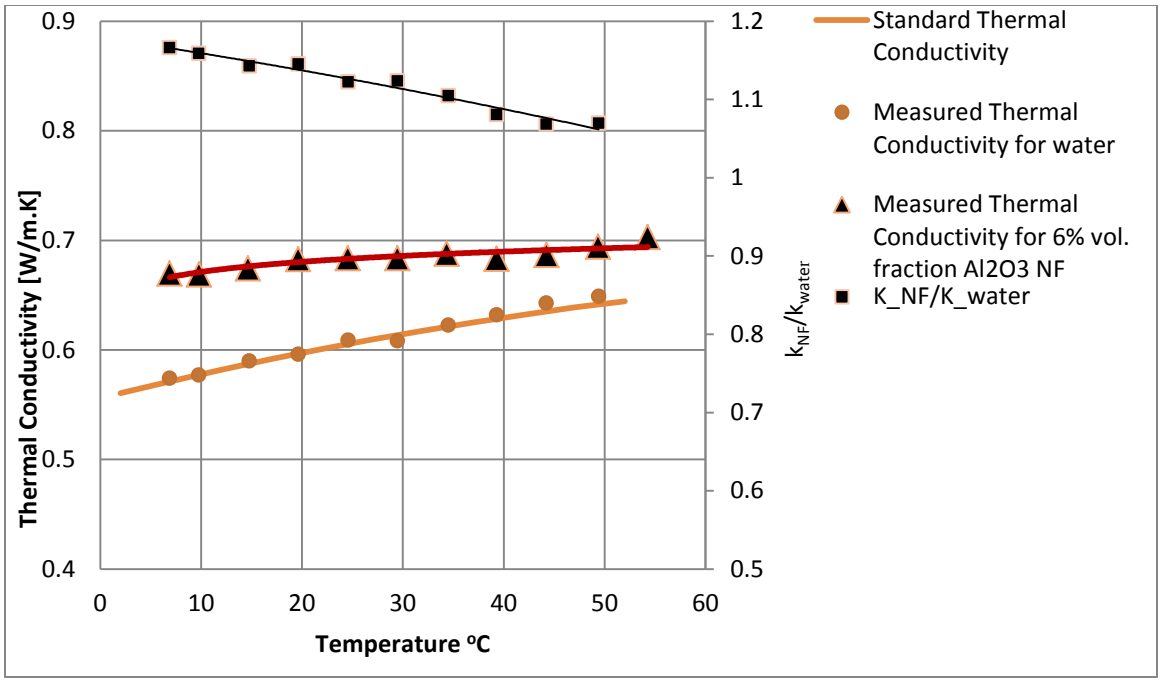

Figure 4.14. Plot showing the thermal conductivity vs. temperature for water and NF. A plot for the thermal conductivity ratio vs. temperature is also shown. The vertical axis on the right represents the thermal conductivity ratio.

Beck et al. (2009) found that the curve of thermal conductivity of Al_2O_3 nanofluids vs. temperature with a particle diameter of 12 nm follows a trend the same as that of water. They report that the temperature dependency of the nanofluid is due to the base fluid and not the nanoparticles. But in our case, the thermal conductivity of NF stayed pretty much constant over the temperature range of 7–50°C and did not follow the same trend as that of water. This suggests that there might be a complex mechanism involved between the base fluid and the nanoparticle depending upon the nanoparticle size, volume fraction and interaction between the base fluid and the nanoparticle.

The plot between the measured thermal conductivity ratio and the temperature is shown in Figure 4.15 along with the values calculated from Maxwell (1892) correlation. It can

be seen that the Maxwell (1892) correlation clearly under predicts the enhancement in thermal conductivity, whereas the correlation developed by Beck et al. (2009) over predicts it. The Maxwell correlation takes into account the thermal conductivity of the base fluid and the volume fraction, while the correlation developed by Beck et al. (2009) takes into account the thermal conductivity of base fluid, volume fraction and diameter. It can be seen that the two correlations seem to be constant for the given temperature range stating that the temperature dependence of thermal conductivity of nanofluid is solely dependent upon the base fluid. However, for our case, addition of Al_2O_3 nanoparticles in base fluid stabilizes the thermal conductivity of the solution over the temperature range of 7°C till 50°C. This adds to the fact that the thermal conductivity enhancement in nanofluid is a complex phenomenon, which takes into account various interactions among the base fluid and the nanoparticle.

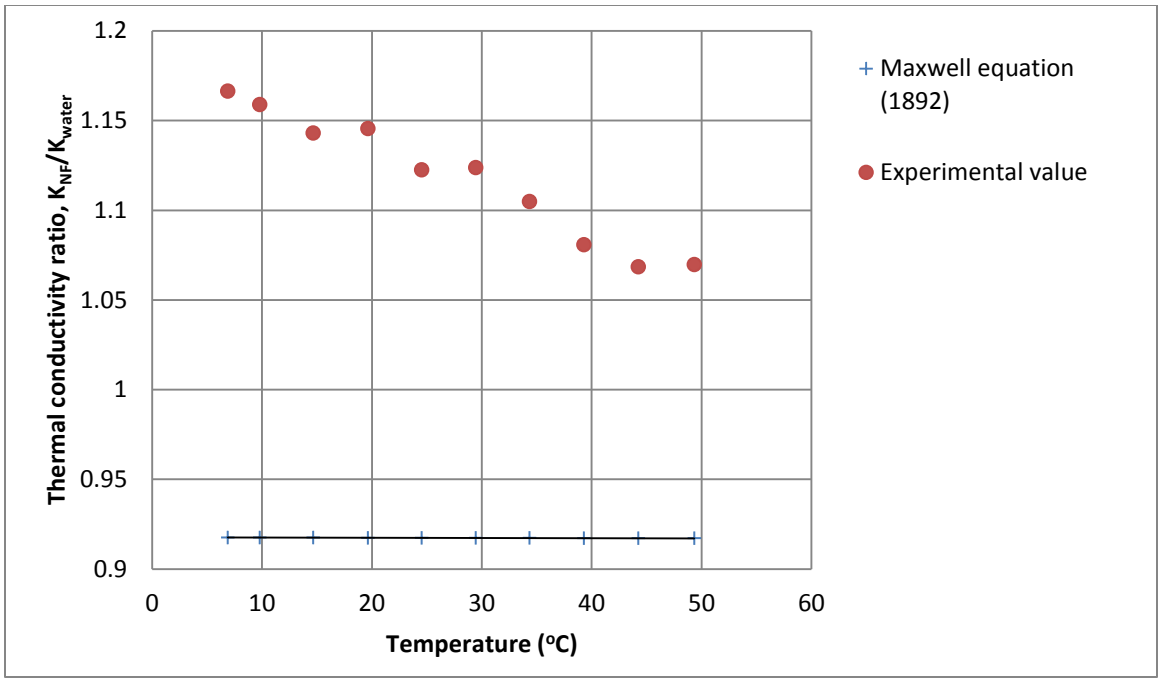

Figure 4.15. Plot comparing the values of measured thermal conductivity ratio and the thermal conductivity ratio given by Maxwell (1892) correlation.

Correlation developed by Prasher et al. (2005) takes into account convection due to the Brownian movement of the nanoparticle, translation Brownian motion and the existence of interparticle potential in addition to thermal conductivity of base fluid, volume fraction and diameter. It can be seen that the thermal conductivity enhancement decreases slightly over the temperature range of 7–50°C. Also our measured values are in good agreement with the correlation developed by Prasher et al. within a ±5% deviation. This shows that the thermal conductivity enhancement of nanofluids is dependent upon several factors including the interaction among the base fluid and the nanoparticle.

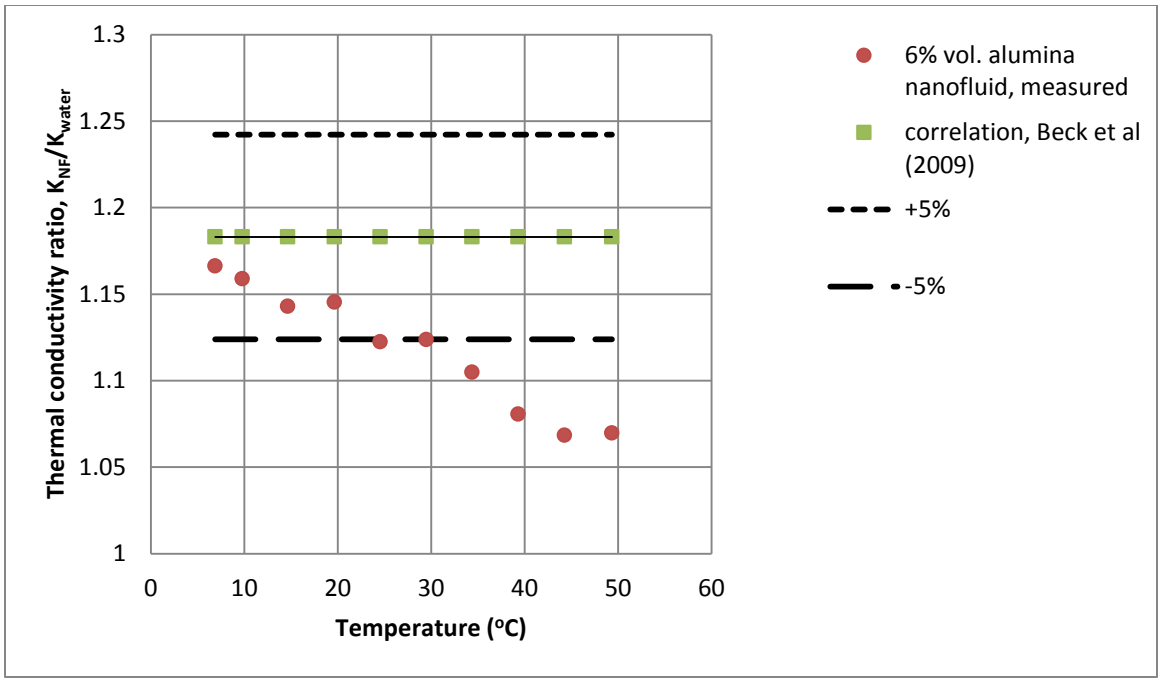

Figure 4.16. Plot comparing the values of measured thermal conductivity ratio and the thermal conductivity ratio given by Beck et al. equation (2009) correlation.

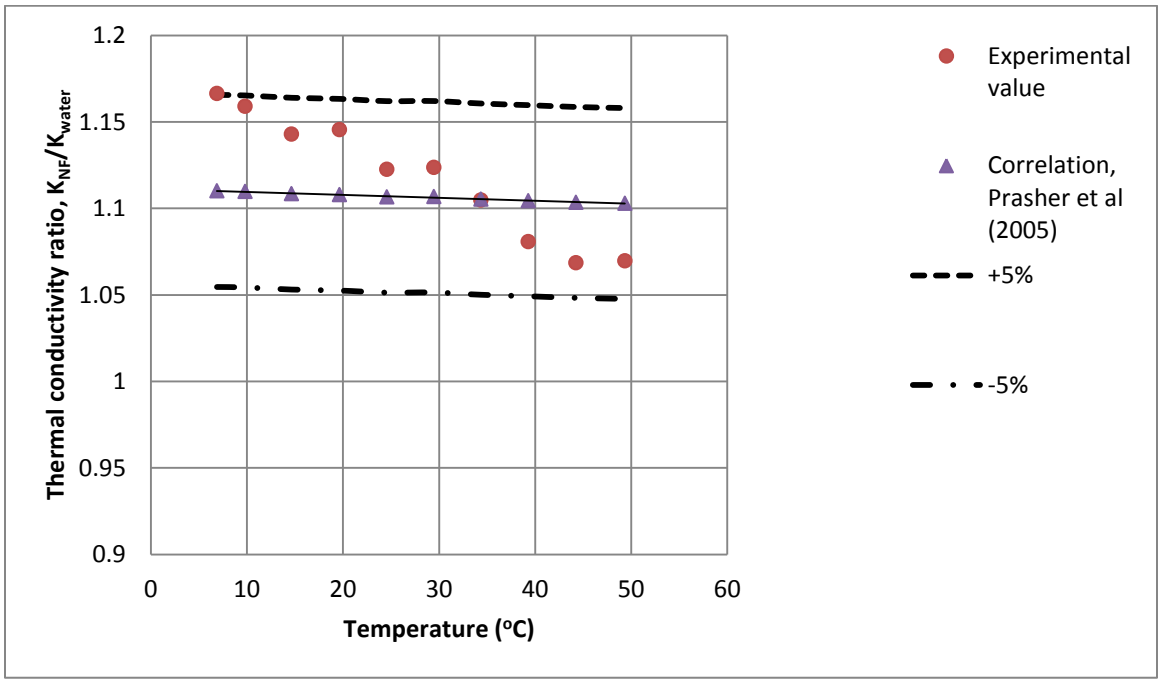

Figure 4.17. Plot comparing the values of measured thermal conductivity ratio and the thermal conductivity ratio given by Prasher et al. (2005) correlation.

4.3 Viscosity Results of Nanofluid

The viscosity of NF is measured at different temperature following the exact procedure outlined in Section 3.2. The plot between the viscosities of NF with temperature is shown in Figure 4.18. It can be seen from the plot that the viscosity of NF decreases sharply with temperature. At a temperature of 6°C, the viscosity is 12.27 cP while at 75°C is 3.45 cP representing a decrease in viscosity by 72% over the temperature range 6–75°C. While for water the change in viscosity is by 74% over the temperature range 6–75°C, which is pretty much comparable to NF.

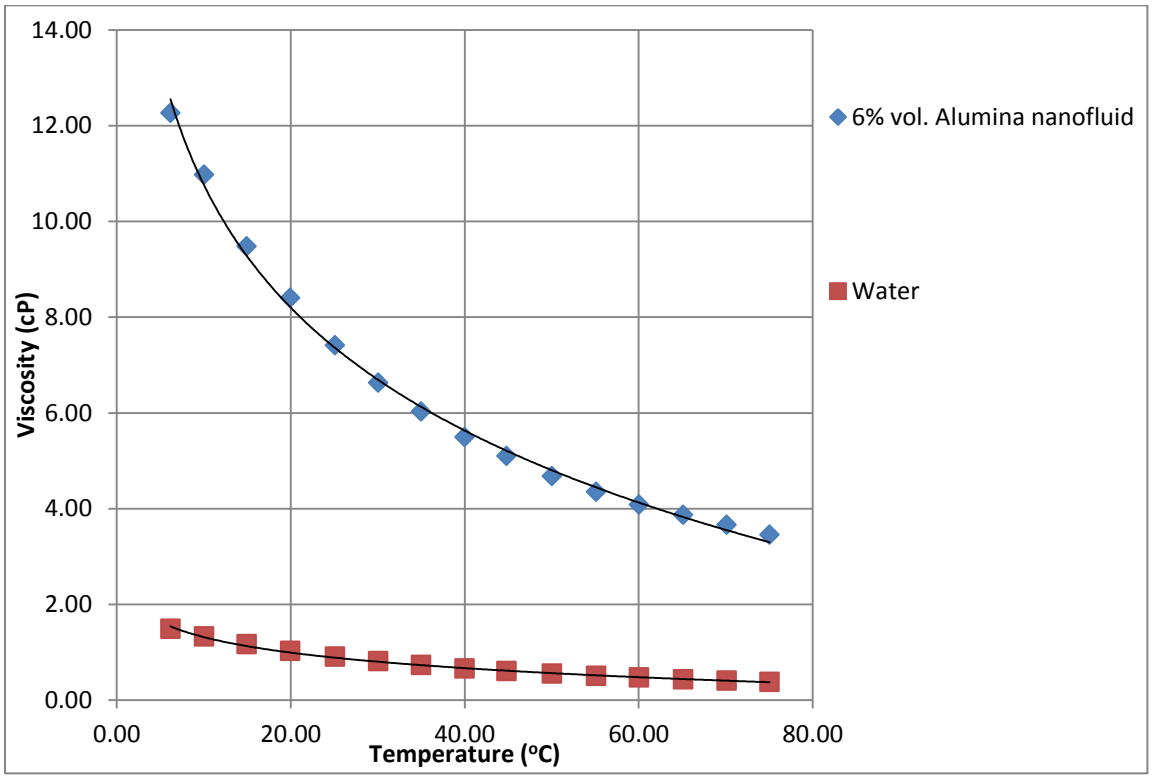

Figure 4.18. Viscosity vs. temperature for water and NF.

A plot between the viscosity of nanofluids and temperature for different concentration of nanofluid is shown in the Figure 4.19. It can be seen that as the concentration of nanoparticles decreases, the viscosity of the nanofluid also decreases and approaches the viscosity curve of water vs temperature at lower volume concentration.

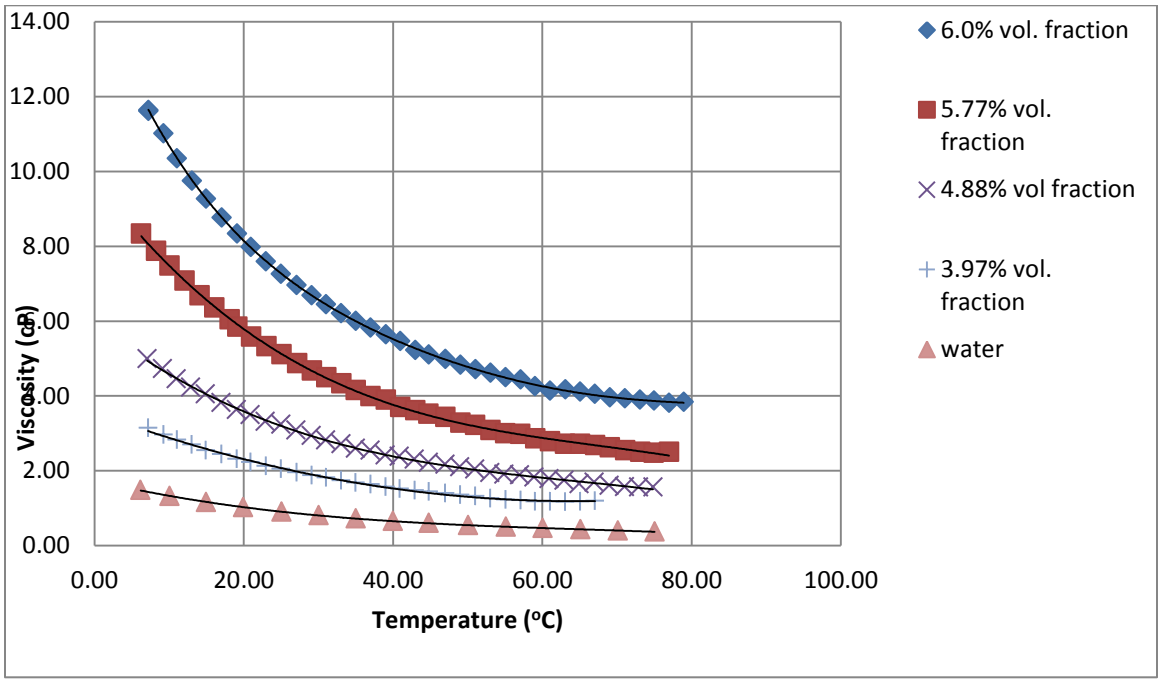

Figure 4.19. Plot showing the viscosity vs. temperature for different concentration Al_2O_3/water nanofluid.

The plot between the relative viscosity of Al_2O_3/water nanofluid and temperature for different concentration of nanoparticle is shown in Figure 4.20. It can be seen from the plot that for 6% vol. fraction Al_20_3/water nanofluid, the relative viscosity increases with temperature much more compared to lower volume fraction nanofluid.

For lower volume fraction, the curve seems to be pretty flat. This indicates that for higher concentration, the viscosity is a strong function of the temperature. For lower concentration, the temperature dependence of viscosity for nanofluid can be predicted to be inherited from the base fluid itself. This phenomenon is also observed by Zhou et al. (2010). Also the relative viscosity of 6 % vol. fraction Al_2O_3/water nanofluid lies within a range of 7.25 to 10.24 for the temperature range from 7 to 75°C, which implies a high viscosity that makes the use of this nanofluid questionable for practical applications. However, if a good balance between the increased viscosity and the rate of heat transfer is achieved, this nanofluid might find its way for practical purpose.

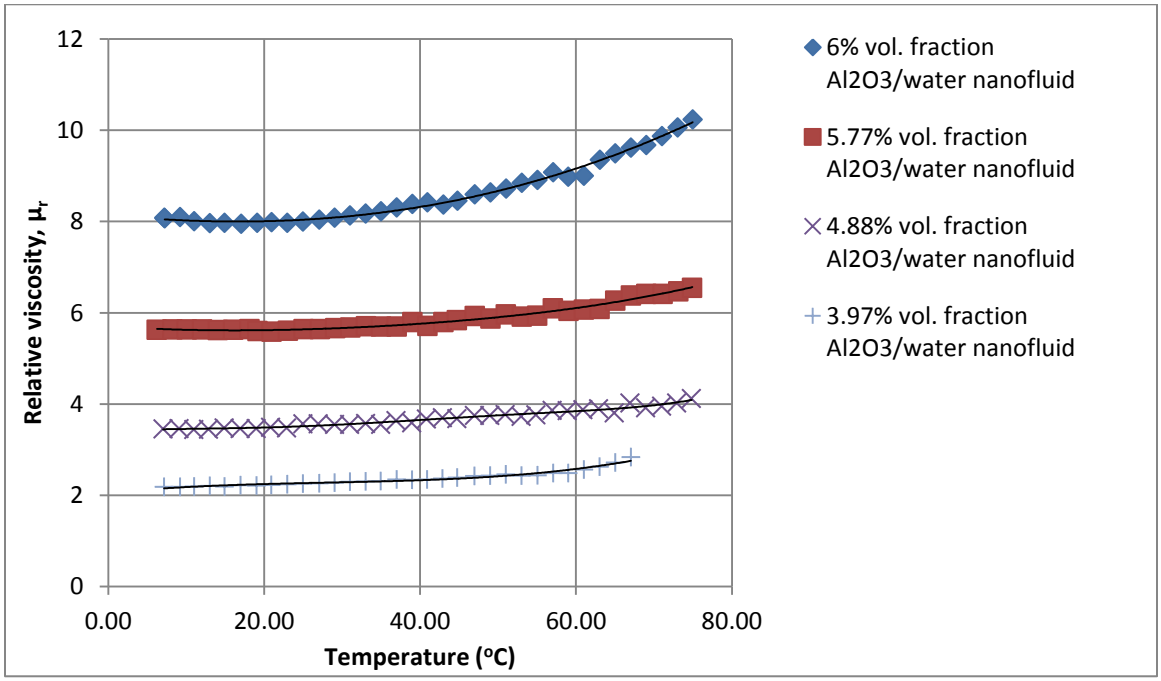

Figure 4.20. Plot showing the relative viscosity vs. temperature for different concentration Al_2O_3/water nanofluid.

A plot between the viscosity of nanofluid and volume concentration of nanoparticles at different temperatures is shown in Figure 4.21. It can be seen that the viscosity of nanofluids increases with increase in volume concentration of nanoparticles. From the plot, we can see that, the increase in viscosity with the volume concentration at different temperatures almost follows the same trend.

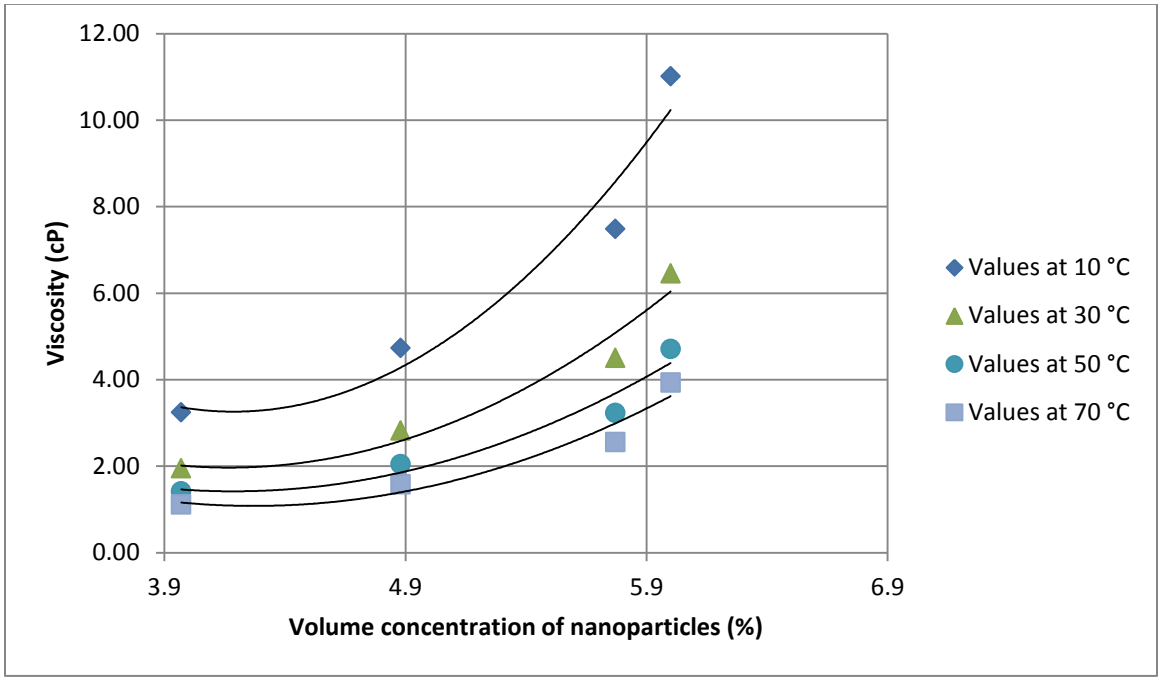

Figure 4.21. Plot showing the viscosity vs. volume concentration of nanoparticles for Al_2O_3/water nanofluid at different temperatures.

The plot between the applied strain rate and the shear stress at three different temperatures of 6°C, 30°C and 75°C for the NF is shown in Figure 4.22. It can be seen that the curves are straight lines passing through the origin. This behaviour represents the NF as a Newtonian fluid for the given shear rates, implying that the viscosity of the fluid

is independent of the applied force. The proportanility constant between these curves represents the viscosity.

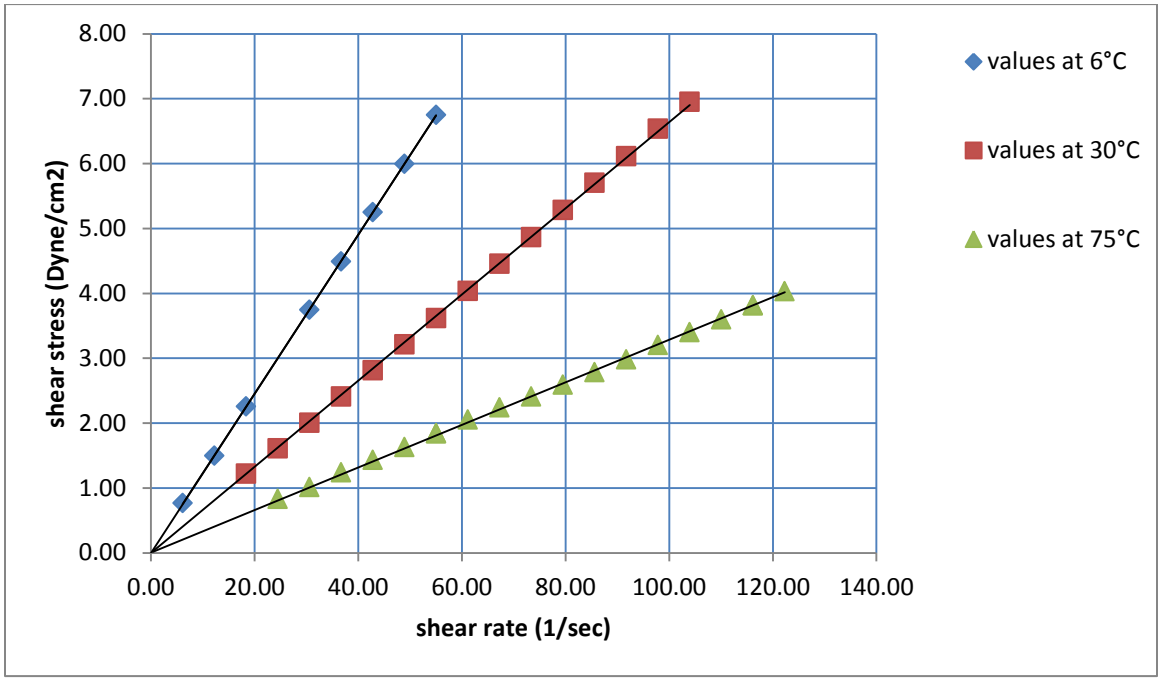

Figure 4.22. Plot between the shear stress and shear rate for NF.

While taking the viscosity measurements for the NF, it was observed that the viscosity vs. temperature curve on cooling did not follow the curve on heating for a temperature range 7°C–75°C showing some hysteresis. Further experiments were carried out by lowering the temperature range. For the temperature range 5−30°C, 5−40°C, 5−50°C, and 5−56.8°C, the viscosity vs. temperature curve on cooling lined up with that for heating (Figures 4.23–4.26). However, for the temperature range of 5−62.65°C (Figure 4.27), the curve on cooling shifted higher than the curve representing the heating phase. This can

conclude that above 62.65°C, some of the alteration in properties of nanofluid occurs, where the particles agglomerate and causes an irrecoverable increase in viscosity. This type of behavior of nanofluid was also observed by Mintsa et al. (2007), where they defined a critical temperature above which the nanofluid property changes and causes an irrecoverable change in viscosity.

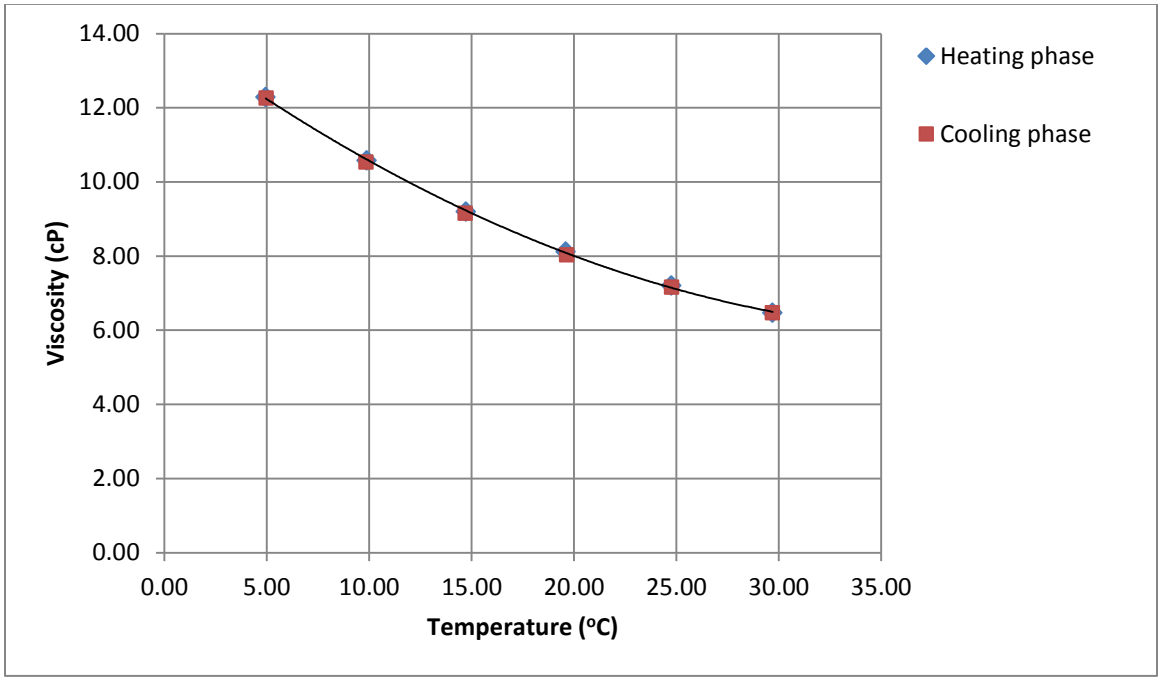

Figure 4.23. Plot showing the viscosity vs. temperature for the NF. The NF is first heated from a temperature of 6°C to 30°C and then again cooled to 6°C.

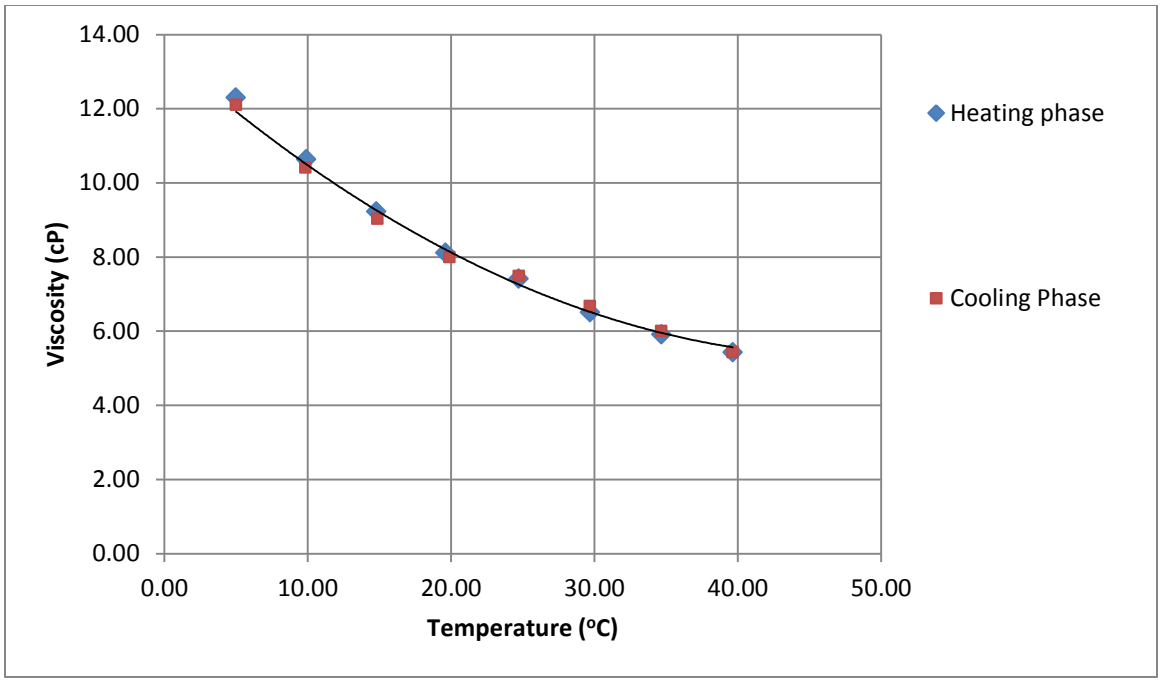

Figure 4.24. Plot showing the viscosity vs. temperature for the NF. The NF is first heated from a temperature of 6°C to 40°C and then again cooled to 6°C.

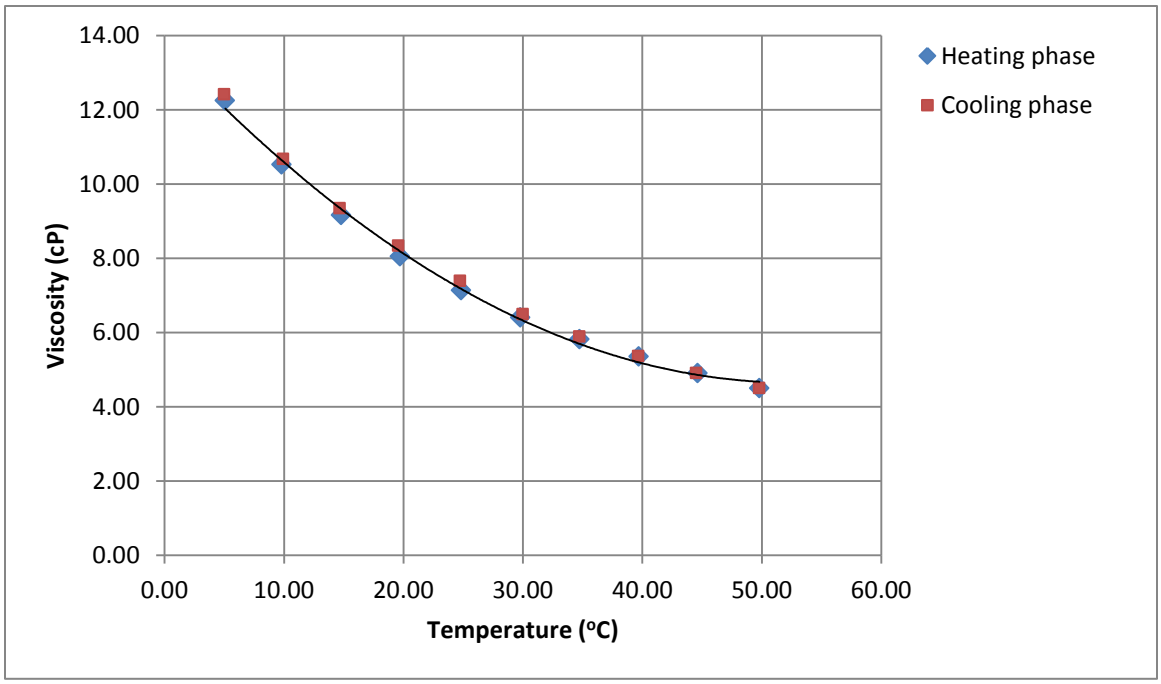

Figure 4.25. Plot showing the viscosity vs. temperature for the NF. The NF is first heated from a temperature of 6°C to 50°C and then again cooled to 6°C.

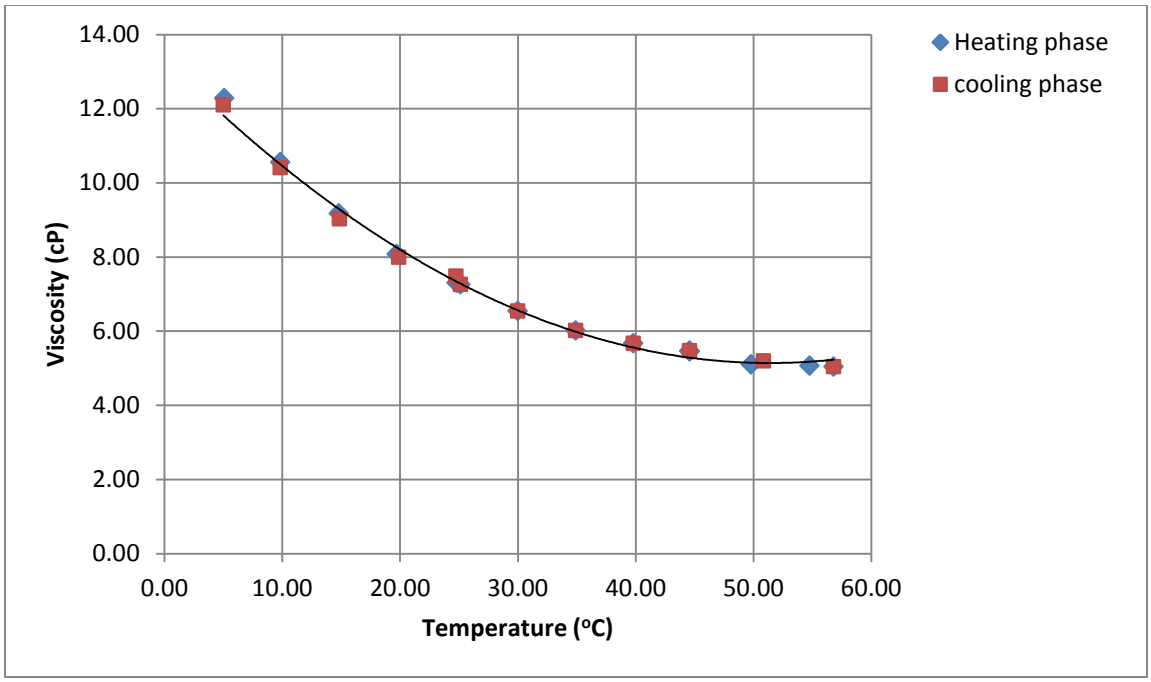

Figure 4.26. Plot showing the viscosity vs. temperature for the NF. The NF is first heated from a temperature of 6°C to 60°C and then again cooled to 6°C.

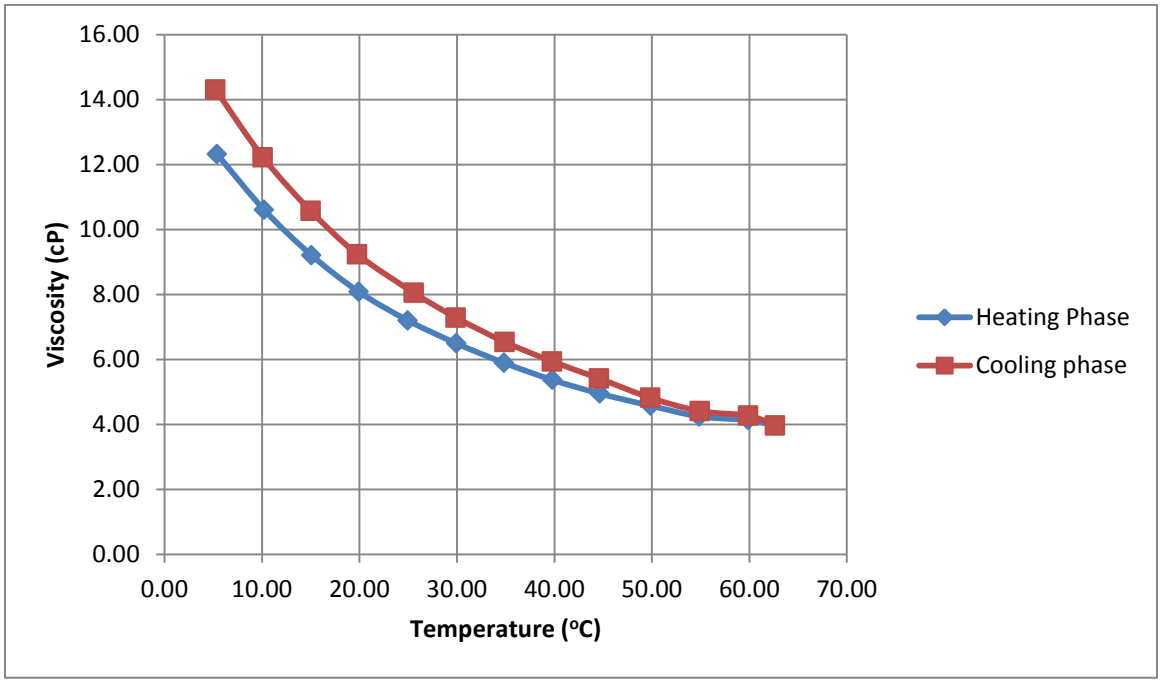

Figure 4.27. Plot showing the viscosity vs. temperature for the NF. The NF is first heated from a temperature of 6°C to 62.65°C and then again cooled to 6°C.

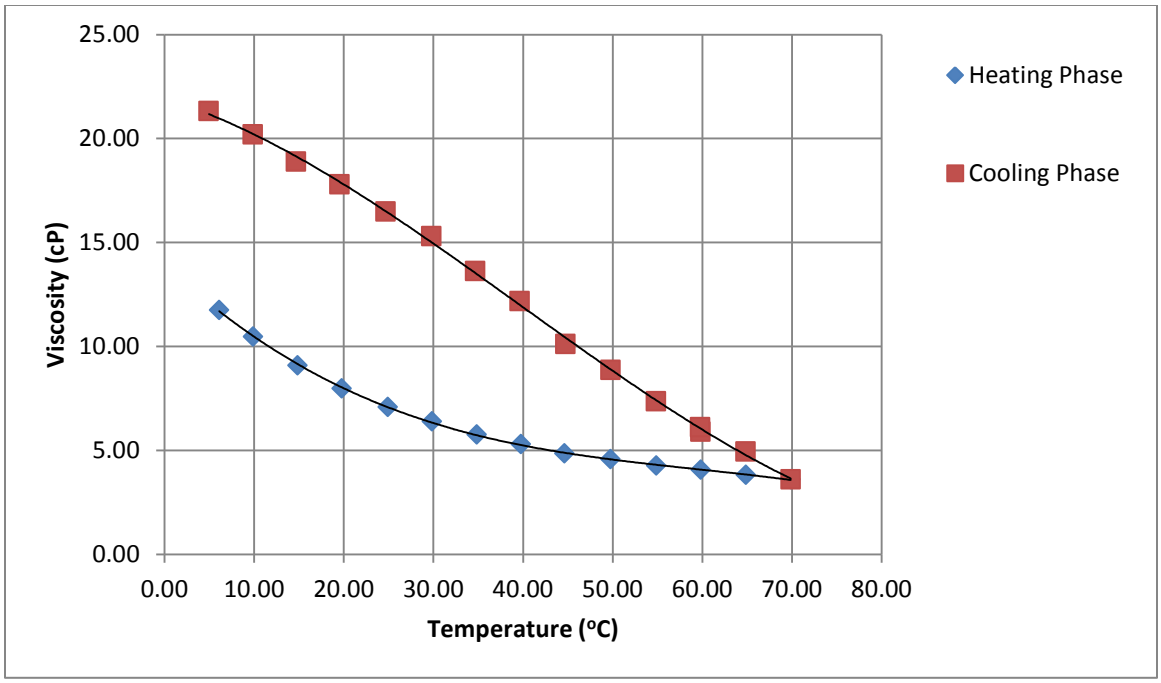

Figure 4.28. Plot showing the viscosity vs. temperature for the NF. The NF is first heated from a temperature of 6°C to 70°C and then again cooled to 6°C.

4.4 Friction Factor Results of Nanofluid

The friction factors for the NF are measured in two different tubes of internal diameter 0.175 inch and 0.118 inch with the same length of 36 inches. Plots between the friction factor for the NF flowing in the 0.118 inch ID and 0.175 inch ID tubes is shown in Figures 4.29 and 4.30. Also, the plot between the Poiseuille number and the Reynolds number for the NF flowing in the 0.118 inch ID and 0.175 inch ID tubes is shown in Figures 4.31 and 4.32. It can be seen that the friction factor of NF closely matches the Hagen-Poiseuille equation within ±5%. Also, after a Reynolds number of approximately 1500 in both the tubes, the measured value of friction factor starts to rise up from that

predicted by the Hagen Poiseuille equation. This indicates a transition from laminar flow above this Reynolds number.

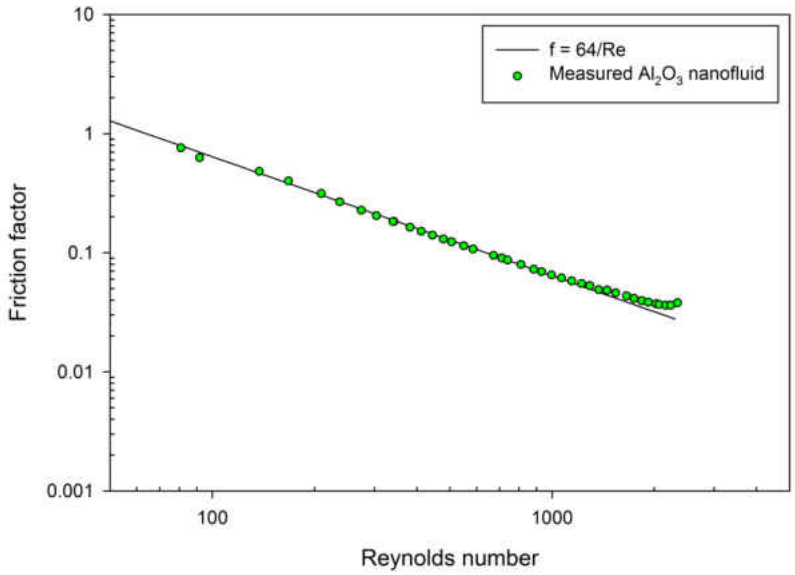

Figure 4.29. Plot between the friction factor and Reynolds number for the NF flowing through 0.118 inch ID, 36 inch long tube.

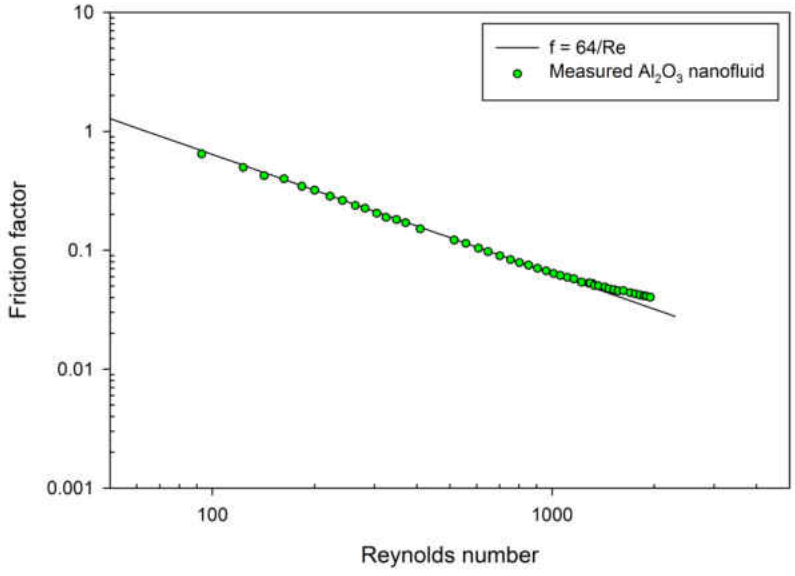

Figure 4.30. Plot between the friction factor and Reynolds number for the NF flowing through 0.175 inch ID, 36 inch long tube.

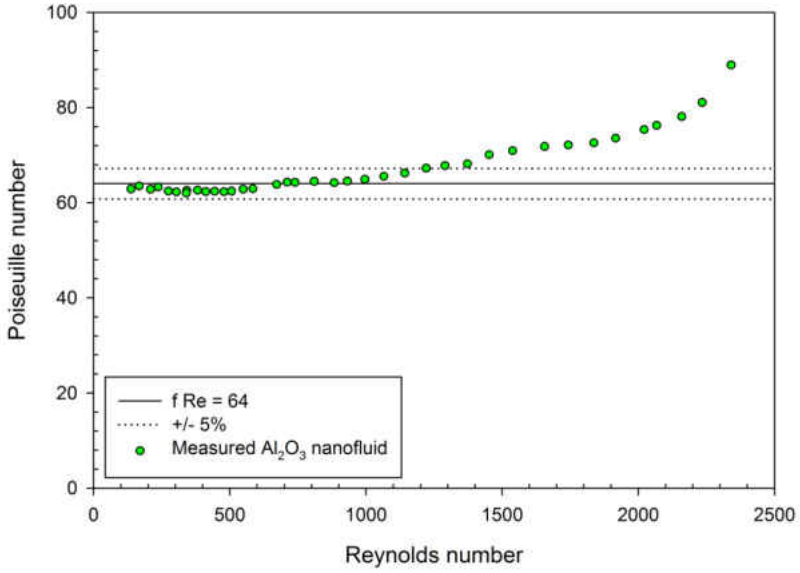

Figure 4.31. Plot between the Poiseuille number vs. the Reynolds number for the NF flowing through the 0.175 inch ID, 36 inch long tube.

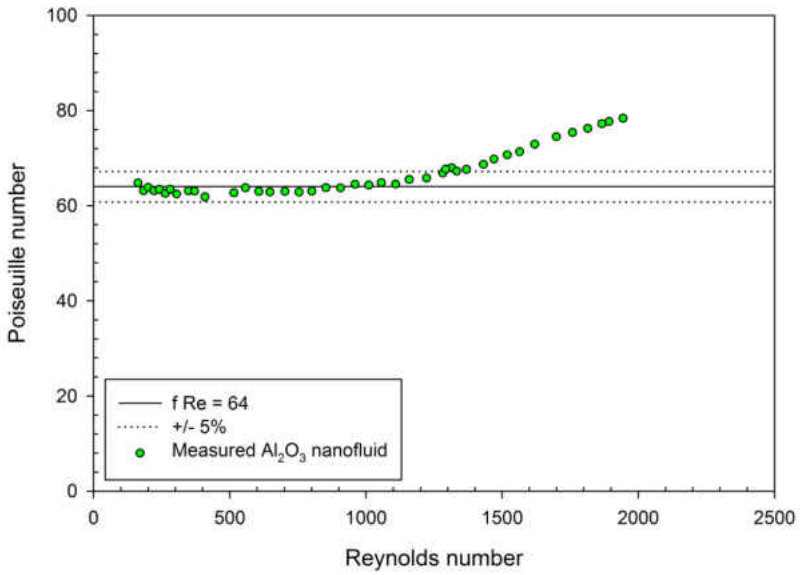

Figure 4.32. Plot between the Poiseuille number vs. the Reynolds number for the NF flowing through the 0.118 inch ID, 36 inch long tube.

4.5 Heat Transfer Results of Nanofluid

Before measuring the heat transfer for a forced convection, an analysis about the entrance length must be carried out. The thermal entrance length is given by Lienhard and Lienhard (2008) and is expressed mathematically as

$$\frac{x_e}{D_i} \cong 0.034 Re_D Pr \tag{4.16}$$

where x_e is the entry length in [m].

The heat transfer results for the NF lies under the laminar regime. Under constant heat flux conditions, the Nusselt number should be Nu = 4.36 for fully developed laminar flow. However, in our case, the thermal profile in the heated test section did not reach fully developed condition except for the 0.175 inch ID, 34 inches long tube and 0.118 inch ID, 34 inches tube, when the Reynolds number is less than 150 and 200, respectively. For the 0.175 inch ID, 34 inches long tube, at the last station where the flow is fully developed, Nusselt numbers of 4.43, 4.52 and 4.65 were measured for Reynolds numbers of 96, 120 and 136, respectively, which is within ±7% of the standard value. For the 0.118 inch ID, 34 inches long tube, at the last station where the flow is fully developed, Nusselt numbers of 4.35, 4.42 and 4.40 were measured for Reynolds numbers of 133, 175 and 195, respectively, which is within ±1.37% of the standard value.

For other Reynolds number a comparison is done with the correlation developed by Lienhard and Lienhard (2008) which gives the Nusselt number for a thermally developing flow and is expressed mathematically as

$$Nu = 4.364 + 0.263 \left(\frac{x^+}{2}\right)^{-0.506} exp\left(-41\frac{x^+}{2}\right) \tag{4.17}$$

where x^+ is the dimensionless distance given by

$$x^+ = \frac{2x}{D_i RePr} \tag{4.18}$$

For all the three tubes, plots between the Nusselt number and the dimensionless distance are shown in Figures 4.33 to 4.35. It can be seen that all the measured values lie within ±10% with those predicted by Lienhard and Lienhard (2008) correlation and also follows the same trend as predicted by the correlation.

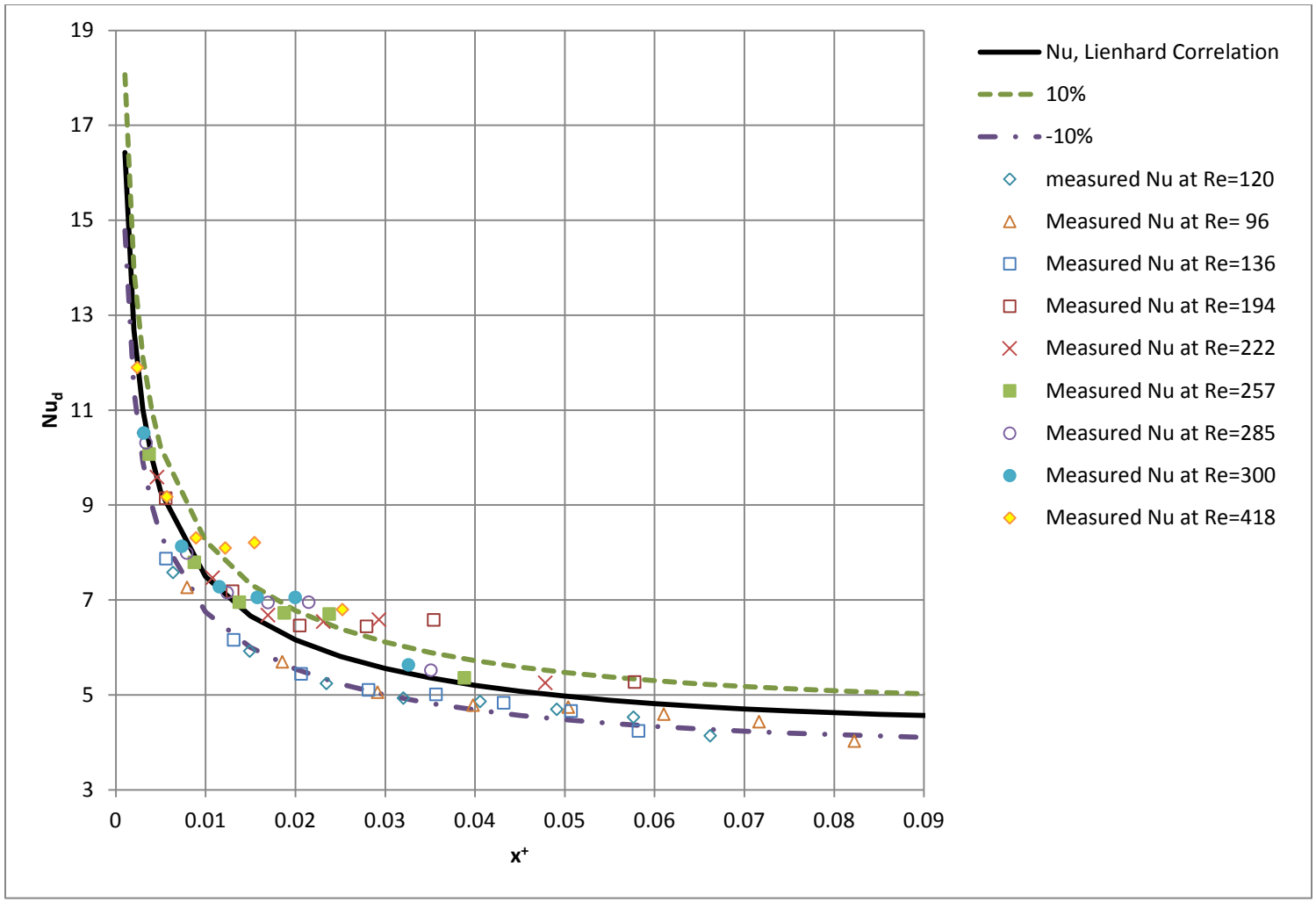

Figure 4.33. Nusselt number vs. x^+ for 6% vol. alumina/water nanofluid flowing through a 0.175 inch ID, 34 inch long heated test section. The solid line represents the correlation by Lienhard and Lienhard (2008). Dash lines represent ±10% error.

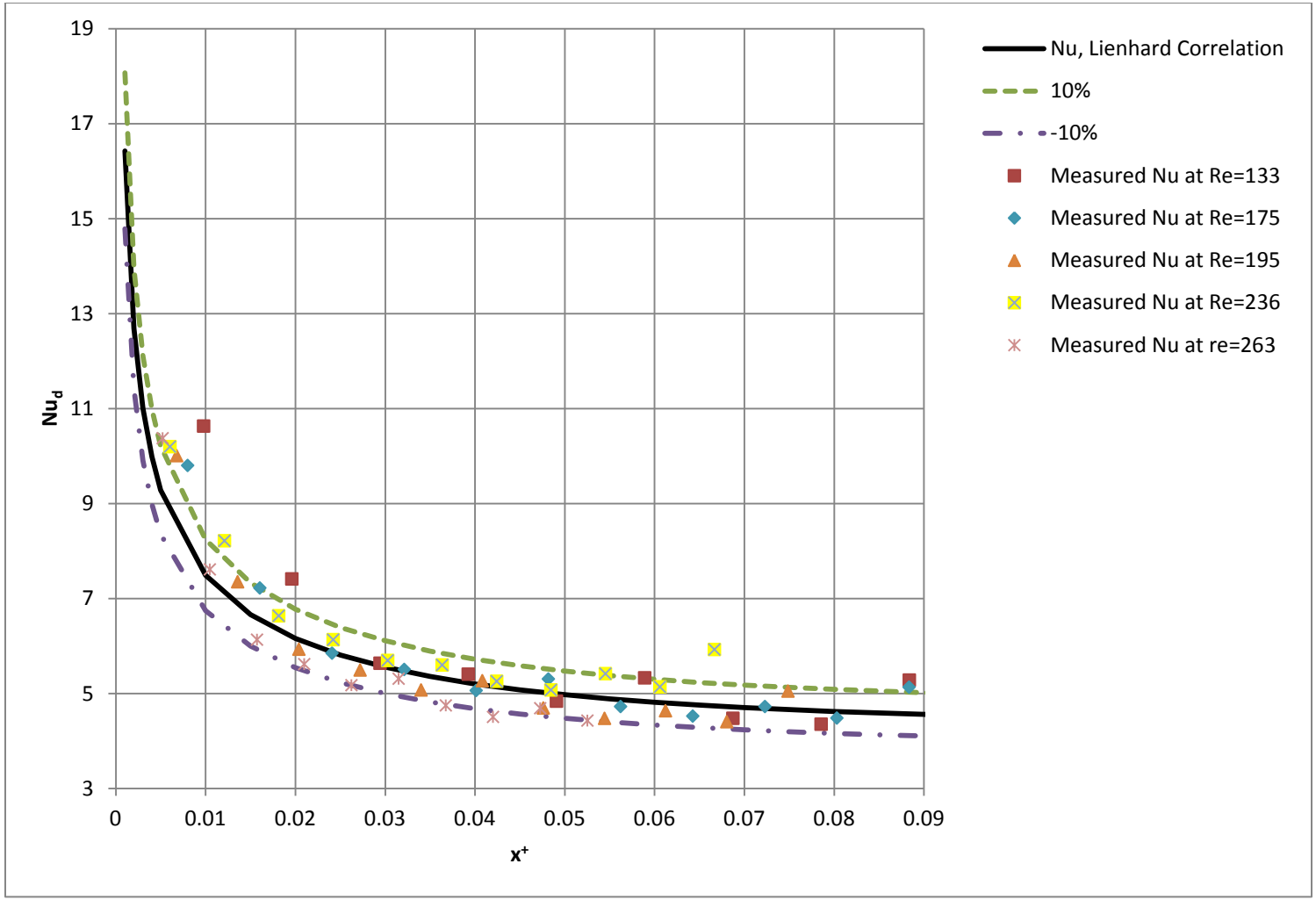

Figure 4.34. Nusselt number vs. x^+ for 6% vol. alumina/water nanofluid flowing through a 0.118 inch ID, 34 inch long heated test section. The solid line represents the correlation by Lienhard and Lienhard (2008). Dash lines represent ±10% error.

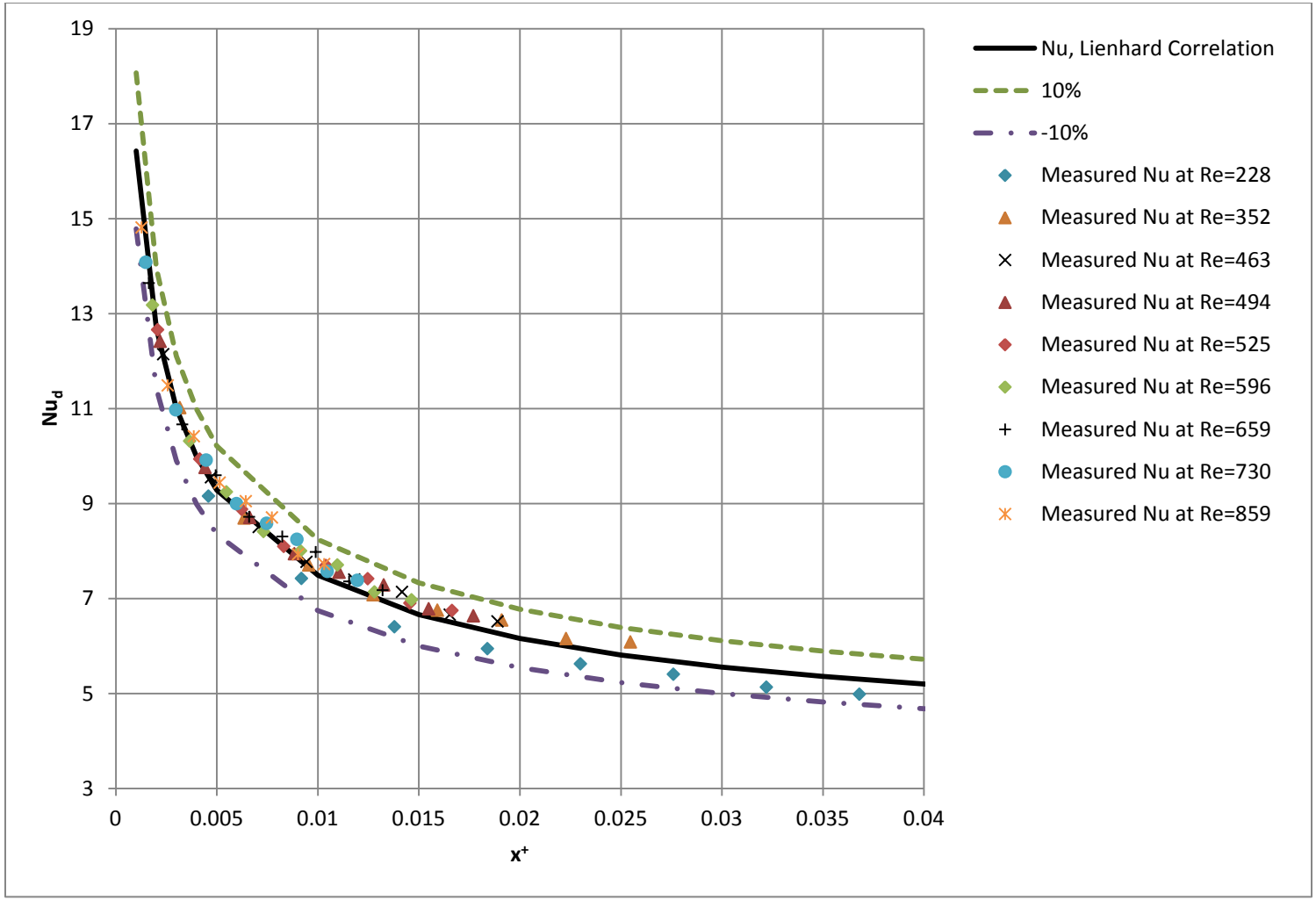

Figure 4.35. Nusselt number vs. x^+ for 6% vol. alumina/water nanofluid flowing through a 0.118 inch ID, 18 inch long heated test section. The solid line represents the correlation by Lienhard and Lienhard (2008). Dash lines represent ±10% error.

CHAPTER V

CONCLUSIONS AND RECOMMENDATIONS

This chapter discusses on the conclusions derived from the results of the experiment and recommends further procedure and experiments which could have been done if limitations in experimental instruments and time were not a factor to conduct this research.

5.1 Conclusions

An experimental study was carried out to investigate the thermophysical properties, friction factor and heat transfer characteristics of 6% vol. concentration AL_2O_3/water nanofluid. The conclusions derived from this experiment and its results are discussed in this chapter.

The thermal conductivity of the nanofluid was measured and it was found out that there is certain enhancement in thermal conductivity when using alumina/water nanofluid instead of water. Within the temperature range from 7 to 50°C, the enhancement is higher at a lower temperature and vice versa. This is because addition of nanoparticle into base fluid stabilizes its thermal conductivity and the nanofluid thermal conductivity will not be a

strong function of temperature whereas for water the thermal conductivity rises with temperature. The thermal conductivity of nanofluid is a complex phenomenon which takes into account not only thermal conductivity of the base fluid, thermal conductivity of the nanoparticles, diameter of the particle, volume fraction but also several interactions among the base fluid and the nanoparticle.

The viscosity of NF is higher than that of the base fluid by a factor of 8 at 7°C which increases to a factor of nearly 10 at 75°C. The viscosity of the nanofluid decreases with the volume concentration of the nanoparticles and at different temperatures follows the same trend. The plot between the shear stress and the shear rate (6 to 122 s^{-1}) for the NF shows that it is a Newtonian fluid indicated by the linear line passing through the origin. After 62.65°C, the NF experiences an irrecoverable increase in viscosity and shows a hysteresis effect on viscosity when heated beyond this temperature and cooled.

The friction factor of the NF in the laminar region can be well approximated by the Hagen-Poiseuille equation, $f = 64 / Re$. It is also seen that the transition from laminar flow starts to occur at a Reynolds number approximately 1500.

The convective heat transfer for fully developed thermal flow indicated a Nusselt number close to 4.36 within ±7%. For a thermally developing flow, the measured values of Nusselt number was in well agreement with the correlation given by Lienhard and Lienhard (2008) within ±10%. Also, the heat transfer of nanofluid can be accurately predicted by the correlation given for a single phase fluid.

5.2 Recommendations

The thermal conductivity measurement is very susceptible to error caused by external disturbances. However, if measurements are conducted by placing the apparatus in a vibration isolation table, a more accurate reading can be obtained. As indicated by the hysteresis effect on viscosity, the measurement of thermal conductivity should also be done by considering cyclic heating and cooling to see if we get a similar trend in thermal conductivity. Also, the effect of different nanoparticle material, volume concentration and particle size on thermal conductivity as well as the viscosity should be determined to understand the thermophysical behavior of the nanofluid in a greater extent. The nanofluid taken into concentration showed a Newtonian behavior for a value of applied shear rate between 6 and 122 s^{-1}. The range was limited due to the limitation in the range of shear rate of the measuring instrument. The nanofluid might or might not show a Newtonian behavior at higher shear rates. However, to understand the behavior of nanofluids fully, its behavior must be determined by subjecting it to a greater shear rate (>500 s^{-1}).

The friction factor and heat transfer results for the nanofluid was measured mostly in the laminar region. A turbulent flow could not be reached due to the limitation of the gear pump. A pump capable of producing turbulent flow in the test channel for the nanofluid should be taken into consideration to understand the friction factor and heat transfer behavior in the turbulent region. The high tolerance given by the manufacturer led to a high uncertainty in friction factor measurement. To lessen the uncertainty, an accurate

method of determining the dimensions of the test section like Laser scanning microscopy techniques should be applied.

The idea of using nanofluid is to get an increase in the heat transfer rate than when using conventional fluids. A study conducted by Ghajar and Tang (2007) showed that when using two phase air-water mixture, after a certain gas flow rate the convective heat transfer increases to be greater than that of single-phase fluid, as shown in Figure 5.1. Since the thermal conductivity of nanofluid is more than that of water, similar procedure can be followed by using nanofluid-air mixture which may further increase the heat transfer characteristic.

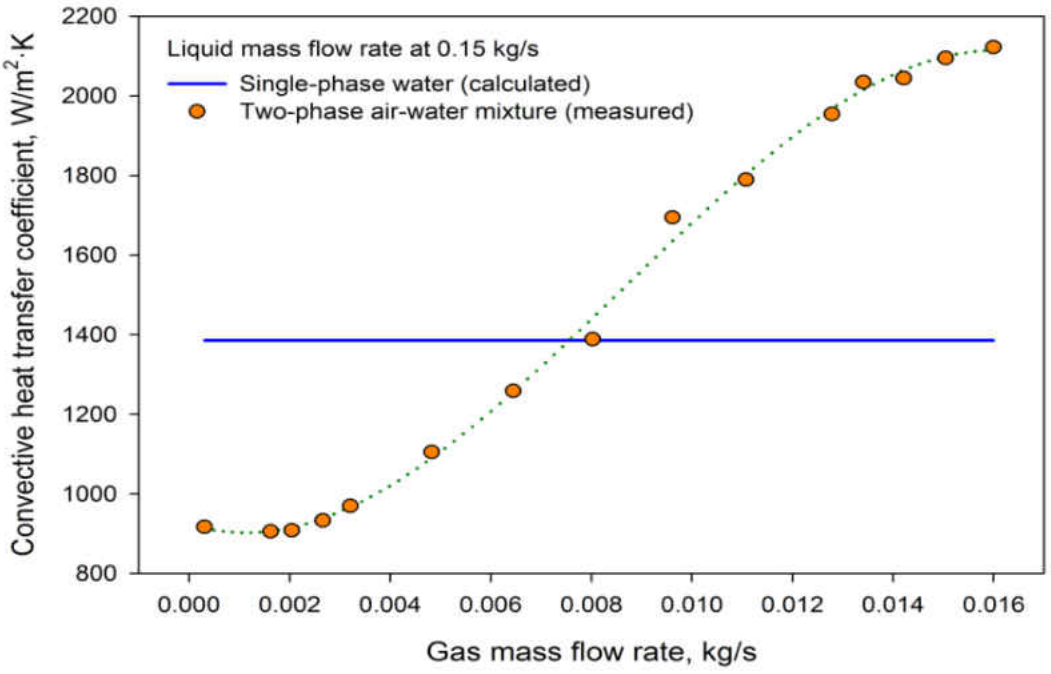

Figure 5.1. Plot showing the convective heat transfer coefficient vs. gas mass flow rate for a two phase air-water mixture (Ghajar and Tang, 2007).

REFERENCES

Abbaspoursani, K., Allahyari, M., Rahmani, M., (2011). An Improved Model for Prediction of the Effective Thermal Conductivity of Nanofluids, *World Academy of Science, Engineering and Technology,* 58.

Beck, M.P., Yuan, Y., Warrier, P., Teja, A.S., (2009), The Effect of Particle Size on the Thermal Conductivity of Alumina Nanofluids, *Journal Nanoparticle Research,*11, pp. 1129-1136.

Beck, M.P., Yuan, Y., Warrier, P., Teja, A.S., (2010), The Thermal Conductivity of Alumina Nanofluids in Water, Ethylene glycol, and Ethylene glycol + Water Mixtures, *Journal Nanoparticle Research,* 12, pp.1469-1477.

Bhatti, M. S. and Shah, R. K., 1987, "Turbulent and Transition Flow Convective Heat Transfer in Ducts," *Handbook of Single-Phase Convective Heat Transfer*, S. Kakaç, R. K. Shah and W. Aung, Eds., John Wiley and Sons, New York, pp.4.1–4.166.

Blasius, H., 1913, "Das Ähnlichkeitsgesetz Bei Reibungsvorgängen in Flüssigkeiten," *Forschungsarbeiten auf dem Gebiete des Ingenieurwesens*, 131, pp. 1–40.

Buongirno, J., (2006) Convective Transport in Nanofluids, *Journal of Heat Transfer,* 128, pp. 240-250.

Chandrasekar, M., (2008) New Analytical Models to Investigate Thermal Conductivity of Nanofluids, *Journal of Nanoscience and Nanotechnolog,* 9, pp. 533-538.

Chandrasekar, M., Suresh, S., Bose, A. C., (2010), Experimental Studies on Heat Transfer and Friction Factor Characteristics of Al_2O_3/Water Nanofluid in a Circular Pipe Under Laminar Flow with Wire Coil Inserts, *Experimental Thermal and Fluid Science,* 34 pp. 122-130.

Chon, C.H., Kihm, K.D., Lee, S. P., Choi, S.U.S., (2005), Empirical Correlation Finding The Role Of Temperature And Particle Size For Nanofluid (Al_2O_3) thermal conductivity enhancement, *Applied Physics Letters,* 87, 153107.

Churchill, S. W., 1977, "Friction Factor Equation Spans All Fluid- Flow Regimes," *Chemical Engineering*, vol. 7, pp. 91–92.

Das, S.K., Putra, N., Thiesen, P., (2003) Temperature Dependence of Thermal Conductivity Enhancement for Nanofluids, *Journal of Heat Transfer ASME*, 125, pp. 567-574.

Dey, T.K. and Kole, M., (2010), Thermal Conductivity and Viscosity of Al2O3 Nanofluid Based on Car Engine Coolant, *Journal of Applied Physics D: Applied Physics,* 43, 315501, (10pp).

Dittus, F.W. and Boelter, L.M.K., (1930). *Univ. Calif. (Berkeley) Pub. Eng.,* vol. 2, p. 443.

Drew, T. B., Koo, E. C. and McAdams, W. H., 1932, "The Friction Factor for Clean Round Pipes, *Trans. AIChE*, vol. 28, pp. 56–72.

Eastman, J.A., Choi, U.S., Li, S., Thompson, I.J., Lee, S., (1996), Enhanced Thermal Conductivity Through The Development of Nanofluids, *Material Research Society 1996 Fall Meeting*, Boston, MA.

Fang, K.C., Weng, C.I., Ju, S.P., (2006) An Investigation into the Structural Features and Thermal Conductivity of Silicon Nanoparticles Using Molecular Dynamics Simulations, *Nanotechnology*, 17, pp. 3909-3914.

Ghajar, A. J. and Tang, C. C., 2007, "Heat Transfer Measurements, Flow Pattern Maps and Flow Visualization for Non-Boiling Two-Phase Flow in Horizontal and Slightly Inclined Pipe," Heat Transfer Engineering, 28, pp. 525-540.

Gnielinski, V., (1976) New Equations for Heat and Mass Transfer in Turbulent Pipe and Channel Flow, *Int. Chem. Engng.,* vol. 16, pp. 359-68.

Hamilton, R.L., Crosser, O.K., (1962) Thermal Conductivity of Heterogeneous Two Component Systems, *IEC Fundam,* 1, pp.187-91.

Heris, S.Z., Etemad, S.G., Esfahany, M.N., (2007) Experimental Investigation of Convective Heat Transfer of Al_2O_3-Water Nanofluid in a Circular Tube, *International Journal of Fluids Flow,* 28(2).

Heris, S.Z., Etemad, S.G., Esfahany, M.N., (2007) Experimental Investigation of Oxide Nanofluids Laminar Flow Convective Heat Transfer, *International Communication of Heat and Mass Transfer,* 33.

Ho, C. Y. , Chu, T. K., (1977), Electrical Resistivity And Thermal Conductivity of Nine Selected Aisi Stainless Steels, CINDAS Report 45.

Holman, J.P., (2010). *Heat Transfer*. New York: McGraw-Hills Companies.

Hosseini, S.M., Moghadassi, A.R., Henneke, D.E., (2010), A New Dimensonless Group for Determining the Viscosity of Nanofluids. *J Therm Anal Calorim,* 100, pp. 873-877.

Hu, L., Rea, U., McKrell, T., Buongiorno, J., (2009), Laminar Convective Heat Transfer and Viscous Pressure Loss of Alumina-Water and Zirconia-Water Nanofluids, *International Journal of Heat and Mass Transfer,* 52, pp. 2042-2048.

Incropera, F.P., Dewitt, D.P., (2009) Fundamentals of Heat and Mass Transfer, 6th edition, John Wiley and Sons, New York, USA.

Jang, P.S., Choi, S.U.S., (2004), Role of Brownian Motion in the Enhanced Thermal Conductivity of Nanofluids, *App. Phys. Lett.*, 84, 4316-8.

Koo, J., Kleinstreuer, C., (2004) A New Thermal Conductivity Model for Nanofluids, *Journal of Nanoparticle Research,* 6, pp.577-588.

Lee, J.H., Hwang, K.S., Jang, S.P., Lee, B.H., Kim, J.H., Choi, S.U.S., Choi, C.J., (2008) Effective Viscosities and Thermal Conductivities of Aqueous Nanofluids Containing Low Volume Concentration of Al2O3 Nanoparticles, *International Journal of Heat and Mass Transfer,* 51, pp. 2651-2656.

Lee, S., (1999) Measuring Thermal Conductivity of Fluids Containing Oxide Nanoparticles, *Journal of Heat Transfer,* 121, pp. 280-289.

Li, C.H., Peterson, G.P., (2007) The Effect of Particle Size on the Effective Thermal Conductivity of Al_2O_3-Water Nanofluids, *Journal of Applied Physics,* 101.

Lianmin, H., Mohamed, S.E., (2001), Thermal Conductivity Measurements of Alumina Powders and Molded Min-K in Vacuum, *Energy Conversion and Management*, 42(5), pp. 599-612.

IV Lienhard, J.H., V Lienhard, J.H., (2008), *A Heat Transfer Textbook Third Edition*, Cambridge MA, Phlogiston Press, Retrived Date 09/14/2012, http://web.mit.edu/lienhard/www/ahttv131.pdf.

Maxwell, J.C., (1892), *A Treatise on Electricity and Magnetism, 2 unabridged 3rd ed.*, Oxford UK: Clarendon Press.

Mintsa, H.A., Boucher, S., Nguyen, C.T., Roy, G., Desgranges, F., Galanis, N., Mare, T., (2007), Temperature and Particle-size Dependent Viscosity data for Water-based Nanofluids-Hysteresis Phenomenon, *International Journal of Heat and Fluid Flow,* 28, pp. 1492-1506.

Mintsa, A.H., Roy, G., Nguyen, C.T., (2007), New Temperature Dependent Thermal Conductivity Data of Water Based Nanofluids, Proceedings of the 5th IASME/WSEAS Int. Athens, Greece, August 25-27, 2007, 290

Murshed, S.M.S., Leong, K.C., Yang, C., (2008) Investigations of Thermal Conductivity and Viscosity of Nanofluids, *International Journal of Thermal Sciences,* 91(7), pp. 560-568.

Murshed, S.M.S., Leong, K.C., Yang, C., (2008) Thermophysical and Electrokinetics Properties of Nanofluids-A Critical Review, *Applied Thermal Engineering,* 28(17), pp. 2109-2125.

Murugesan, C., Sivan, S., (2010), Limits for Thermal Conductivity of Nanofluids, *Thermal Science,* 14(1), pp. 65-71.

Nguyen, C.T., Roy, G., Gauthier, N., Galanis,N.,(2008) Heat Transfer Enhancement Using Al_2O_3-Water Nanofluid for Electronic Liquid Cooling System, *Applied Thermal Engineering,* 28.

Prasher, R., Bhattacharya, P., Phelan, P.E., (2005), Thermal Conductivity of Nanoscale Colloidal Solutions, *Physics Review Letters,* 94, 025901.

Selvakumar, P., Chandrasekar, M., Suresh, S., (2012), Experimental Studies on Heat Transfer and Friction Factor Characteristics of Cuo/Water Nanofluid Under Laminar Flow in a Helically Dimpled Tube, *Heat and Mass Transfer,* 48, pp. 683-694.

Shah, A.K, London, A.L., (1978), *Laminar Flow Forced Convection in Ducts: A Source Book for Compact Heat Exchanger Analytical Data*, New York: Academic Press.

Shanthi, R., Anandan, S.S., Ramalingam, V., (2012), Heat Transfer Enhancement Using Nanofluids, *Thermal Science*, 16(2), pp. 423-444.

Shukla, R.K., Dhir, V.K., (2005) Study of the Effective Thermal Conductivity of Nanofluids, *Proceedings ASME IMECE*, Orlando, Fl., pp. 1-5.

Sobhan, C.B.P. and Thomas, S., (2011), A Review of Experimental Investigations on Thermal Phenomena in Nanofluids, *Nanoscale Research Letters*, 6, pg. 377.

Sridhara, V., Satapathy, L.N., (2011), Al2O3-Based Nanofluids: A Review, *Nanoscale Research Letters*, 6, pg. 456.

Wang, X., Xu, X., Choi, S.U.S., (1999) Thermal Conductivity of Nanoparticle-Fluid Mixture, *Journal of Thermophysics and Heat Transfer*, 13(4), pp. 474-480.

Wongwises, S., Duangthongsuk, W.,(2009), Heat Transfer Enhancement and Pressure Drop Characteristics of Tio2-Water Nanofluid in a Double-Tube Counter Flow Heat Exchanger, *International Journal of Heat and Mass Transfer*, 52, pp. 2059-2067.

Xie, H.Q., (2002) Thermal Conductivity Enhancement of Suspensions Containing Nanosized Alumina Particles, *Journal of Applied Physics*, 91(7), pp. 4568-4572.

Xuan, Y., Li, Q., (2000) Heat Transfer Enhancements of Nanofluids, *International Journal of Heat and Fluid Flow*, 21(1), pp.58-64.

Xuan, Y., Li, Q., (2003) Investigation on Convective Heat Transfer and Flow Features on Nanofluids, *Journal of Heat Transfer*, 125, pp. 151-155.

Xuan, Y., Roetzel, W., (2000) Conceptions for Heat Transfer Correlations of Nanofluids, *International Journal of Heat and Mass Transfer*, 43, pp. 3701-3707.

Yoo, D.H., Hong, K.S., Yang, H., (2007), Study of Thermal Conductivity of Nanofluids for the Application of Heat Transfer, *Thermochimica Acta*, 455, pp. 66-69.

Yu, L., Liu, D., Botz, F., (2012), Laminar Convective Heat Transfer of Alumina-Polyalphaolefin Nanofluids Containing Spherical and Non-Spherical Nanoparticles, *Experimental Thermal and Fluid Science*, 37, pp. 72-83.

Yu, W.H., France, D.M., Routbort, JL, Choi, U.S., (2008), Review and Comparison of Nanofluid Thermal Conductivity and Heat Transfer Enhancements, *Heat Transfer Engineering*, 29, pp.432-460.

Wong, K.V., Leon O.D., (2010), Applications of Nanofluids: Current and Future, *Advances in Mechanical Engineering*, vol. 2010, Article ID 519659, 11 pages, 2010. doi:10.1155/2010/519659.

Zhou, S., Ni, R., Funfschilling, D., (2010), Effects of Shear Rate and Temperature on Viscosity of Alumina Polyalphaolefins Nanofluids, *Journal of Applied Physics*, 107, 054317.